UC Davis

UC Davis Electronic Theses and Dissertations

Title

Musculoskeletal response during mechanical unloading: Effects of age, alendronate, and Semaglutide

Permalink

https://escholarship.org/uc/item/4zf4k78k

ISBN

9798290614991

Author

Orr, Sophie Victoria

Publication Date

2025-06-15

Peer reviewed|Thesis/dissertation

eScholarship.org Powered by the California Digital Library
University of California

Musculoskeletal Response During Mechanical Unloading: Effects of Age, Alendronate, and Semaglutide

By

SOPHIE VICTORIA ORR

DISSERTATION

Submitted in partial satisfaction of the requirements for the degree of

DOCTOR OF PHILOSOPHY

in

Biomedical Engineering

in the

OFFICE OF GRADUATE STUDIES

of the

UNIVERSITY OF CALIFORNIA

DAVIS

Approved:

_____

Blaine A. Christiansen, Chair

_____

Keith Baar

_____

Clare Yellowley

Committee in Charge

2025

Dedication

To those who made this research obtainable: sertraline, my therapists, & the mice.

Acknowledgements

I'd like to say thank you to:

- Dr. Blaine Christiansen, the best mentor I have ever had, for teaching me how to do research and giving me every opportunity to explore the topics that are important to me. I will always remember and cherish your endless support.
- To my family for constantly reminding me they love me and sending See's Candies when necessary.
- To Connor, for always being supportive and loving, even when I was hungry.
- My dear friends Alita D'Almeida and Adam Weiner, who made every coffee break the reset I needed to relax and refuel before getting back to it.
- My other friends, near and far, who cheered me on the whole way.
- My lab mates for endless dissections, with special thanks to Will Lin, the best lab twin I could have hoped for. I can't wait for our next PhDs.
- The professors who took the time to work with me, whether on my dissertation or QE committee, or through training, teaching, equipment use, or work on the Health, Equity, Wellness committee. Special thanks to Dr. Keith Baar, Dr. Gaby Loots, and Dr. Ele Grandi for all their help.
- Lastly, thank you to Christal Wintersmith for creating a home at BMEGG for all of us.

Table of Contents

List of Figures

List of Tables

Abstract

Every year, millions of Americans are affected by illnesses and injuries that force them into periods of limited mechanical loading, such as bed rest, wheelchair usage, limb casting, or spaceflight. Disuse can occur at any point throughout life for many reasons, even in otherwise healthy individuals. During disuse, bones and muscles atrophy from a lack of mechanical loading. This tissue loss can have implications for those already at risk of low bone and muscle mass, including older individuals, those undergoing weight loss, or individuals with preexisting conditions. It is also an area ripe for innovation, as new pharmaceuticals and supplements for bone and muscle mass gain have well-established medical and wellness niches. Unfortunately, bone and muscle growth research often focuses on a single age group, despite differences in musculoskeletal remodeling throughout the lifespan. Additionally, the understanding of the effect that commonly prescribed pharmaceuticals have during unloading has not been fully explored. This dissertation overcomes this limitation by including different ages and sexes in bone and muscle health investigations during unloading with pharmaceutical interventions. First, it investigates the effect of mechanical unloading across the lifespan by utilizing young, middle-aged, and old mice. Next, it explores how bone mass maintenance might support muscle mass maintenance with alendronate treatment and identifies the effect of bone-muscle crosstalk proteins. Finally, it identifies the side effects of the blockbuster pharmaceutical Semaglutide, also known as Ozempic, during periods of unloading and reloading, which could impact bone and muscle atrophy and growth. Together, these studies offer novel insight into the impact of different medications during mechanical unloading. This research also supports the hypothesis that changes in response to mechanical unloading occur across the lifespan.

Chapter 1: Background

1.1 Significance: Bone and Muscle Loss During Unloading with Pharmaceutical Use

Mechanical unloading is a common following of injury and disease in all age groups, and can lead to bone and muscle loss. Disuse can be as transient as recovery from a sprained ankle or as long-lasting as bed rest for patients experiencing chronic pain. While these conditions affect all ages, musculoskeletal tissues vary tremendously across the lifespan in terms of both tissue mass and mechanical function. This impacts the rate of bone and muscle loss and the ability to regain lost tissue during recovery. These tissues may also adapt differently to different medications used during mechanical unloading, such as bisphosphonates and GLP1-receptor agonists. Bisphosphonates are prescribed to maintain bone in individuals at risk of low bone mass, particularly those with osteoporosis. As a mediator of bone resorption, bisphosphonates can also be used to investigate the impact of bone resorption on muscle health through biological crosstalk. However, bisphosphonates are usually only prescribed to older individuals. GLP-1 receptor agonists, including Ozempic, are meant to cause significant weight loss, which reduces mechanical loading in response to physical activity. How weight loss may impact musculoskeletal tissue loss during periods of unloading is unknown. The effect of biological crosstalk and pharmaceutical usage during mechanical unloading needs to be better understood if we hope to improve clinical outcomes in patients.

1.2 Musculoskeletal Response to Mechanical Loading and Unloading

Understanding the mechanisms of mechanotransduction in these tissues is essential for researching the effect of crosstalk and pharmaceuticals on bones and muscles during mechanical unloading.

1.2.1 Bone Anatomy & Physiology

Approximately 90% of bone cells in the body are osteocytes (Fig. 1.1[1]), the primary cellular regulators of bone remodeling [2]. These cells live in holes in the bone called lacuna and connect through dendritic processes that span canals in the bone called canaliculi. The lacuno-canalicular network is encased within the extracellular matrix (ECM) of bone and filled with interstitial fluid. The ECM is comprised of organic and inorganic compounds, mainly collagen and hydroxyapatite, that give bone its hard yet resilient properties. Cell-to-cell connections in the osteocyte dendritic processes, known as gap junctions, allow material and signal transfer between osteocytes and other bone cells and facilitate the regulation of bone growth, remodeling, and resorption [3].

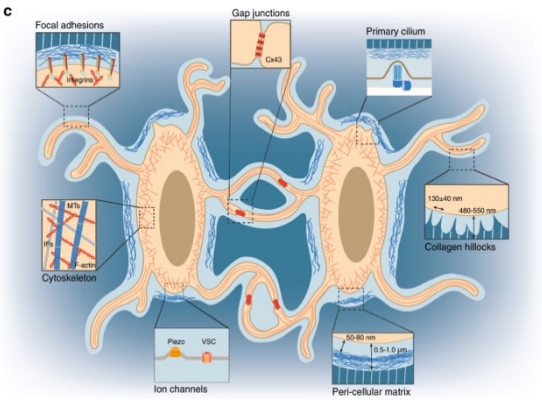

Figure 1.1. Osteocytes. Altered from Qin et Al. 2021 [1].

Bone remodeling occurs when damaged or excess bone is resorbed and new bone is created (Fig. 1.2[4]). Bone resorption is triggered to replace damaged bone, or to reduce bone mass in response to many stimuli, including disuse. Osteocytes release receptor activator of NF-κB ligand (RANKL) to trigger osteoclastogenesis, the proliferation of osteoclasts. RANKL and macrophage colony-stimulating factor (M-CSF, released by osteoblasts) bind to their respective receptors on osteoclast

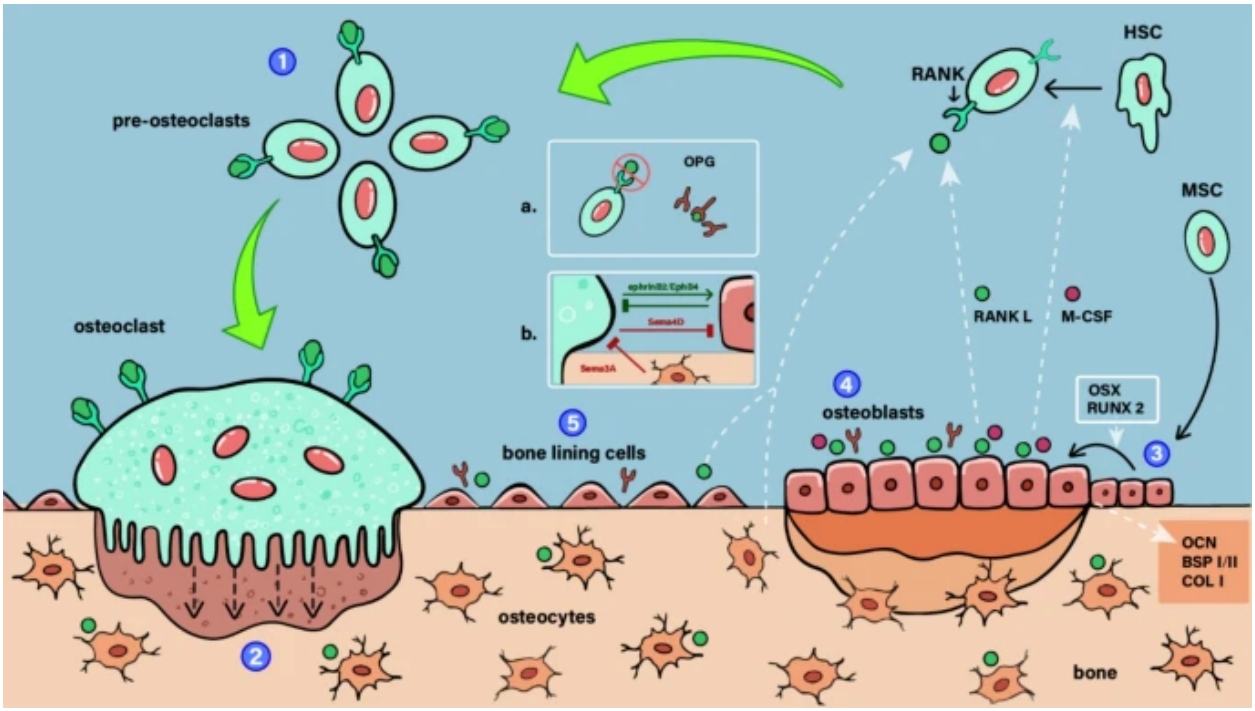

Figure 1.2. Bone Remodeling. From Maciel et al. (2023).

progenitor cells. These monocytic cells fuse into a multinucleated osteoclast and, with additional stimulation from RANKL and M-CSF, mature and attach to the bone surface, creating a sealed pocket called the Howship's lacunae. Osteoclasts then secrete HCl, Cathepsin K, and other enzymes to dissolve mineral and collagenous bone components[5-7] (Fig. 1.3[8]). Hydroxyapatite is broken down into Ca^{2+} and $(PO_4)^{3-}$, which are released into the bloodstream. Once the damaged tissue is dissolved, osteoblasts produce osteoprotegerin (OPG), which binds to RANKL so it cannot bind to RANK trimers on osteoclast progenitor cells or immature osteoclasts. Osteocytes and osteoblasts regulate osteoclast differentiation through the RANKL/OPG pathway in this manner, encouraging osteoclast apoptosis and effectively halting bone resorption.

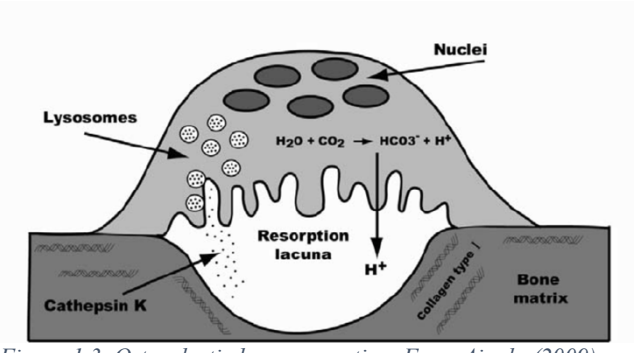

Figure 1.3. Osteoclastic bone resorption. From Ainola (2009)

To form new bone, osteoblasts are recruited to the resorption site and secrete an osteoid seam in the crater created by osteoclasts during resorption [9, 10]. Some osteoblasts undergo apoptosis while others embed themselves in the mineralized matrix and differentiate into osteocytes with newly formed dendritic processes. Bone lining cells then cover the surface of newly formed bone, connecting with osteocytes via gap junctions to participate in remodeling signaling. Once bone formation is complete, osteocytes secrete sclerostin, a protein that halts osteoblast activity by inhibiting BMP2 [11, 12].

1.2.2 Mechanotransduction in Bone

Maintaining bone throughout a person's lifespan requires efficient mechanotransduction, which is how cells convert mechanical stimuli into electrochemical signals transmittable throughout tissue [13]. Mechanotransduction has four distinct phases: 1) mechanocoupling, 2) biochemical coupling, 3) transmission of signal, and 4) effector cell response [14-16].

1.2.2.1 Mechanocoupling

For cells to react to an environmental mechanical stimulus, it must first be converted into a local mechanical signal. Local signals are measured in microstrain (με), where 1 με = 1 micron (μm) of deformation per meter (m). Strains result from the culmination of peak forces exerted on the bone from bending and compression from locomotion or other coordinated movements, which must be dynamic to create an osteogenic response [17-19]. Osteocytes are biaxially loaded during strain. Additionally, as the bone matrix bends, the strain gradients across the bone matrix produce an extracellular fluid flow sensed by osteocytes as fluid sheer stress on the cell process membrane (Fig. 1.4 [20]) [14, 20-22]. Osteocytes are connected to the walls of the lacuno-canalicular network

via a pericellular matrix composed of fibroblast intermediate filaments that connect to the osteocytic intracellular actin cytoskeleton [23, 24]. Upon bending, the fluid flow exerts drag on the pericellular matrix filaments, causing a deformation in the osteocyte cell membrane and actin cytoskeleton [23]. The formation of the pericellular matrix and cytoskeleton connection causes a hoop strain, producing approximately 10 times the force compared to fluid shear stress on the cell process membrane and 20 to 100 times the forces exerted on osteocytes through a direct transference of force from the ECM [23].

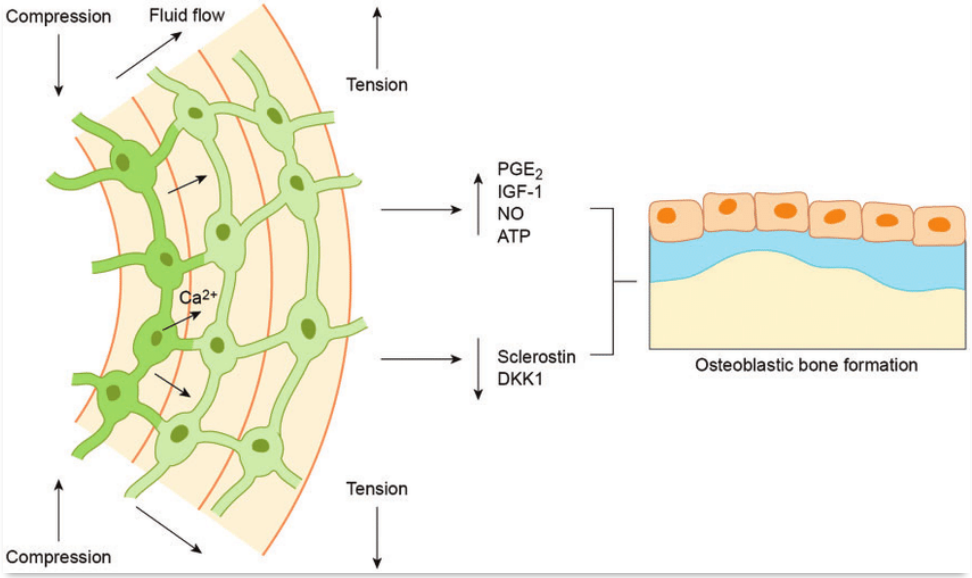

Figure 1.4. Interstitial fluid flow in response to mechanical loading on bone. From Hughes et Al. (2016).

1.2.2.2 Biochemical Coupling

Once a local mechanical signal is detected, it can be converted into a biochemical signal. One method of biochemical coupling is the activation of ligand-integrin-cytoskeleton linkages, which translate external mechanical stimuli into signaling cascades inside the cell. Proteins and integrins comprise extracellular organelles called focal adhesions that connect the ECM to the cytoskeleton through the cell membrane [15]. Cytoskeleton changes alter phenotype expression. The activation

of this pathway upregulates osteogenic transcription of factors, such as RUNX2, which leads to osteoblast differentiation [15]. Transmembrane ion channels, such as calcium channels and connexins (grouped in hemichannels as part of gap junctions (Fig. 1.5[25]), allow for the flow of Ca^{2+}, ATP, cAMP, and other signaling molecules [3, 26]. Protruding tubes on the cell membrane surface called primary cilia activate Ca^{2+} ion translocation into bone sensory cells through polycystin channels that open during mechanical stimulation, causing cell membrane depolarization [15]. This catalyzes STAT and Wnt signaling pathways [27], and oscillatory fluid flow (OFF) sensed by the cilia increases COX-2 and BMP2 expression, driving osteogenesis and MSC proliferation [28].

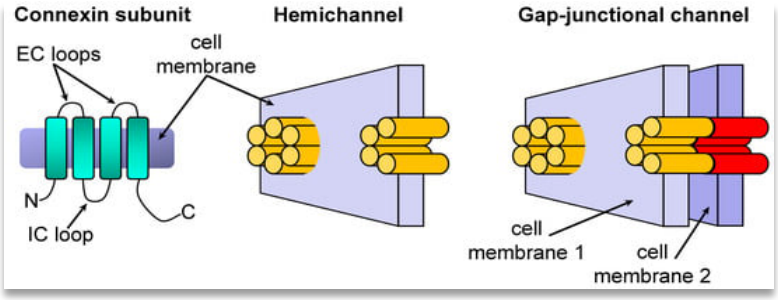

Figure 1.5. Gap junctions. From Fiori et Al. (2017).

Transmembrane glycoproteins called cadherins also regulate biochemical coupling by α-catenin and β-catenin association. During fluid shear stress, cadherin disassociates with β-catenin [29], which then fills the cell and is available to trigger the canonical Wnt signaling pathway [30-32].

1.2.2.3 Transmission of Signal

The biochemical signal then transmits to the nucleus. Kinase enzymes such as those in Akt, FAK, and MAPK subgroups phosphorylate signal molecules, starting many bone-regulating pathways that lead to osteogenesis [15, 33, 34]. Intracellular calcium ion (Ca^{2+}) concentrations are regulated by Piezo channel responses to fluid shear stress [35, 36]. Increased Ca^{2+} triggers ATP, NO, and kinase signaling cascades/pathways. This is also essential for increasing PGE_2 inside osteocytes, regulating mechanosensory response and PGE_2 intercellular signal transmission through proliferation of Connexin 43 (Cx43) [37]. The canonical Wnt signaling pathway, activated through β-catenin, transmits mechanosensory signals to increase osteogenesis.

Once the biochemical signal has reached the nucleus, the signal can then be transmitted from the sensor cell to the effector cell via direct or indirect methods. Gap junctions are connections between cells that allow for direct transmission of signals and cytoplasmic materials. A hemichannel composed of six connexin (Cx) subunits permeates the cell membrane and connects with another cell hemichannel to create a pathway for material transfer (Fig. 1.5 [25]) [38, 39]. Connexin 43 (Cx43) is responsible for many gap junction functions that exist between osteocytes in the lacuno-canalicular network, allowing particles up to 1kDa to pass between cells [3, 39-41]. Compression and tension of bone tissue cause a calcium ion signal to be transmitted through these gap junctions, leading to an increase in bone formation signaling (Fig. 1.4 [20]). Indirect signal transfer occurs when molecules are secreted by sensor cells and later absorbed or sensed by other cells through paracrine or endocrine signaling. Different types of multi-tissue crosstalk occur through these channels, including bone-muscle crosstalk.

1.2.2.4 Effector Cell Response

When the effector cell finally receives the biochemical signal, it reacts as necessary to maintain the equilibrium of bone strain. Bone remodeling is significantly tied to physical forces placed on musculoskeletal tissue by loading and movement. As first proposed by Wolff's Law, bone reacts to mechanical force by altering modeling and resorption rates based on the force applied [42]. In his Mechanostat theory, Frost proposed that there is an ideal strain for bone and mechanisms within the bone reacting to different amounts of strain [43-45]. Bone mass remains at equilibrium under an intrinsically preferred physiologic load. At the same time, periods of low magnitude strain promote resorption, while high strain stimulates modeling (Fig. 1.4 [46]). If a strain is too high, woven bone is produced to prevent fracture caused by overloading the bone tissue**.** These loading "zones" are differentiated by a minimum effective strain (MES) sensed by bone tissue. Loading must be large enough and cyclical in nature to produce most bone-forming responses [19, 47].

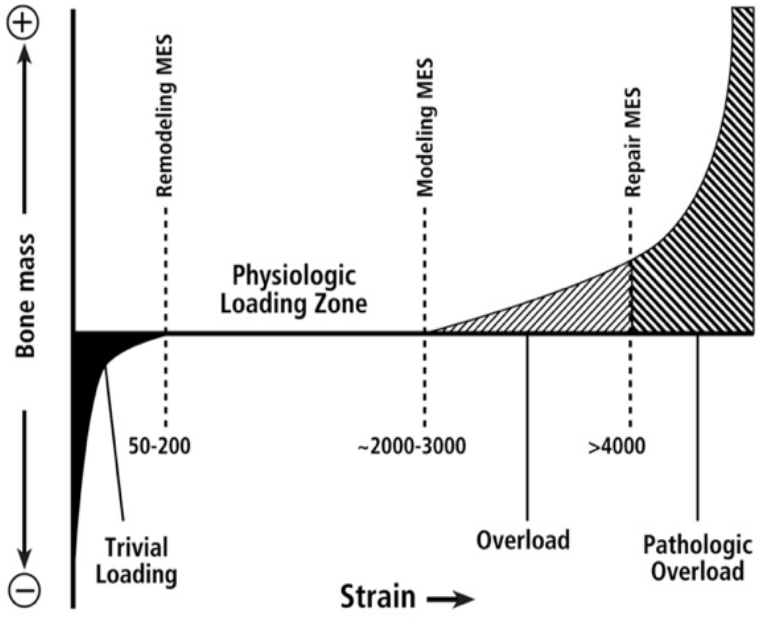

Figure 1.6. Skedros' rendition of Frost's Mechanostat theory. From Skedros et Al. (2001).

1.2.3 Mechanical Unloading

During periods of unloading, or disuse, there is not enough strain to prompt bone mass maintenance through mechanotransduction pathways. Transcription of osteogenic and osteoblast proliferating genes is downregulated, while osteoclastogenesis-promoting genes are upregulated. In muscle, protein synthesis is decreased, and degradation rises, resulting in muscle atrophy. These effects start in as one week or less, depending on mechanical stimulation, age, sex, and gravity of the local environment. However, the full impact of these factors is not wholly characterized. The rodent tail suspension hindlimb unloading model is used to study disuse in situations like prolonged bed rest and spaceflight, and as a proxy for wasting diseases (Fig. 1.7) [48, 49]. This model also allows researchers to investigate biological factors of mechanical unloading, such as gene expression and cytokine transfer.

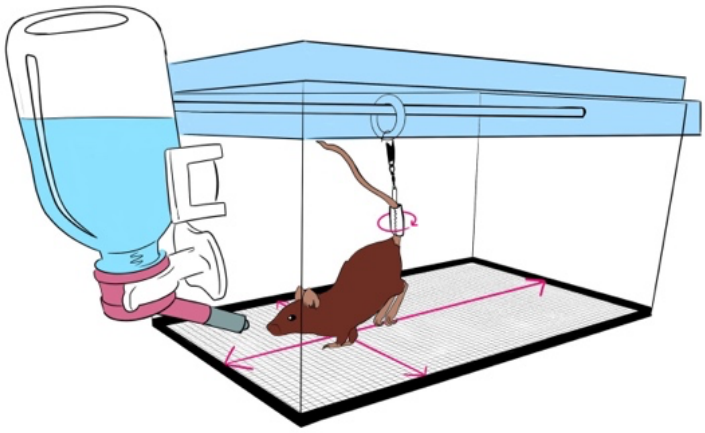

Figure 1.7. Murine hindlimb unloading cage.

1.2.4. Muscles and Tendons During Periods of Unloading

Muscles and tendons are also directly affected by mechanical loading and periods of unloading. Skeletal muscle cells are long, multinucleated fibers composed of sarcomeres arranged end to end in myofibrils. Myofibrils are bound together in a series of bundles surrounded by a sarcoplasmic reticulum (for Ca^{2+} storage and transfer); a protective sheet called the endomysium encircles each

individual muscle cell/fiber, and contains both vascular and neuronal networks (Fig. 1.8 [50]). Each muscle is individually structured to produce the desired force on bone when contracted. Muscles are attached to bones by tendons, which are strong connective tissue structures made from collagen that transmit forces from muscle to bone, act as a shock absorber, and prevent muscles from being damaged during movement. During contraction, myosin heads traverse actin filaments, hydrolyzing ATP with each step. This causes a shortening of sarcomeres, producing a force in the tendon and the attached bone. Like bone, muscle and tendon cells rely on mechanotransduction that creates appropriate intracellular responses to prevent atrophy and adapt to loading[51-55]. Unloading causes muscle and tendon adaptations, including atrophy and loss of function.

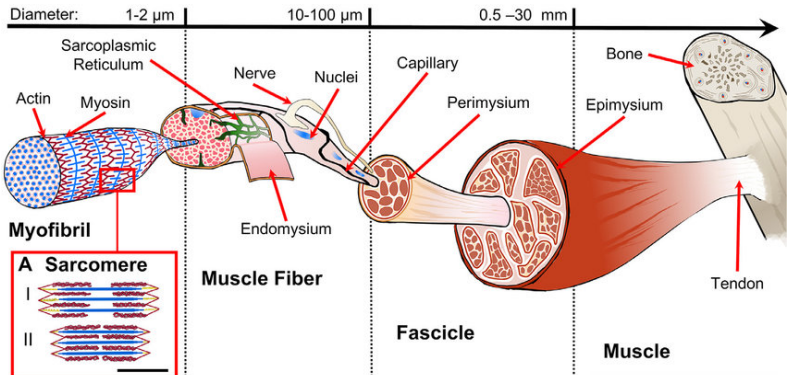

Figure 1.8. Skeletal Muscle Structure. Modified from Gottie et Al.(2020).

1.3 Musculoskeletal Cytokines

Many factors are involved in responses to mechanical unloading, including cytokines: small signaling proteins that regulate biological function. Many cytokines have multiple pathways of action throughout the body, including in musculoskeletal tissues. Mechanotransduction alters transcription of several key cytokines, including RANKL, OPG, TGF-β, and myostatin.

1.3.1 RANKL

Receptor activator of NF-kappa B (RANKL) is a type of Tumor Necrosis Factor (TNF) found throughout the body. In bone, it is released by osteoclasts and osteoblasts to promote osteoclastogenesis (Fig. 1.9[56]). The RANKL receptor RANK is located on osteoclast progenitors, osteoclasts, and some immune cells [57]. Mutations of the genes that encode RANK and RANKL can result in osteopetrosis, a disease characterized by abnormal bone growth leading to brittle, dense bones [58, 59]. RANK gene mutations can also present as early-onset Paget disease, osteolysis, panostotic expansile bone disease, and expansile skeletal hyperphosphatasia [57].

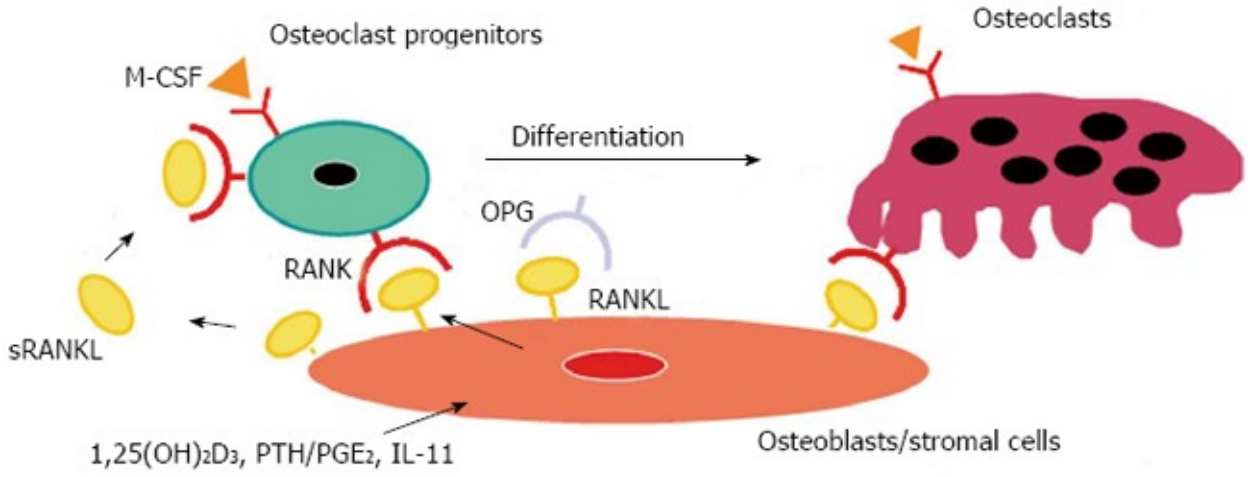

Figure 1.9. RANKL in osteoclastogenesis. From Yasuda (2013).

Many pathways modulate RANKL concentration and transcription. Mechanical loading causes fluid shear stress on bone cell walls, which reduces RANKL expression by upregulating the expression of nitric oxide (NO) synthase (NOS) mRNA and related proteins [60, 61]. L-arginine is then converted to NO by NOS, allowing NO to inhibit RANKL in response to mechanical loading. Biaxial mechanical strain also reduces RANKL mRNA expression by up to 50% [62]. This is partially attributed to mitogen-activated protein kinase (MAPK) signaling pathways,

specifically Extracellular signal-regulated kinase (ERK) and N-terminal Jun kinase (JNK) subfamilies. ERK 1 & 2 inhibit RANKL mRNA expression as a response to biaxial strain.

1.3.2 RANKL/OPG Ratio

Osteoprotegerin (OPG) is a tumor necrosis factor that regulates the release of RANKL into serum. OPG binds to RANKL, making it unavailable to bind to RANK, preventing bone resorption (Fig. 1.10 [63]) [63, 64]. The RANKL/OPG ratio is often used to discuss the availability of RANKL for binding, as low RANKL/OPG ratios are inversely correlated with RANKL levels in serum. RANKL and OPG concentrations change with mechanical loading [65, 66]. Additionally, hormones and other cytokines can influence RANKL/OPG ratios. Parathyroid hormone (PTH) and sclerostin upregulate RANKL and inhibit OPG expression [67, 68]. Inflammatory cytokine IL-6 concentrations also increase the RANKL/OPG ratio by reducing OPG concentrations *in vitro* [69]. Estrogen is a positive regulator of OPG, decreasing osteoclastogenesis and suggesting how hormone changes during and after menopause can decrease bone mass [70].

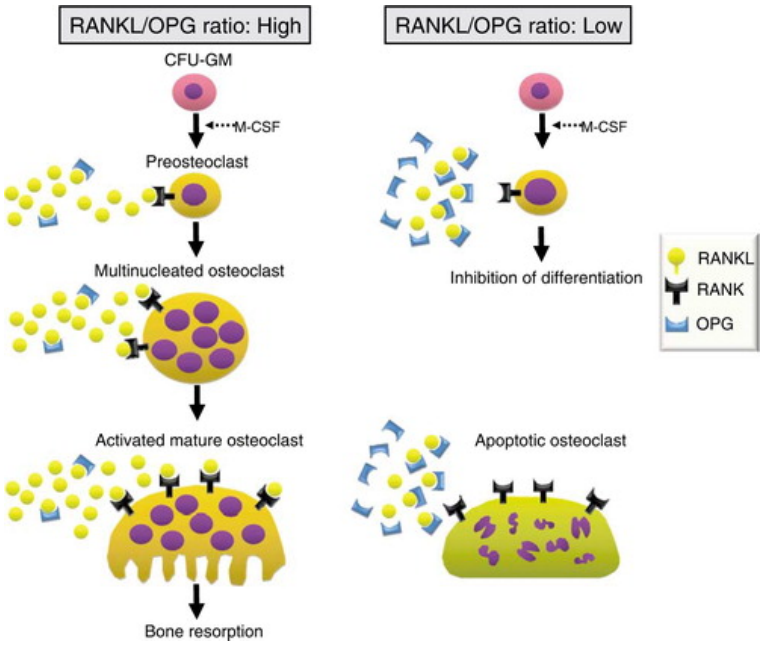

Figure 1.10. RANKL/OPG Ratio from Kajiya et al. (2010).

Oscillatory fluid flow (OFF) occurs in bone due to the compressive strain experienced by this tissue during mechanical loading, pushing fluid through the lacuna-canalicular network [71]. This fluid flow is considered oscillatory as mechanical movements such as walking are often repetitive,

creating a consistent cyclical pattern of fluid flow to and from regions of bone [26, 72]. During OFF, ATP, PGE_2, and OPG concentrations are increased while RANKL concentrations are decreased [26, 73]. The reduction of the RANKL/OPG ratio decreases osteoclastogenesis [73].

1.3.3 TGF-β

Transforming growth factor β1 (TGF-β1) is a cytokine from a family of growth factors that modulate cell growth and inhibition throughout the body [74-76]. In bone, TGF-β1 is bound to latency-associated protein (LAPs) inside the bone matrix, where it is inactive [77-79]. LAP is cleaved from TGF-β1 during osteoclastic bone resorption, releasing bioactive TGF-β1 into the interstitial fluid [79, 80]. TGF-β1 is then available to bind to TβRI receptors and trigger phosphorylation of SMAD2/3 which bind to co-SMAD4, allowing for transcription of TGF- β dependent genes (Fig. 1.11 [81]) [81]. TGF-β1 dysregulation and genetic mutations can cause musculoskeletal diseases, such muscular dystrophy [82], hairy cell leukemia [83], and Camurati-Engelmann disease [84, 85],

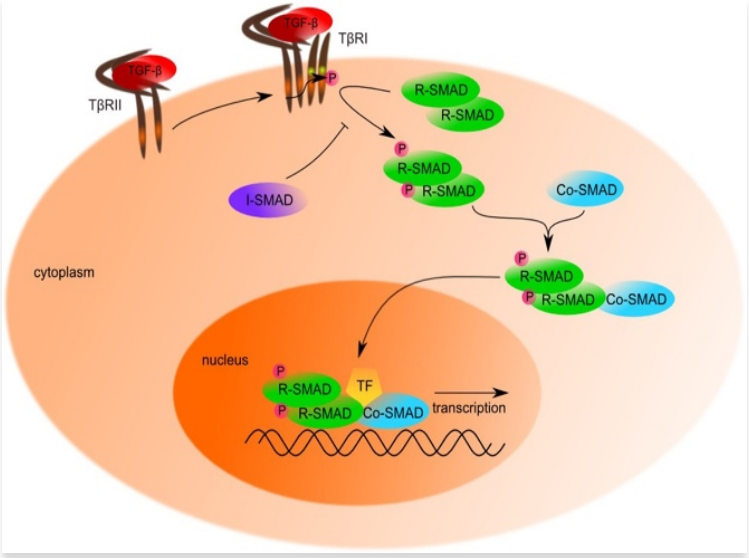

Figure 1.11. TGF-β pathway in bone cells. From Kubiczkova et Al 2023.

TGF-β signaling pathways are robust and are influenced by many factors, including mechanical stimuli. This stimulation can affect TGF-β concentrations, but the response depends on the force magnitude and application method. Activated TGF-β release increases after intermittent hydrostatic compression (IHC) [86]. Alternatively, fluid shear stress induces TGF-β signaling, increasing production of TGF-β and bone mineralization protein Type 1 receptors [87]. This increase manifests in increased Smad 2 & 3 phosphorylation. Some studies suggest that the effect of mechanical stimuli from mechanical loading on TGF-β concentrations appears to be localized to long bones, at least in rodent models [88, 89] . However, this contradicts studies where increases in systemic TGF-β concentration were observed. There may be additional forces at play *in vivo* that could not be controlled for in cell culture experiments. Investigation into the transfer of TGF-β from bone to muscle during mechanical unloading must be conducted to determine if it plays a key role in muscle atrophy during unloading *in vivo*.

1.3.4 Myostatin

Growth differentiation factor 8 (GDF8), colloquially known as Myostatin, is a negative regulator of muscle mass in both embryonic and adult mammals. During periods of disuse, such as bed rest, wheelchair usage, or space flight, myostatin expression increases. Acting through the ActRIIB pathway, myostatin binds with activin to activate the same Smad 2/3 phosphorylation pathway previously described for TGF-β1. In muscle, this inhibits production of MyoD, a protein essential for muscle differentiation, leading to atrophy (Fig. 1.12 [90]) [90, 91]. AKT expression and subsequent phosphorylation of FOXO are also diminished by myostatin, leading to muscle protein ubiquitination. In this process, proteins are degraded by the ubiquitin-proteasome system (UPS) [91-93]. The result of this ubiquitination is a reduction of muscle mass, which can manifest in short-term muscle wasting or long-term pathologies like sarcopenia or cachexia.

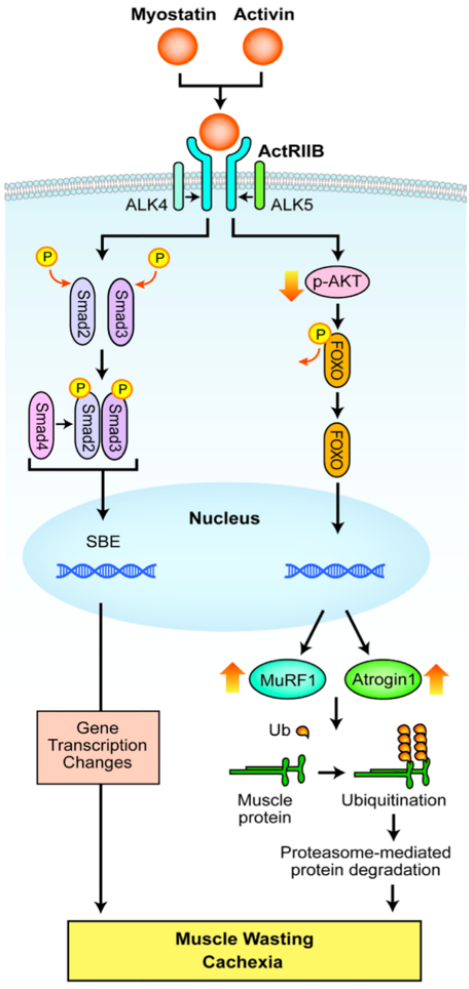

Figure 1.12. Myostatin Pathways in Muscle. From Han and Mitch (2011).

1.4 Bone-Muscle Crosstalk

Bone and muscle are intrinsically connected – each tissue acts on the other mechanically during movement and locomotion. Even wasting diseases like osteopenia and sarcopenia are considered the same disease to some researchers, who coined osteosarcopenia to demonstrate that the diseases are one and the same. As these tissues are so interconnected, it shouldn't come as a surprise that bone and muscle also communicate via protein transfer, or crosstalk [94-99]. Cytokines are proteins excreted from cells that can trigger action in the secretory cell itself (autocrine signaling), other cells in proximity (paracrine signaling), or cells in distant areas of an organism (endocrine signaling). These proteins are often categorized by their tissue of origin; osteokines originate in bone, while myokines originate in muscle. Biological crosstalk between bone and muscle tissues involves cytokines regulating different aspects of bone and muscle activity [94-99].

During disuse, osteoclasts break down existing bone tissue, releasing osteokines that can affect muscle metabolism. Two of these signaling proteins are TGF-β [100-102] and RANKL [57, 102-109], both of which initiate myopathy through their respective pathways. TGF-β release during bone metastasis decreases muscle Ca^{2+} concentration, driving muscle weakness [101]. TGF-β also activates the same pathway in muscle as myostatin, driving muscle atrophy in high concentrations [100]. RANKL inhibits myogenesis through regulation of Ca^{2+} storage in the sarcoplasmic reticulum [104]. As a result, circulating RANKL contributes to muscle weakness in ovarian cancer patients [110]. Similarly, the myokine myostatin triggers muscle resorption, inhibits new muscle growth, reduces muscle mass and strength [111-113], and affects bone. Myostatin can regulate osteoblast differentiation, osteoclast development, and bone morphology and atrophy in normal and unloaded conditions [94, 95, 97, 112-114]. Myostatin inhibition increases bone BMD, BMC,

length, and other key characteristics of many bones in the murine skeleton (Fig. 1.13 [115]) [115]. Inhibiting Myostatin receptor ActIIB can prevent trabecular bone loss in chemotherapy patients [116].

While these interactions are well characterized during periods of bone resorption caused by disuse and disease, it is unknown how crosstalk interacts with the biological changes caused by reductions in mechanical stimuli. Bisphosphonates maintain bone volume by reducing bone resorption by osteoclasts. In theory, decreased bone resorption should prevent the release of osteokines that drive muscle atrophy, such as TGF-β. Similarly, myostatin concentration is increased with muscle atrophy. Myostatin should not cause bone quantity and quality reductions if muscles are maintained during unloading. However, these biological crosstalk interactions have not yet been investigated.

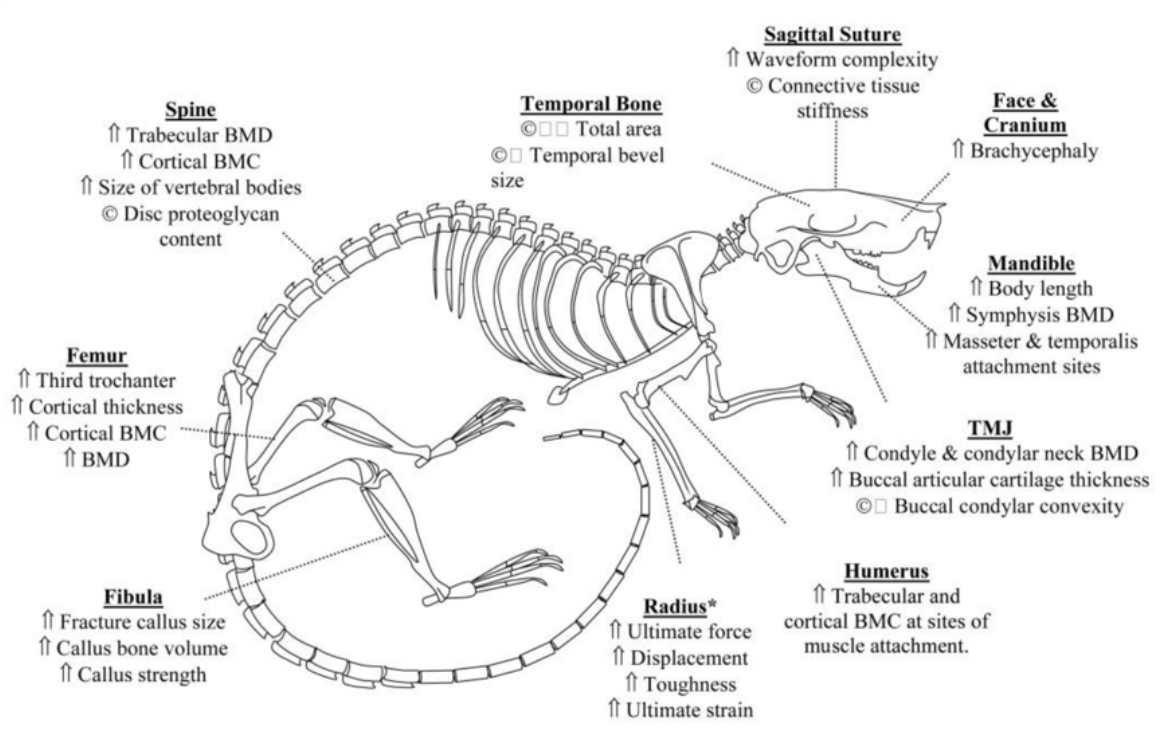

Figure 1.13. Effect of myostatin inhibition in murine skeleton. From Elkasrawy and Hamrick (2010).

1.5 Pharmaceutical Treatments

Medications used to directly or indirectly maintain bone can also affect multiple musculoskeletal tissues. This can be especially true during periods of modified or complete mechanical unloading. Bone-maintenance drugs, such as bisphosphonates, can prevent the deleterious effects of disuse. These medications can therefore be used to research the biological crosstalk present during unloading. Other medications, such as GLP-1 receptor agonists, which are used for treating diseases such as Type 2 Diabetes Mellitus, or for weight loss, are not prescribed for the direct treatment of bone. However, these drugs may have positive or negative impacts on bone without unloading, and unknown interactions with these tissues during unloading. Investigating these pharmaceuticals can help us understand mechanical unloading as it impacts current patient populations.

1.5.1 Bisphosphonates

Bisphosphonate usage is common in older patients who wish to maintain bone volume due to osteopenia, osteoporosis, and other diseases that directly or indirectly impact bone. Bisphosphonates maintain bone mass by interfering with normal osteoclast function and inhibiting bone resorption [117-119], and may reduce loss of muscle mass and function [120, 121]. Bisphosphonate treatment is prescribed to populations needing to retain bone mass, such as those with osteoporosis or bone atrophy due to certain cancers. It is also used in aerospace applications to prevent bone loss in astronauts during long-duration spaceflight missions [122]. Alendronate is an FDA-approved aminobisphosphonate commonly prescribed under the drug name Fosamax®. Alendronate binds to bone surfaces and prevents osteoclastic resorption by promoting apoptosis [6, 123] and interfering with the production of geranylgeraniol during the mevalonate pathway,

preventing cholesterol synthesis [124]. This ultimately interrupts cytoskeleton function [6, 119, 124]. Alendronate that is not absorbed by osteoclasts can remain in mineralized bone for several years, possibly interfering with osteoclasts during subsequent periods of resorption [125]. Osteocytes and osteoblasts are protected from alendronate-instigated transduction of extracellular signal-regulated kinase activation of connexin 43 (Cx43) found in bone gap junctions [41, 126].

Osteonecrosis of the jaw is a rare but serious side effect of bisphosphonate treatment, especially for patients with dental issues. Some doctors may suggest drug holidays (scheduled gaps in treatment) to prevent this. They may also prescribe other medications to maintain bone mass depending on the age, sex, and other conditions a patient might have. Other treatment options include Denosumab, Romosozumab, and hormone therapies. Denosumab is an FDA-approved treatment to prevent bone resorption and cancer metastases by inhibiting RANKL binding to RANK during osteoclastogenesis [127]. Romosozumab is also FDA approved and is used to inhibit sclerostin, a protein encoded by the SOST gene that interferes with osteoblastogenesis and osteoblast function [128, 129]. Hormone therapies can also be used, and many doctors prescribe vitamin C and D during osteoporosis treatment.

1.5.1.1 Bisphosphonate-Related Mechanotransduction Signal Disruption

As bisphosphonates interfere with osteoclast processes, they inherently alter the ability of the skeletal system to regulate bone mass. Amino and non-amino bisphosphates and specific drugs have different implications for the molecules present in the bone environment. The current consensus is that the effects of bisphosphonates on RANKL and OPG transcription, production, and serum levels vary widely depending on the specific drug mechanisms of action,

musculoskeletal disease status, and the affected tissue types [130-133]. These variations introduce uncertainty in the effect of these medications on different age groups, as bone and muscle tissue function and abundance change throughout the lifespan.

1.5.2 GLP-1 & GLP-1 Receptor Agonists

Glucagon-like peptide-1 (GLP-1) is a type of gut hormone called an incretin that modulates glucose homeostasis (Fig. 1.14) [134]. Incretins work by regulating the release of insulin, which transports glucose from the blood into cells [135]. Insulin secretion by pancreatic β-cells is increased during periods of high blood glucose, such as after a meal, and reduced when blood glucose levels return to basal levels. Incretins modulate this release and reduce glucagon secretion from the pancreas, reducing blood glucose levels. Glucagon would otherwise trigger the breakdown of glycogen and its release as glucose from the liver. Once blood glucose levels have stabilized, these glucose-dependent hormones will no longer activate insulin release. This insulin regulation in response to regular glucose shifts caused by eating and exercise is essential to preventing pathologically dangerous blood glucose levels.

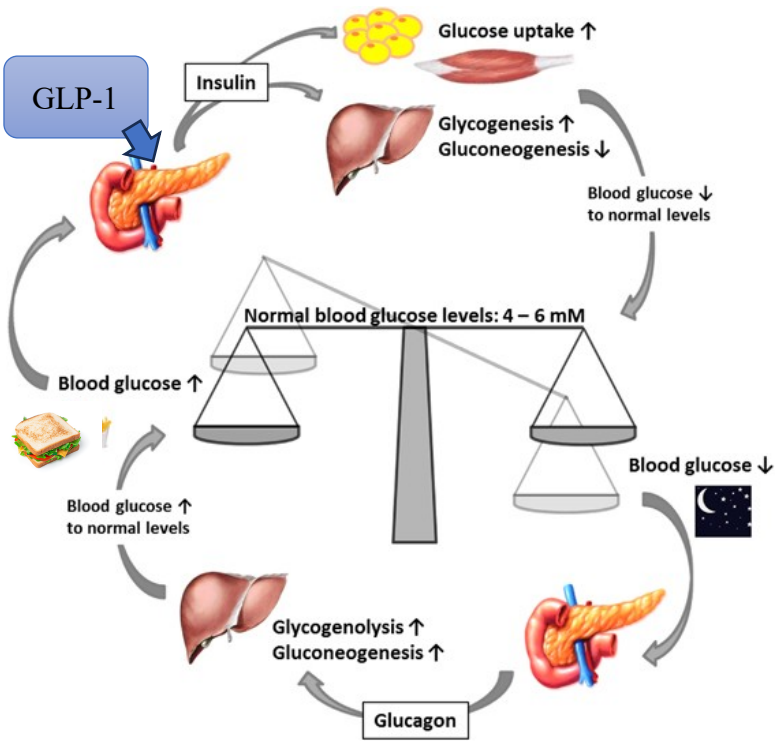

Figure 1.13. Glucose homeostasis, modified from Röder et al. (2016).

During Type 2 Diabetes Mellitus (T2D), insulin sensitivity of cells is reduced, preventing the transfer of glucose into cells and resulting in hyperglycemia, an elevated blood glucose level. If not treated, hyperglycemia can lead to a variety of dangerous health problems[136-138], such as heart disease[139], kidney disease[140, 141], nerve damage[142, 143], and vision loss[144]. To treat this, many T2D patients receive medical injections of insulin to reduce blood glucose levels [145, 146]. However, insulin treatment can cause hypoglycemia [147, 148], or low blood glucose levels, which can cause seizures [149], loss of consciousness or coma [148-150], brain damage [151, 152], or death [152, 153]. These glucose-independent treatments require patients and caretakers to consistently monitor insulin and blood sugar levels to prevent the dangerous extremes of blood glucose concentration [154]. Whereas insulin injections are glucose-independent, a newer class of drug known as GLP-1 receptor agonists (GLP-1RAs) act on the same glucose-dependent pathway as GLP-1 (Fig. 1.15 [155]). In this pathway, GLP-1 binds to its receptor in pancreatic B-cells, allowing for the coupled G protein to release from the receptor to bind to Adenylyl cyclase. Adenylyl cyclase then catalyzes the conversion of ATP to cAMP. Glucose is required for ATP availability in the cell, though high levels of ATP restrict the channels that allow for intracellular glucose uptake. cAMP can then activate PKA, which is needed for changes in ion transfer necessary for insulin secretion. These medications simulate GLP-1 but have a significantly longer half-life. Unlike GLP-1, which has a half-life of 1-7 minutes[156], these analogs can remain active for up to 168 hours (1 week) due to their designed resistance to the enzyme dipeptidyl-peptidase IV (DPP-4), which breaks down excess GLP-1[156-158]. They therefore remain in the blood until they are needed to reduce blood glucose levels.

Additionally, like GLP-1, these agonists also reduce the pancreas secretion of glucagon, slow gastric emptying, and reduce appetite[135]. Semaglutide and other GLP-1RAs have also been

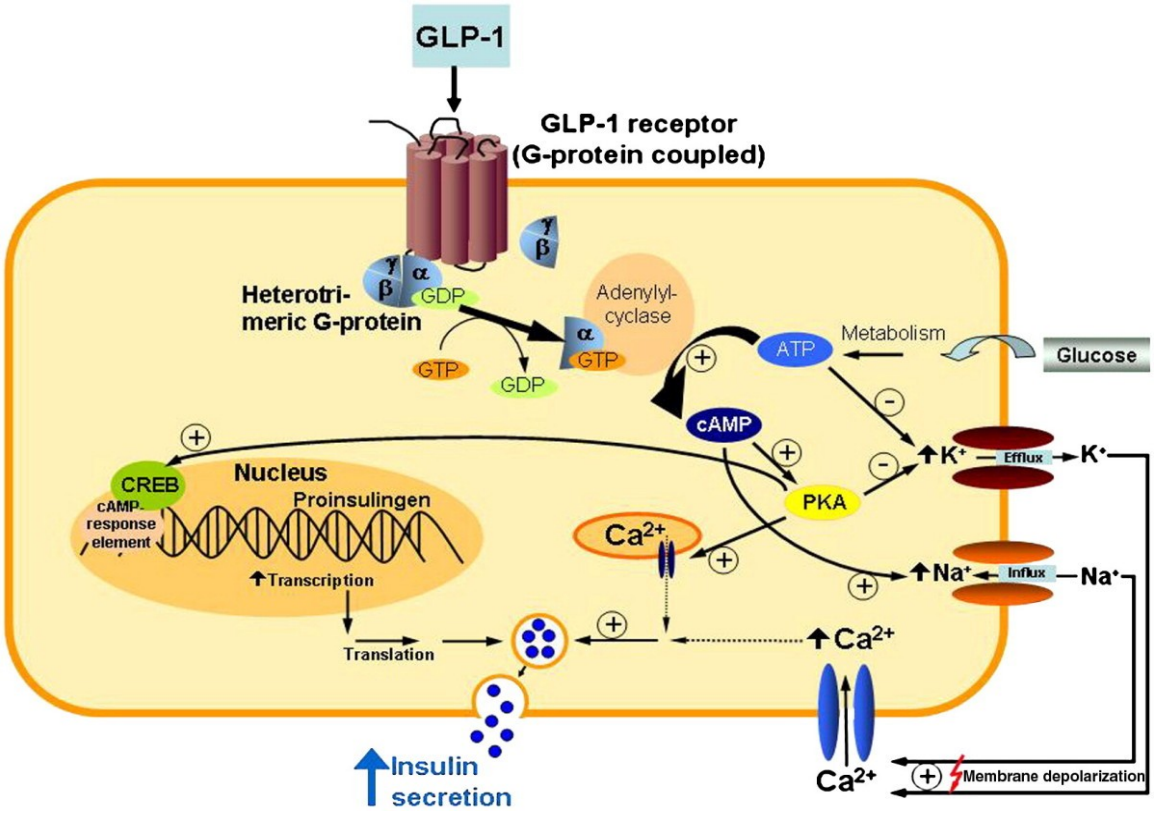

Figure 1.14. The GLP-1 mechanism in the pancreas (glucose-dependent). From Verspohl (2009). GLP-1 stimulates the GLP-1 receptor, which is coupled to a heterotrimeric G-protein. This allows for the exchange of GDP and GTP, releasing the G-protein α subunit to bind with Adenylyl cyclase, which catalyzes the production of cAMP from ATP. cAMP then increases insulin mRNA transcription and activates protein kinase A(PKA). Together, cAMP and PKA depolarize the cellular membrane, driving ion channel activation. An influx of Ca2+ ions then triggers secretion of insulin.

shown to penetrate the blood-brain barrier with potential central nervous system effects that may modulate satiety and craving responses, though further investigation is needed[159]. Together, these effects modulate blood glucose levels and, in many patients, contribute to weight loss.

Weight loss, however, does not only come from a reduction in body fat (adipose tissue). Fat-free mass loss, including muscle, can comprise up to 40% of weight loss, depending on the weight loss method [160]. Caloric restriction weight loss results in less overall weight loss, as well as a lower

percentage of fat-free mass (FFM) loss (10-30%), while GLP-1RA-induced weight loss can result in more weight loss but also higher levels of FFM loss (25-39%) [160-162]. Lower-weight individuals may lose little to no muscle mass during low-dose Semaglutide treatment [163], though this retrospective study was only focused on 25 T2D patients. While some researchers argue that the muscle loss during GLP-1RA-induced weight loss may not be clinically relevant due to the health benefits of weight loss and improvement in muscle quality metrics [162], countless others clearly demonstrate the importance of skeletal muscle as a structural and metabolically relevant tissue (Fig.1.16[160]) [2, 95, 160, 164]. Sarcopenia, a progressive loss of muscle mass, is a growing concern in larger-bodied patients who lose and regain weight [165, 166], especially in older adults [167-169]. Older patients with T2D have increased loss of muscle mass and function compared to those with normal insulin susceptibility [170], making this an even more threatening condition.

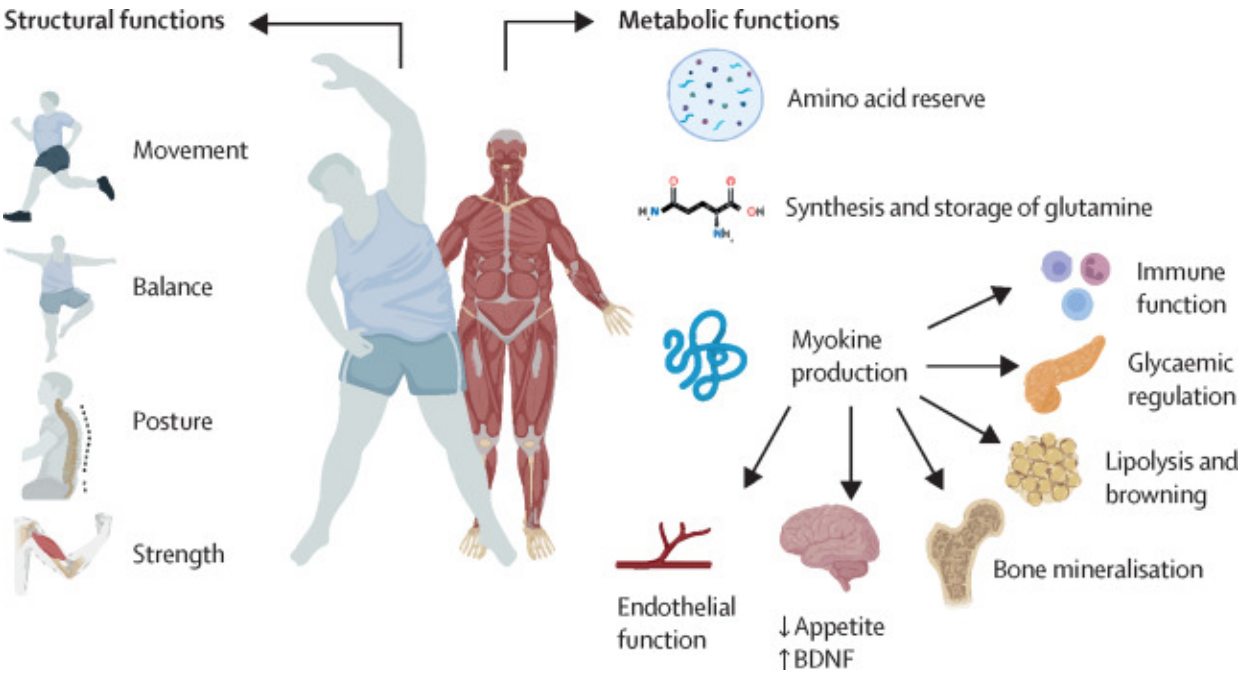

Figure 1.15. Muscle functions. From Prado et al (2024).

Weight reduction can also lead to bone loss due to decreased mechanical loading, nutrient reduction, and hormone changes [171-176]. As discussed previously, loading is required for bone remodeling homeostasis. Reductions in caloric intake can interrupt nutrient intake, and low-fat diets can also impact nutrient absorption. For example, vitamin D is fat-soluble and required for calcium absorption, so low fat diets may further increase these nutrient deficiencies without additional interventions [177]. Changes in hormone production caused by fat and muscle loss, such as reductions in adiponectin and estrogen, can also impact bone resorption through various pathways [178-181]. Increases in bone marrow adipose tissue might also contribute to bone dysfunction after weight loss [182]. Similar to muscle loss, rapid weight loss leads to increased bone loss compared to more gradual and less severe weight loss [176]. Bone loss can also accelerate after weight regain [183].

Currently, 2 out of 3 patients stop taking GLP-1 RAs as a weight loss medication within one year[184]. Given that patients who stop taking these medications regain most of the weight lost, if not more, the danger of weight cycling is increased for patients who take Semaglutide for weight loss reasons. Patients who have success on the medication and regain weight may decide to retake it. This may be especially true as Semaglutide medication is currently cost-prohibitive for many Americans[185], which could cause gaps in medication. Weight cycling increases the risk of sarcopenia and high body mass[165, 166], as well as increasing fracture risk [171] and reducing BMD[186]. Additionally, weight regain often occurs with less muscle or bone mass returning compared to the amount lost [183, 187-189]. For example, a study by Beavers et al. discovered

that for every 1kg of weight lost, 0.26kg was lean mass, but only 0.12kg of lean mass was gained back per 1kg regained[187].

1.5.2.1 GLP-1 & Bone

GLP-1 has direct and indirect effects on bone (Fig. 1.17 [190]). The prevalence of GLP-1 receptors on different bone cells is currently under investigation. Some studies suggest that GLP-1 receptors are not expressed in bone cells [191, 192], while others indicate that they are[193-196]. *In vitro* studies using mouse-derived cells demonstrate that GLP-1 receptors are expressed in osteoclasts[193, 196], and osteoclasts treated with GLP-1RAs exendin-4 and liraglutide have increased proliferation but reduced activity and similar levels of viability[193, 196]. MLO-Y4 cells and rat femoral osteocytes were also shown to express GLP-1R [195]. However, it is unclear whether mature osteoblasts express GLP-1R[192], though it is present during osteogenesis of several stem cell lines[192, 194, 197, 198]. GLP-1RA expression may also be regulated in a glucose-dependent manner [194].

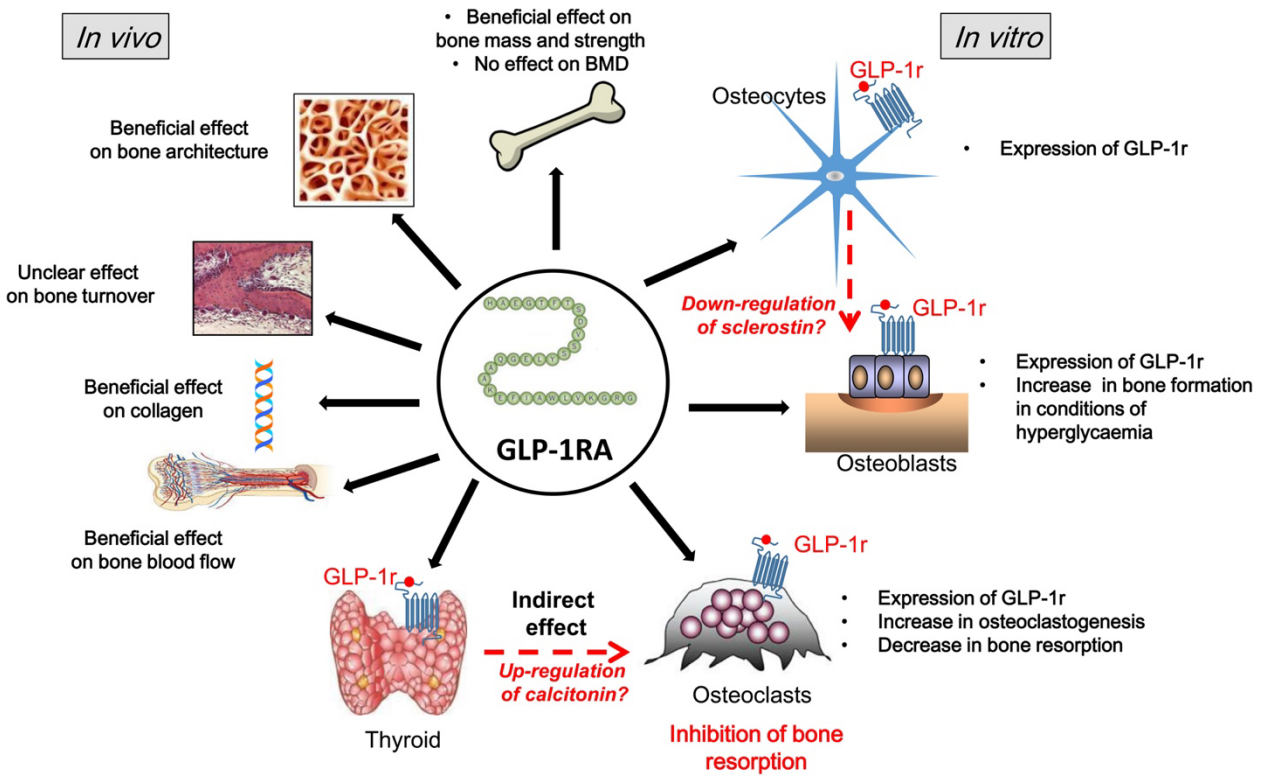

Figure 1.16. GLP-1 effects on bone. From Mabilleau (2018).

Relevant phenotypes and suggested mechanisms have been identified for the effects of GLP-1 and GLP-1RAs on bone. GLP-1RA treatment increases trabecular bone mass in mouse models [196]. Rodent models with reduced bone mass and quality saw improvements in max load, stiffness, and Young's Modulus with GLP-1RA treatment [192, 199]. Glp-1r$^{-/-}$ knockout mice have increased bone resorption, reduced cortical bone density, and increased fragility[200]. Glp1r-deficient mice show decreases in bone structural and material strength, possibly due to reductions in collagen-crosslinking [191]. The GLP-1RA exendin-4 has been shown to bind to GLP-1R in bone marrow stromal cells, increasing osteogenic differentiation through protein kinase A(PKA)/ β-catenin signaling pathways[192]. GLP-1 may also stabilize β-catenin in the canonical Wnt/ β-catenin pathway by increasing cAMP expression in the cytoplasm of relevant cells[201].

Osteoclastogenesis was also reduced in cultured mouse cells through NF-κB and MAPK signaling pathways[193].

However, some of this research may only apply to rodent models, not clinical studies or primates. For example, thyroid calcitonin production increases with GLP-1RA in rats but not primates [202]. In mice, GLP-1 may act in a calcitonin-dependent way to regulate bone homeostasis, but this has not been investigated in primates [200]. *In vivo*, *in vitro*, and clinical studies with different GLP-1RAs have been comparatively inconsistent [190, 203]. More research is therefore needed to solidify relevant direct mechanisms of GLP-1, GLP-1RAs, and Semaglutide specifically, especially in humans.

Different GLP-1RAs also exhibit different bone-altering effects given their various structures and mechanisms [204, 205]. Mice treated with exendin-4 have shown increased calcitonin, while those treated with liraglutide saw no increase [196]. In human patients, a weight loss clinical trial with liraglutide noted increased bone formation markers [206], while another study with weight loss using Semaglutide demonstrated no change in bone formation markers and an increase in bone resorption markers in patients at risk of fracture [207]. Given the difference in bone response between GLP-1RAs and a significant increase in half-life between Semaglutide and other more established but less prescribed GLP-1RAs, research already conducted on other compounds should be repeated with Semaglutide. The exponential increase of biological availability compared to GLP-1 and other GLP-1RAs is likely biologically relevant.

1.5.2.2. GLP-1 & Muscle

GLP-1 also directly and indirectly affects skeletal muscle, with expression of GLP-1 receptors in skeletal muscle cells being well demonstrated [208]. GLP-1 regulates many functions in muscle tissue, including glucose metabolism, insulin sensitivity, and remodeling. GLP-1 is involved in AMPK (AMP-activated protein kinase) signaling [209, 210]. The GLP-1/AMPK pathway has been shown to prevent glucotoxicity by preventing p47phox translocation in cardiac muscle cells [209]. GLP-1 also increases the expression of GLUT4, a glucose transporter expressed in adipose cells, and cardiac and skeletal muscle cells. Insulin is required to translocate GLUT4 to the cell membrane, allowing glucose uptake in these tissues [211]. However, exercise can also trigger GLUT4 translocation through the AMPK pathway. Circulating GLP-1 increases after exercise [212], and cell glucose uptake can be induced through exercise-regulated AMPK pathways [213].

The impact of GLP-1RA on body composition and muscle is not fully understood. In one study, Glp1r-/- mice had no changes in body weight or composition compared to Glp1r+/+ mice when fed standard chow [214]. However, when fed a high-fat diet, lean mass was reduced in Glp1r-/- female mice compared to functional controls. Female Glp1r-/- mice also gained less weight under a high-fat diet than Glp1r+/+, while male mice had the same level of fat accumulation between both genotypes. Muscle glycogen levels were also elevated in Glp1r-/- mice. Fasting glucose levels were reduced in Glp1r-/- mice compared to Glp1r+/+ mice, suggesting a reduction in insulin resistance in muscle tissue, even when fed a high-fat diet[214]. GLP-1RAs interventions have been successful in maintaining muscle mass in animal models. Exendin-4 reduced muscle loss in a dexamethasone-induced muscle atrophy mouse model by downregulating myostatin expression

and upregulating myogenic growth factors [215]. Further investigation into these effects, including their impact on tissue during unloading, is warranted.

1.5.2.3. Semaglutide

Semaglutide is a GLP-1RA produced and sold in the US by Novo Nordisk as several different medications: Rybelsus (pill, 7mg or 14mg, daily), Ozempic (injected, 1mg, weekly), and Wegovy (injected, 2.4mg, weekly). Ozempic and Rybelsus were FDA-approved for T2D treatment in 2017 and 2019, respectively, and Wegovy was approved as a weight loss treatment in 2021 [216].

Semaglutide has been shown to reduce life-threatening symptoms of T2D. Semaglutide treatments reduce blood glucose levels [217], reduce the severity of cardiovascular disease [218-221], kidney disease [218, 220, 222, 223], and osteoarthritis [224, 225]. It also reduces patient weight [226-228]. Wegovy also decreased cardiovascular events such as heart attack and stroke in patients with high BMI and preexisting cardiovascular disease[219]. However, cessation of medication can cause patients to regain weight and a reversal of health improvements [227].

Semaglutide treatment has multiple side effects in both animal models and humans, most notably gastrointestinal concerns and suspected increases in pancreatitis and cancer[229]. As with other GLP-1RA research, these studies have shown conflicting results in animals and humans. However, the FDA has still issued warnings based on some of these studies. Ozempic and Wegovy are contraindicated in those with a family history of medullary thyroid carcinoma and Multiple Endocrine Neoplasia syndrome type 2 because of an increase in thyroid c-cell tumors during rodent studies [230-232]. In clinical trials, Wegovy had higher instances of most side effects compared

to Ozempic and placebo (Table 1), though the patient population was slightly different; Wegovy trials did not require patients to have T2D, where Ozempic did [231, 232]. Gastrointestinal side effects could explain reductions in food consumption in both treatment groups. No musculoskeletal side effects have been listed on Semaglutide prescription labels other than fetal growth defects. Therefore, the investigation of Semaglutide effects on bone and muscle is overdue.

Table 1.1. Wegovy and Ozempic Clinical Trial Adverse Effects. Modified from WEGOVY and OZEMPIC drug labels.

	Wegovy Clinical Trial		Ozempic Clinical Trial	
	Placebo	WEGOVY (2.4mg)	Placebo	OZEMPIC (1mg)
	n=1,261	n=2,166	n=262	n=261
	%	%	%	%
Nausea	16	44	6.1	20.3
Diarrhea	16	30	1.9	8.8
Vomiting	6	24	2.3	9.2
Constipation	11	24	1.5	3.1
Abdominal Pain	10	20	4.6	5.7
Headache	10	14	Not Reported	Not Reported
Fatigue	5	11	Not Reported	Not Reported

1.6 Summary and Knowledge Gaps

First, bone and muscle morphology and function change throughout the lifespan, but the impact of unloading has not been fully characterized across all age groups. Investigation into the unloading response of young, middle-aged, and old mice is needed to address the lack of consensus observed in current research literature. Secondly, the effects of biological crosstalk between bone

and muscle during periods of disuse have not been satisfactorily explored *in vivo*. Many bone-muscle crosstalk agents have been identified, but whether they contribute to tissue atrophy during disuse because of biological crosstalk instead of a lack of mechanical cues remains to be seen. Lastly, pharmaceutical interventions on bone and muscle atrophy during unloading and recovery during reloading have not been well explored. This is particularly relevant to populations at risk for low bone quantity and quality, such as older patients or those who are undergoing extreme weight loss. More information is needed regarding the adverse side effects of medical interventions during disuse, which may exacerbate the loss of bone and muscle during unloading. Without this knowledge, medications intended to prevent one disease may inadvertently compromise musculoskeletal tissue temporarily or permanently.

This dissertation aims to close these research gaps. Chapter 2 will explore bone, muscle, and crosstalk-related adaptation to unloading and bone mass maintenance in young, middle-aged, and old mice. Chapter 3 will elucidate the effect of the popular weight loss drug Semaglutide on musculoskeletal tissue during periods of unloading and reloading. Together, this research will help define the roles of age, biological bone-muscle crosstalk, and common pharmaceuticals in adaptation to unloading.

Chapter 2: Age-Dependent Musculoskeletal Changes During Mechanical Unloading with Bisphosphonate Treatment

Abstract

Mechanical unloading (disuse) leads to reductions in bone and muscle mass. Bone and muscle health are often studied together in terms of mechanical stimulus, but non-mechanical (biological) crosstalk during periods of disuse and how this is affected by bone-preserving pharmaceuticals has not been assessed. This study aimed to determine how mechanical unloading and concurrent bisphosphonate treatment affect bone and muscle structure and function in young, middle-aged, and old mice. We hypothesized that unloading would cause bone loss in all mice, but bisphosphonate treatment would prevent this loss. Additionally, we expected to see muscle atrophy and weakness with unloading. We hypothesized that these reductions would be partially mitigated by bisphosphonate treatment due to decreased release of osteokines, and that this mitigation will decrease with age. This study used young (3-mo, n=40), middle-aged (12-mo, n=40), and old (20-m, n=40) male C57BL/6J mice. Mice received biweekly subcutaneous bisphosphonate injections (0.03 mg alendronate/mouse in PBS) or PBS control injections starting one week before unloading. Mice underwent hindlimb unloading (HLU) via tail suspension for 14 days. Maximum hindlimb force was measured after 14 days of unloading. Femurs were imaged with micro-computed tomography (μCT 35, SCANCO Medical AG) with a 6 μm nominal voxel size; cortical bone was analyzed at the mid-diaphysis, and trabecular bone was analyzed at the distal femur to determine bone microstructural outcomes. Muscle volume and fiber type were analyzed via IHC. Muscle myostatin and serum TGF-β1 levels were tested via ELISA. Tendon mechanical properties were also investigated. HLU conditions decreased the mass of the Triceps surae muscles regardless of

bisphosphonate treatment. Muscle mass was only maintained in the Tibialis anterior of treated middle-aged mice during HLU. Old mouse muscle mass decreased after HLU with bisphosphate treatment. Limb force production did not correlate with bone or muscle changes. Maximum hindlimb force production and respective force to muscle mass ratio differed between all age groups. Muscle myostatin concentrations increased with age($p=0.040$), bisphosphonate treatment ($p=0.003$), and unloading($p=0.002$), as well as due to the interaction of treatment and unloading ($p=0.0239$). Serum levels of TGF-β1 increased with age ($p<0.0001$) and unloading ($p=0.012$), as well as with interactions between both age and treatment($p=0.006$) and age and unloading ($p=0.013$). The main effect of age impacted muscle, tendon, and bone responses to unloading and/or bisphosphonate treatment. Bone and muscle adaptation to unloading are different across the lifespan, as are the effects of bisphosphonate treatment. Characterizing these changes is essential for understanding clinical outcomes related to periods of disuse and clinical bone and muscle preserving treatments during bedrest, immobilization, or even spaceflight across different age groups.

1. Introduction

Osteoporosis & sarcopenia are debilitating age-related diseases with high morbidity & mortality risks that impact millions. Osteoporosis is a degenerative disease characterized by reduced bone mass, leading to bone weakness and frailty [233], that impacts millions annually in the United States [234]. The incidence of the disease increases with age and is dependent on gender, with women being 4 times more likely to develop osteoporosis than men [235]. Osteoporosis is often closely associated with sarcopenia, the wasting of skeletal muscle that occurs later in life, with both conditions leading to increased frailty, fracture risk, and mortality rates [236, 237]. Age is an essential factor in treatment of bone and muscle due to these conditions.

Preventing bone and muscle atrophy during unloading can reduce the burden to at-risk populations. Bone and muscle wasting are accelerated during extended periods of mechanical unloading (disuse) [238, 239], especially in situations such as bed rest and spaceflight [240-243]. Mechanical loading (i.e., exercise) can theoretically be used to regenerate atrophied tissue through mechanotransduction [13]. However, with age, people's ability to perform weight-bearing exercise is diminished, and bone and muscle tissue are less responsive to mechanical stimuli [244]. This is important because elderly patients make up a disproportionately large number of hospitalizations, and their length of stay for hospitalizations is longer on average than that of younger adults [245, 246]. Preventing atrophy during unloading periods can benefit multiple at-risk populations, but these treatments will most likely vary depending on age. High-performance populations like athletes and astronauts could benefit from bone and muscle maintenance to rebound from injury or prevent atrophy in microgravity. In contrast, older populations could benefit from avoiding bone and muscle loss during bed rest, which could contribute to accelerated onset of osteoporosis or sarcopenia.

While bone and muscle atrophy are often researched together in the context of exercise or unloading due to their force-transmitting interaction, the non-mechanical (e.g. biological) crosstalk between these tissues may also be critical but has not been as well characterized. Cytokines are proteins excreted from cells that can trigger action in the secretory cell itself, other cells in proximity, or distant areas of an organism. These proteins are often categorized by their tissue of origin; osteokines originate in bone, while myokines originate in muscle. Biological crosstalk between bone and muscle involves cytokines regulating different aspects of bone and muscle activity [94, 95]. During disuse, osteoclasts break down existing bone tissue, releasing osteokines that can affect muscle. Two of these signaling proteins are transforming growth factor beta (TGF-β) [100, 101] and Receptor activator of NF-κB ligand (RANKL) [57, 103-108], both of which initiate myopathy through their respective pathways. Similarly, the myokine myostatin (GDF-8) inhibits new muscle growth, and reduces muscle mass and strength [111-113], but also affects bone. Myostatin can regulate osteoblast differentiation, osteoclast development, bone morphology, and atrophy in normal and unloaded conditions [94, 95, 97, 112-114]. These cytokines play essential functions in both tissue types, and crosstalk can therefore contribute to tissue health, especially during periods of unloading. Understanding the transfer of cytokines between bone and muscle tissues at different ages during mechanical unloading may help define pathways that influence bone and muscle health.

Current treatments for bone atrophy prevent bone remodeling, while research on muscle atrophy treatments is focused on promoting muscle tissue growth. Bisphosphonates maintain bone mass by interfering with normal osteoclast function and inhibiting bone resorption [117-119]. This

treatment is prescribed to populations that need to retain bone mass, such as those who have osteoporosis or bone atrophy due to cancer. It is also used in aerospace applications to prevent astronaut bone loss during long-duration spaceflight missions [122]. Myostatin inhibitors are being studied for clinical applications to systemically inhibit myostatin, a myokine that blocks muscle growth[247, 248], from binding to its receptor on muscle cells[249, 250]. While this treatment is currently successful in research models such as mice [251, 252], clinical therapies have not been successful in combating atrophic diseases such as muscular dystrophy [252]. It is presently unknown whether preserving muscle tissue with these treatments affects bone tissue by preventing release and binding of myokines, or if bisphosphonate treatments prevent osteokine transfer to, and subsequent effects on, muscle function. Differences in cytokine transfer between these tissues across the lifespan are also poorly understood.

This study outlines the investigation of bone-muscle crosstalk-related mechanisms that may lead to therapeutic strategies to reduce musculoskeletal atrophy during disuse. We **hypothesized** that the release of cytokines during unloading-induced atrophy of bone and muscle tissue contributes to atrophy of the other tissue, that preventing the atrophy of one of these tissues during unloading will also mitigate the atrophy of the other by inhibiting the release of catabolic cytokines, and that this inhibition will diminish with age. The goal of this work is to open new areas of study in orthopaedic research that may ultimately inform clinical practice.

This study aims to determine whether maintaining bone volume via alendronate during unloading will affect:

1) bone morphology at different ages;

2) muscle volume, composition, and function;

3) tendon mechanical properties and composition;

and 4) how these changes will vary across the lifespan.

2. Methods

2.1 Hindlimb Unloading

Mice were single-housed and suspended by their tails at approximately 30-degree head-down angle so that their hindlimbs could not touch the cage floor [48]. Tail suspension fixtures were attached to a swivel and slider on a bar across the top of the cage, allowing them to reach the entire cage, with access to food (Chow # 2918, Teklad Global, West Lafayette, Indiana, USA), water, and bedding. The vivarium was held at a thermoneutral temperature of 90º F.

2.2 Bisphosphonate Treatment:

Alendronate sodium trihydrate, 97% (Thermo Scientific, Waltham, MA), was administered at a dose of 1.0 mg/kg body weight in phosphate-buffered saline (PBS) subcutaneously biweekly [253] starting 7 days before the beginning of HLU. PBS was administered to control groups at a dose of 0.1 mL subcutaneously biweekly starting on day 7 [253].

2.3 Micro-Computed Tomography (μCT) Analysis of Bone Microstructure

Femurs were collected and placed in 4% paraformaldehyde on a rocker for 3 days at 4°C. The PFA was discarded, and the femurs were stored in 70% EtOH until scanning. Femurs were scanned using micro-computed tomography (SCANCO μCT 35, Brüttisellen, Switzerland) with a 6 μm nominal voxel size. Trabecular bone was analyzed in the distal femoral metaphysis, and cortical bone was examined at the femoral diaphysis.

2.4 Muscle Contractile Force Measurements

Mice were anesthetized prior to euthanasia, and maximum muscle contractile force was measured via electrical stimulation of the tibialis anterior and gastrocnemius via a 305C-LR dual-mode muscle lever and footplate system [254]. After euthanasia, the tibialis anterior, triceps surae (gastrocnemius, plantaris, and soleus muscles) were removed and weighed.

2.5 Muscle Fiber Type Analysis

The triceps surae were pinned to cork at fixed length, and flash-frozen in LN_2-cooled isopentane (2-methylbutane) before being stored at -80°C [255]. They were then sectioned into 8-micron sections via cryotome and stored at -20°C. Immunohistology (IHC) staining was performed to differentiate between Type I, IIa, and IIb fiber types. Briefly: Tissue sections were blocked with MOM and NGS in PBST. The following Sant Cruz Biotechnology (Santa Cruz, CA, USA) antibodies were used: IgG2B (blue, 350λ, type I), IgG1 (red, 555λ, type IIa), IgM (green, 488λ, type IIb), and RB 647λ (laminin). Changes in muscle fiber size and type were quantified using immunohistochemistry and analyzed using SMASH software [256].

2.6 Myostatin (GDF-8) and TGF-β1 Analysis

Immediately before euthanasia, mice were anesthetized, and 0.5-1 ml of blood was collected via cardiac puncture. Tibialis anterior and triceps surae muscles were collected and flash-frozen after dissection. Tissues were powdered and used to create supernatant samples. Muscle supernatant samples were analyzed via enzyme linked immunosorbent assay (ELISA) for myostatin (GDF-8) following the manufacturer's guidelines: Myostatin ELISA on Muscle supernatant (GDF8/Myostatin Quantikine ELISA kit, Cat #DGDF80, R&D Systems, Minneapolis, MN, USA) Serum samples were also analyzed via ELISA for circulating TGF-β following the manufacturer's guidelines: (Human/Mouse/Rat/Porcine/Canine TGF-β1 Quantikine ELISA kit, Cat #DB100C, R&D Systems, Minneapolis, MN, USA)

2.7 Tendon Mechanical Properties

Tendons were removed during dissection, and the mechanical and material properties (load-deformation and stress-strain curves, maximal tensile load) were quantified using a custom tensile testing apparatus as previously described [257, 258]. Briefly: The Width and thickness of each tendon were determined with spectral-domain optical coherence tomography (OCT) using an OQ Labscope (Lumedica, Durham, NC). Cross-sectional area was calculated by measuring the width and thickness at the narrowest point and assuming the tendons have a rectangular shape. Tendons were stretched to failure using a Model 68SC-1 single-column tensile tester with a BioPuls Body Temperature Bath and BioPuls Submersible Pneumatic Side Action Grips (Instron, Norwood, MA) with a 100-Newton (N) load cell. During testing, tissues were submerged in 0.9% saline at 37°C. Grip tension was held at 80 lb./in^2 (56245.57 kg/m^2). The mechanical testing protocol

included 10 preconditioning cycles (0.10-0.25 N) at a rate of 0.25 mm/s before loading to failure at a constant rate of 0.25 mm/s until the force dropped 80% from the maximum.

2.8 Statistical Analysis

Statistical analysis was performed with a 3-way analysis of variance (ANOVA) stratified by age (3, 12, or 20 months old), treatment (saline or bisphosphonate), and loading condition (loaded or unloaded). Post hoc analysis was performed using Tukey's Honest Significant Difference (HSD) test. All statistical tests were performed using Prism 10.4.1 for Mac (Graphpad Software, San Diego, CA). Statistically significant differences were identified at $p<0.05$; some non-significant trends were noted at $p \leq 0.10$.

3. Results

Age impacts skeletal response to unloading and bisphosphonate treatment.

Bone mass maintenance during hindlimb unloading (HLU) was facilitated by alendronate treatment, which we have previously shown can maintain bone during unloading in young and old mice [259]. MicroCT analysis of cortical and trabecular bone of the femur demonstrates changes in skeletal response to unloading and alendronate treatment. Unloading (HLU) reduced bone morphology in 3-month-old mice groups, but not in 12-month-old mice. 20-month-old mice exhibited a reduced response to HLU. The selected alendronate dose successfully maintained bone volume lost during HLU in young animals and increased bone in middle-aged and old groups during HLU (Figs. 1 & 2). Several bone microarchitecture factors changed across the lifespan, including reduced metaphyseal bone volume, bone volume fraction (BV/TV), and trabecular number (TB.N). Cortical bone volume fraction (BA/TA) also decreased. Trabecular thickness (Tb.Th) and trabecular separation (Tb.Sp) increased with age (Fig. 2.1B, 2.2B). Age altered the effect of HLU and alendronate treatment in trabecular bone, but not cortical bone (Fig.2. 2 B-D).

3.1 MicroCT Analysis

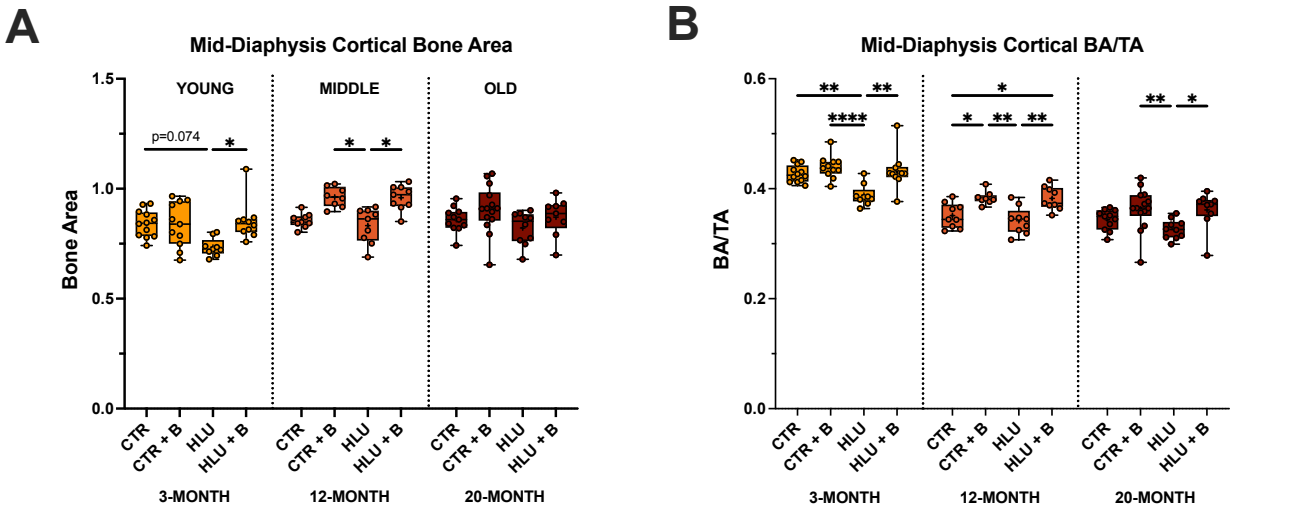

Source of Variation	% of total variation	P value	P value summary
Age	14.29	<0.0001	****
HLU	16.21	<0.0001	****
Bisphosphonate Treatment	2.970	0.0245	*
Age x HLU	2.601	0.1073	ns
Age x Bisphosphonate Treatment	0.5271	0.6314	ns
HLU x Bisphosphonate Treatment	1.693	0.0878	ns
Age x HLU x Bisphosphonate Treatment	2.160	0.1556	ns

Source of Variation	% of total variation	P value	P value summary
Age	52.64	<0.0001	****
HLU	1.988	0.0076	**
Bisphosphonate Treatment	11.89	<0.0001	****
Age x HLU	0.7255	0.2642	ns
Age x Bisphosphonate Treatment	0.1994	0.6913	ns
HLU x Bisphosphonate Treatment	1.110	0.0447	*
Age x HLU x Bisphosphonate Treatment	0.3246	0.5490	ns

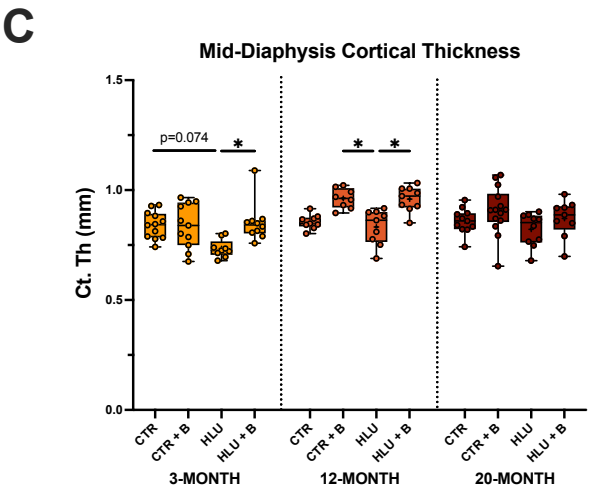

Source of Variation	% of total variation	P value	P value summary
Age	7.247	0.0067	**
HLU	2.049	0.0880	ns
Bisphosphonate Treatment	11.92	<0.0001	****
Age x HLU	0.06683	0.9528	ns
Age x Bisphosphonate Treatment	2.651	0.1519	ns
HLU x Bisphosphonate Treatment	1.314	0.1708	ns
Age x HLU x Bisphosphonate Treatment	0.5325	0.6813	ns

*Figure 2.1. µCT analysis of cortical bone at the femoral mid-diaphysis during hindlimb unloading (HLU) and bisphosphonate (alendronate) treatment (+B) in 3-,12-, and 20-month-old mice. Cortical bone microarchitecture: A) bone area (BA); B) bone volume fraction (BA/TA); C) cortical thickness (Ct.Th). Significance values of 3-way ANOVA with Tukey's post-hoc analysis: * p-value < 0.05, ** p-value <0.01, *** p-value < 0.001, **** p-value < 0.0001.*

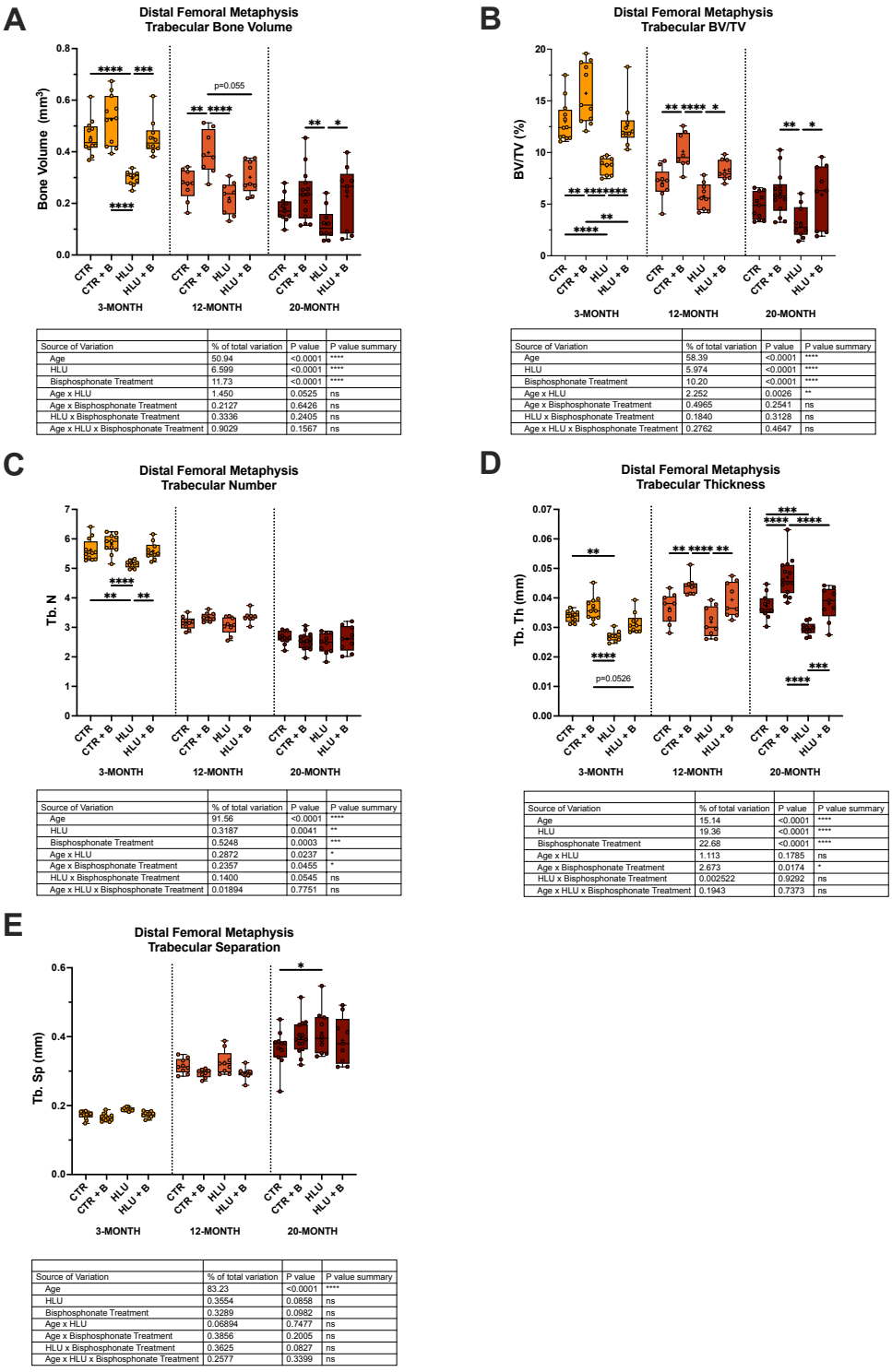

Source of Variation	% of total variation	P value	P value summary
Age	50.94	<0.0001	****
HLU	6.599	<0.0001	****
Bisphosphonate Treatment	11.73	<0.0001	****
Age x HLU	1.450	0.0525	ns
Age x Bisphosphonate Treatment	0.2127	0.6426	ns
HLU x Bisphosphonate Treatment	0.3336	0.2405	ns
Age x HLU x Bisphosphonate Treatment	0.9029	0.1567	ns

Source of Variation	% of total variation	P value	P value summary
Age	58.39	<0.0001	****
HLU	5.974	<0.0001	****
Bisphosphonate Treatment	10.20	<0.0001	****
Age x HLU	2.252	0.0026	**
Age x Bisphosphonate Treatment	0.4965	0.2541	ns
HLU x Bisphosphonate Treatment	0.1840	0.3128	ns
Age x HLU x Bisphosphonate Treatment	0.2762	0.4647	ns

Source of Variation	% of total variation	P value	P value summary
Age	91.56	<0.0001	****
HLU	0.3187	0.0041	**
Bisphosphonate Treatment	0.5248	0.0003	***
Age x HLU	0.2872	0.0237	*
Age x Bisphosphonate Treatment	0.2357	0.0455	*
HLU x Bisphosphonate Treatment	0.1400	0.0545	ns
Age x HLU x Bisphosphonate Treatment	0.01894	0.7751	ns

Source of Variation	% of total variation	P value	P value summary
Age	15.14	<0.0001	****
HLU	19.36	<0.0001	****
Bisphosphonate Treatment	22.68	<0.0001	****
Age x HLU	1.113	0.1785	ns
Age x Bisphosphonate Treatment	2.673	0.0174	*
HLU x Bisphosphonate Treatment	0.002522	0.9292	ns
Age x HLU x Bisphosphonate Treatment	0.1943	0.7373	ns

Source of Variation	% of total variation	P value	P value summary
Age	83.23	<0.0001	****
HLU	0.3554	0.0858	ns
Bisphosphonate Treatment	0.3289	0.0982	ns
Age x HLU	0.06894	0.7477	ns
Age x Bisphosphonate Treatment	0.3856	0.2005	ns
HLU x Bisphosphonate Treatment	0.3625	0.0827	ns
Age x HLU x Bisphosphonate Treatment	0.2577	0.3399	ns

*Figure 2.2. µCT analysis of trabecular bone af the distal femoral metaphysis during hindlimb unloading (HLU) and bisphosphonate (alendronate) treatment (+B) in 3-,12-, and 20-month-old mice. Trabecular bone microarchitecture: A) bone volume (BV); B) bone volume fraction (BV/TV); C) trabecular number (Tb.N); D) trabecular thickness (Tb.Th); E) Trabecular Separation (Tb.Sp). Significance values of 3-way ANOVA with Tukey's post-hoc analysis: * p-value < 0.05, ** p-value <0.01, *** p-value < 0.001, **** p-value < 0.0001.*

Table 2.1. Bone Microstructure Values: Means & St.Devs

			3 months		12 months		20 months	
			mean	stdev	mean	stdev	mean	stdev
Metaphysis	BV	CONTROL	0.456933	0.068006	0.272578	0.059133	0.1797	0.051758
		+B	0.524645	0.097382	0.396813	0.084937	0.233657	0.098818
		HLU	0.297367	0.027676	0.220722	0.06085	0.11934	0.061537
		HLU+B	0.45402	0.067735	0.301011	0.062096	0.228078	0.122553
	BV/TV	CONTROL	0.130067	0.019929	0.070344	0.015243	0.048373	0.012741
		+B	0.1573	0.028736	0.100913	0.017511	0.060007	0.020837
		HLU	0.08688	0.008323	0.057611	0.012979	0.03213	0.015452
		HLU+B	0.12586	0.022386	0.082722	0.009748	0.059022	0.030027
	Tb.N	CONTROL	5.447233	0.804305	3.045933	0.380816	2.69497	0.166052
		+B	5.561091	0.854983	3.290725	0.28058	2.524908	0.294958
		HLU	4.933144	0.701028	2.992389	0.343322	2.450367	0.360867
		HLU+B	5.37028	0.779875	3.276767	0.309264	2.613888	0.458979
	Tb.Th	CONTROL	0.03365	0.0018	0.036489	0.005002	0.037264	0.004093
		+B	0.036482	0.004008	0.044113	0.003304	0.04695	0.006411
		HLU	0.026967	0.001797	0.031833	0.005045	0.02958	0.002121
		HLU+B	0.03154	0.003461	0.039356	0.005781	0.038056	0.00571
	Tb.Sp	CONTROL	0.172817	0.011325	0.314844	0.021447	0.366827	0.052651
		+B	0.1656	0.010801	0.293663	0.012576	0.39695	0.049949
		HLU	0.189589	0.00528	0.325789	0.034149	0.4113	0.064154
		HLU+B	0.1735	0.008766	0.293222	0.017122	0.389133	0.06759
Diaphysis	BV	CONTROL	0.840545	0.061475	0.854929	0.032636	0.859379	0.057415
		+B	0.733976	0.040884	0.832347	0.079463	0.82152	0.074586
		HLU	0.836839	0.101433	0.962279	0.045663	0.906209	0.108222
		HLU+B	0.85239	0.089987	0.958973	0.057044	0.870654	0.08484
	BV/TV	CONTROL	0.427206	0.015275	0.351071	0.022543	0.343604	0.018927
		+B	0.439104	0.020695	0.383353	0.012015	0.363154	0.037892
		HLU	0.388119	0.019269	0.341947	0.02478	0.326241	0.017753
		HLU+B	0.432425	0.03408	0.382362	0.021141	0.36134	0.034237
	Ct.Th	CONTROL	0.164583	0.008436	0.151889	0.009226	0.153545	0.009202
		+B	0.169	0.013015	0.171875	0.004673	0.155214	0.034154
		HLU	0.150111	0.006112	0.146667	0.012894	0.1441	0.008491
		HLU+B	0.1702	0.014876	0.168667	0.0085	0.154	0.030566

3.2 Muscle Analysis

Bone response to alendronate treatment does not result in muscle mass maintenance.

Alendronate was administered to mice undergoing hindlimb unloading (HLU) to determine whether bone maintenance impacts muscle mass maintenance possibly by bone-muscle crosstalk through cytokines. Body weight, muscle mass, and hindlimb force production were compared to assess muscle atrophy in response to unloading and treatment. Body weight was reduced in HLU animals with and without alendronate treatment compared to controls (Fig. 2.3A). Muscle atrophy of the Triceps surae and Tibialis anterior muscles was apparent in all age groups (Fig. 2.3C & E). 12-month-old mice were the only age group that demonstrated no changes in the weight of tibialis anterior muscles between loaded controls and HLU groups. Maximum hindlimb force production was normalized to body weight, Triceps surae weight, and tibialis anterior weight to investigate possible changes in muscle function. 20-month-old mice had increased normalized force production after HLU with and without treatment, while 3-month and 12-month mice demonstrated no noticeable changes (Fig. 2.3C, D, F). To explain changes in force production across the lifespan, immunohistochemistry was performed to quantify type I, IIa, and IIx fibers in gastrocnemius and soleus muscles.

Age, HLU, and bisphosphonate treatment modified the average fiber type sizes in the soleus and gastrocnemius muscles.

Age reduced the percentage of type I fibers in the soleus muscle (Fig. 2.4). However, soleus type I fiber size (cross-sectional area, CSA) increased with bisphosphonate treatment ($p<0.0001$) and decreased with unloading ($p=0.005$). Age impacted the response to bisphosphonate treatment

(p=0.027), with 12-month-old mice being less affected by these changes than 3-month-old and 20-month-old mice. Conversely, type I fibers in the gastrocnemius were reduced by bisphosphonate treatment (p=0.035) and unloading (p=0.002). Gastrocnemius type IIa fibers were also impacted by age (p=0.016) and unloading (p<0.0001), but not by bisphosphonate treatment. 3- and 20-month-old mice had significantly reduced gastrocnemius type IIa CSA between control mice and HLU bisphosphonate-treated mice.

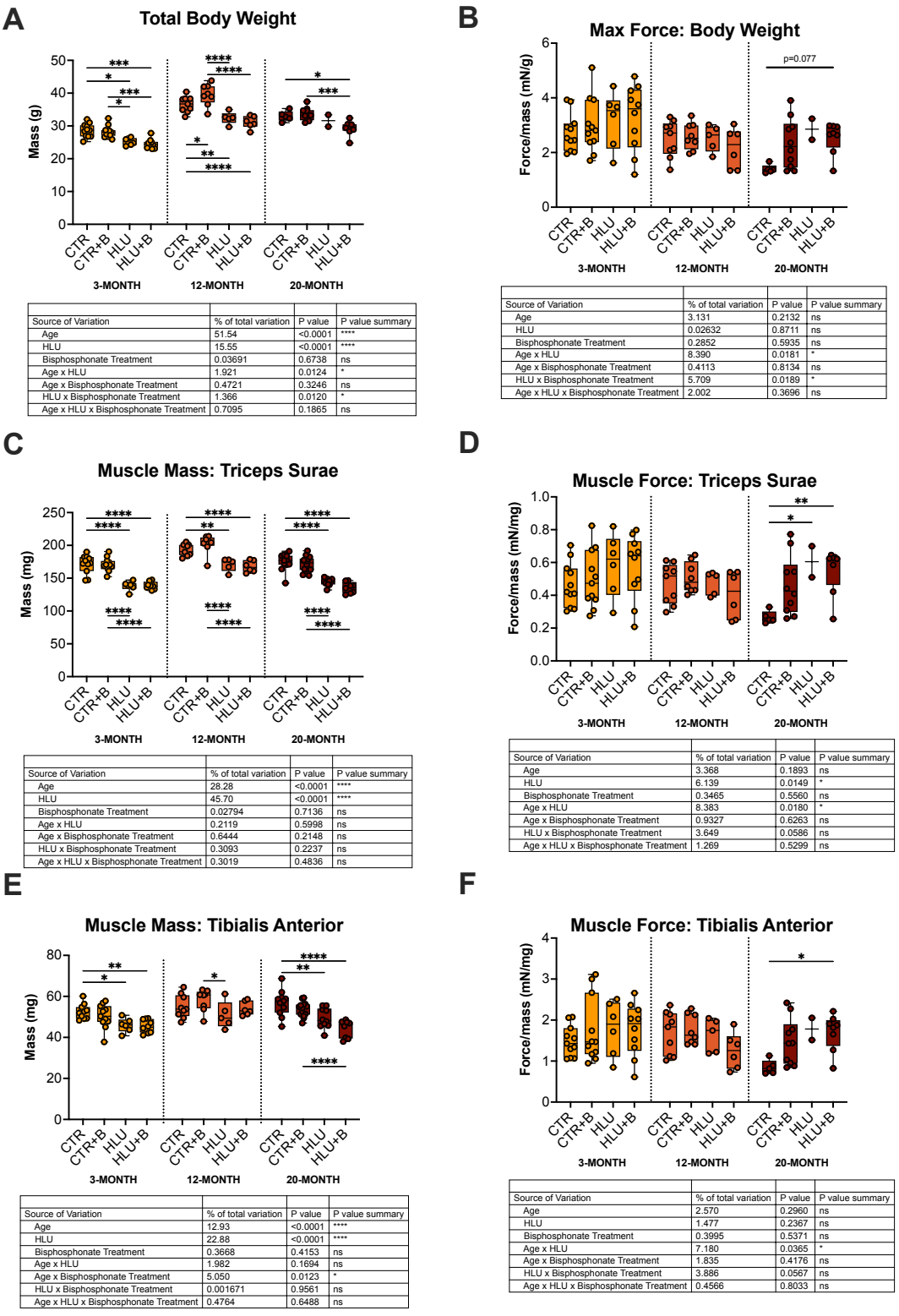

Source of Variation	% of total variation	P value	P value summary
Age	51.54	<0.0001	****
HLU	15.55	<0.0001	****
Bisphosphonate Treatment	0.03691	0.6738	ns
Age x HLU	1.921	0.0124	*
Age x Bisphosphonate Treatment	0.4721	0.3246	ns
HLU x Bisphosphonate Treatment	1.366	0.0120	*
Age x HLU x Bisphosphonate Treatment	0.7095	0.1865	ns

Source of Variation	% of total variation	P value	P value summary
Age	3.131	0.2132	ns
HLU	0.02632	0.8711	ns
Bisphosphonate Treatment	0.2852	0.5935	ns
Age x HLU	8.390	0.0181	*
Age x Bisphosphonate Treatment	0.4113	0.8134	ns
HLU x Bisphosphonate Treatment	5.709	0.0189	*
Age x HLU x Bisphosphonate Treatment	2.002	0.3696	ns

Source of Variation	% of total variation	P value	P value summary
Age	28.28	<0.0001	****
HLU	45.70	<0.0001	****
Bisphosphonate Treatment	0.02794	0.7136	ns
Age x HLU	0.2119	0.5998	ns
Age x Bisphosphonate Treatment	0.6444	0.2148	ns
HLU x Bisphosphonate Treatment	0.3093	0.2237	ns
Age x HLU x Bisphosphonate Treatment	0.3019	0.4836	ns

Source of Variation	% of total variation	P value	P value summary
Age	3.368	0.1893	ns
HLU	6.139	0.0149	*
Bisphosphonate Treatment	0.3465	0.5560	ns
Age x HLU	8.383	0.0180	*
Age x Bisphosphonate Treatment	0.9327	0.6263	ns
HLU x Bisphosphonate Treatment	3.649	0.0586	ns
Age x HLU x Bisphosphonate Treatment	1.269	0.5299	ns

Source of Variation	% of total variation	P value	P value summary
Age	12.93	<0.0001	****
HLU	22.88	<0.0001	****
Bisphosphonate Treatment	0.3668	0.4153	ns
Age x HLU	1.982	0.1694	ns
Age x Bisphosphonate Treatment	5.050	0.0123	*
HLU x Bisphosphonate Treatment	0.001671	0.9561	ns
Age x HLU x Bisphosphonate Treatment	0.4764	0.6488	ns

Source of Variation	% of total variation	P value	P value summary
Age	2.570	0.2960	ns
HLU	1.477	0.2367	ns
Bisphosphonate Treatment	0.3995	0.5371	ns
Age x HLU	7.180	0.0365	*
Age x Bisphosphonate Treatment	1.835	0.4176	ns
HLU x Bisphosphonate Treatment	3.886	0.0567	ns
Age x HLU x Bisphosphonate Treatment	0.4566	0.8033	ns

*Figure 2.3. Mass and force production of triceps surae and tibialis anterior muscles during hindlimb unloading (HLU) and bisphosphonate (alendronate) treatment (+B) in 3-,12-, and 20-month-old mice. A) mouse body weight; B) max force normalized to body weight; C triceps surae mass; D) muscle max force normalized to triceps surae mass; E) Tibialis anterior mass; F) muscle max force normalized to tibialis anterior mass. Significance values of 3-way ANOVA with Tukey's post-hoc analysis: * p-value < 0.05, ** p-value <0.01, *** p-value < 0.001, **** p-value < 0.0001.*

Table 2.2. Muscle Means and St.Devs

			3 months		12 months		20 months	
			mean	stdev	mean	stdev	mean	stdev
Weights	Body weight	CONTROL	28.6273	2.0567	36.5667	2.4182	32.9800	1.5865
		+B	28.2455	1.8124	39.4875	3.2804	33.5700	1.9488
		HLU	25.2667	1.1272	32.4200	1.8833	31.6000	2.5456
		HLU+B	24.5100	1.4587	31.1167	1.9041	29.3000	2.1902
	TS weight	CONTROL	171.1455	14.1262	192.9444	8.7045	174.5182	13.2665
		+B	170.8364	10.4474	201.7000	14.3212	171.4643	11.5765
		HLU	138.0333	7.1469	170.6200	9.7968	143.9500	5.5806
		HLU+B	139.1100	5.3524	167.8167	8.9123	135.6500	8.3022
	TS:body (%)	CONTROL	5.9464	0.4637	5.2430	0.4046	5.3437	0.4150
		+B	5.9652	0.5538	5.1629	0.4616	5.0613	0.2377
		HLU	5.3615	0.3411	5.1882	0.5255	5.0067	N/A
		HLU+B	5.6534	0.3878	5.2273	0.5588	4.7046	0.2820
	TA	CONTROL	52.7091	3.5130	55.0111	5.7093	56.7000	6.2814
		+B	50.3364	5.8138	58.1500	5.3506	53.7500	3.5751
		HLU	45.9000	3.4514	50.8800	6.6556	49.3000	4.9028
		HLU+B	45.3800	3.0767	54.0500	3.3969	44.1500	4.3270
	TA:body (%)	CONTROL	1.8434	0.0772	1.5116	0.2052	1.6698	0.1802
		+B	1.7881	0.2282	1.4760	0.1255	1.5862	0.0855
		HLU	1.8197	0.1578	1.5714	0.2038	1.6269	0.2429
		HLU+B	1.8557	0.1469	1.7404	0.1198	1.5091	0.1286
Hindlimb Force		CONTROL	2.6584	0.7035	2.4375	0.7590	1.4350	0.1615
		+B	2.9038	1.0001	2.5141	0.6350	2.4527	0.8814
		HLU	3.0004	1.0724	2.8005	0.3822	2.4676	#DIV/0!
		HLU+B	3.2107	1.1553	2.1633	0.7356	2.5121	0.6175
	Max force:TS	CONTROL	0.4630	0.1352	0.4714	0.1225	0.2665	0.0380
		+B	0.4978	0.1748	0.5067	0.0932	0.4615	0.1799
		HLU	0.5854	0.1924	0.4762	0.0714	0.6047	0.1340
		HLU+B	0.5710	0.1977	0.4035	0.1437	0.5515	0.1397
	Max force: TA	CONTROL	1.4869	0.3724	1.6839	0.5232	32.5590	77.6691
		+B	1.7476	0.7947	1.7673	0.3676	51.0528	81.6155
		HLU	1.7906	0.6678	1.6327	0.4067	1.7824	0.3809
		HLU+B	1.7608	0.6393	1.2479	0.4403	1.6995	0.4485

A

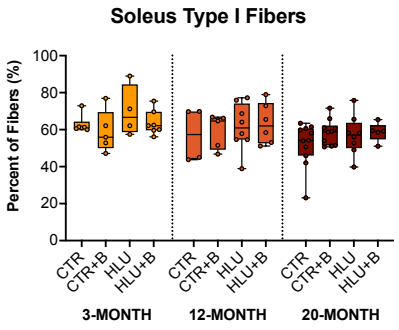

Source of Variation	% of total variation	P value	P value summary	Significant?
Age	8.121	0.0436	*	Yes
HLU	3.817	0.0835	ns	No
Bisphosphonate	0.02126	0.8961	ns	No
Age x HLU	0.4219	0.8435	ns	No
Age x Bisphosphonate	3.244	0.2761	ns	No
HLU x Bisphosphonate	0.3023	0.6226	ns	No
Age x HLU x Bisphosphonate	0.1733	0.9324	ns	No

B

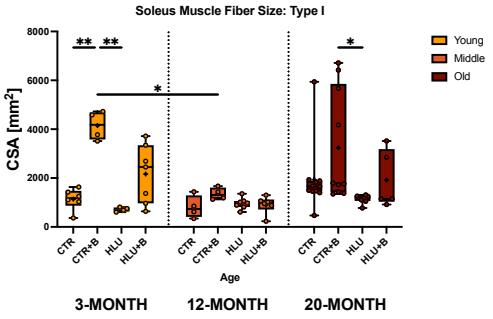

Source of Variation	% of total variation	P value	P value summary
Age	10.14	0.0043	**
HLU	7.124	0.0053	**
Bisphosphonate	15.23	<0.0001	****
Age x HLU	2.196	0.2832	ns
Age x Bisphosphonate	6.520	0.0271	*
HLU x Bisphosphonate	2.229	0.1110	ns
Age x HLU x Bisphosphonate	0.5843	0.7114	ns

C

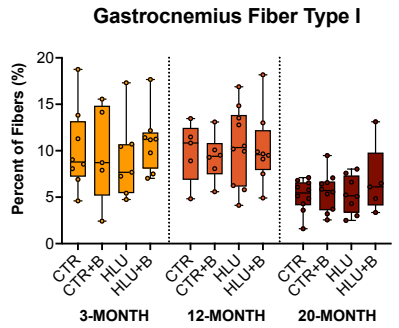

Source of Variation	% of total variation	P value	P value summary	Significant?
Age	26.57	<0.0001	****	Yes
HLU	0.2857	0.5666	ns	No
Bisphosphonate	0.1819	0.6473	ns	No
Age x HLU	0.2334	0.8736	ns	No
Age x Bisphosphonate	0.5261	0.7380	ns	No
HLU x Bisphosphonate	0.7520	0.3533	ns	No
Age x HLU x Bisphosphonate	0.3640	0.8102	ns	No

D

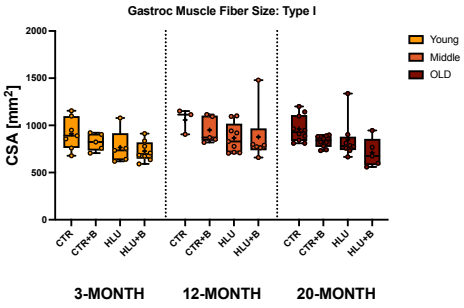

Source of Variation	% of total variation	P value	P value summary
Age	8.292	0.0270	*
HLU	11.49	0.0018	**
Bisphosphonate	5.025	0.0352	*
Age x HLU	0.02440	0.9889	ns
Age x Bisphosphonate	1.142	0.5942	ns
HLU x Bisphosphonate	0.5470	0.4809	ns
Age x HLU x Bisphosphonate	0.4829	0.8017	ns

E

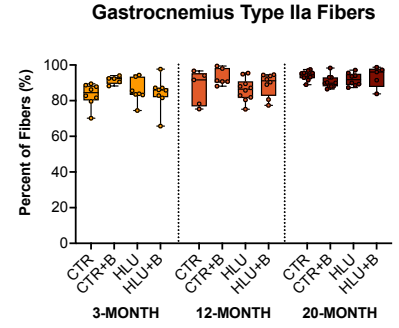

Source of Variation	% of total variation	P value	P value summary	Significant?
Age	14.04	0.0011	**	Yes
HLU	1.637	0.1902	ns	No
Bisphosphonate	2.480	0.1079	ns	No
Age x HLU	1.285	0.5069	ns	No
Age x Bisphosphonate	3.121	0.1959	ns	No
HLU x Bisphosphonate	0.6113	0.4217	ns	No
Age x HLU x Bisphosphonate	4.526	0.0961	ns	No

F

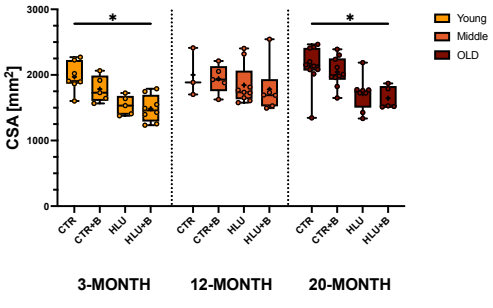

Source of Variation	% of total variation	P value	P value summary
Age	7.458	0.0162	*
HLU	21.47	<0.0001	****
Bisphosphonate	1.648	0.1686	ns
Age x HLU	2.498	0.2377	ns
Age x Bisphosphonate	0.1166	0.9339	ns
HLU x Bisphosphonate	0.1395	0.6869	ns
Age x HLU x Bisphosphonate	0.2104	0.8839	ns

*Figure 2.4. Muscle fiber types and sizes during hindlimb unloading (HLU) and bisphosphonate (alendronate) treatment (+B) in 3-,12-, and 20-month-old mice. Muscle fiber type and cross-sectional area (CSA): A-B) soleus type I; C-D) gastrocnemius type I; E-F) gastrocnemius type IIa. Significance values of 3-way ANOVA with Tukey's post-hoc analysis: * p-value < 0.05, ** p-value <0.01, *** p-value < 0.001, **** p-value < 0.0001.*

3.3 ELISA Analysis

The explored cytokines are not wholly responsible for the muscle response to mechanical unloading.

Bone-muscle crosstalk has been suggested as a driver of bone and muscle health. Circulating concentrations of TGF-β1 and muscle concentrations of myostatin were quantified via Enzyme-Linked Immunosorbent Assay (ELISA) to explore the connection between these tissues. Myostatin concentrations of the Triceps surae increased with alendronate treatment in 3-month-old unloaded mice (HLU vs HLU+B) but not within other age groups (Fig. 2.5). However, overall, unloading, alendronate treatment, and the interaction of unloading and treatment increased myostatin concentrations. 20-month-old mice had lower concentrations of myostatin than 12-month-old mice. Age exhibited no interaction effects with HLU or alendronate treatment. Serum TGF-β1 concentrations increased with age and unloading, though unloading results from old mice may skew this relationship (Fig. 2.6). Only 20-month-old mice exhibited within-groups changes due to unloading and alendronate treatment. HLU increased TGF-β1 concentrations in this age group, and alendronate treatment reduced the concentration. Age interacted with both HLU and alendronate treatment to increase circulating TGF-β1 concentrations.

3.3.1 Muscle Myostatin

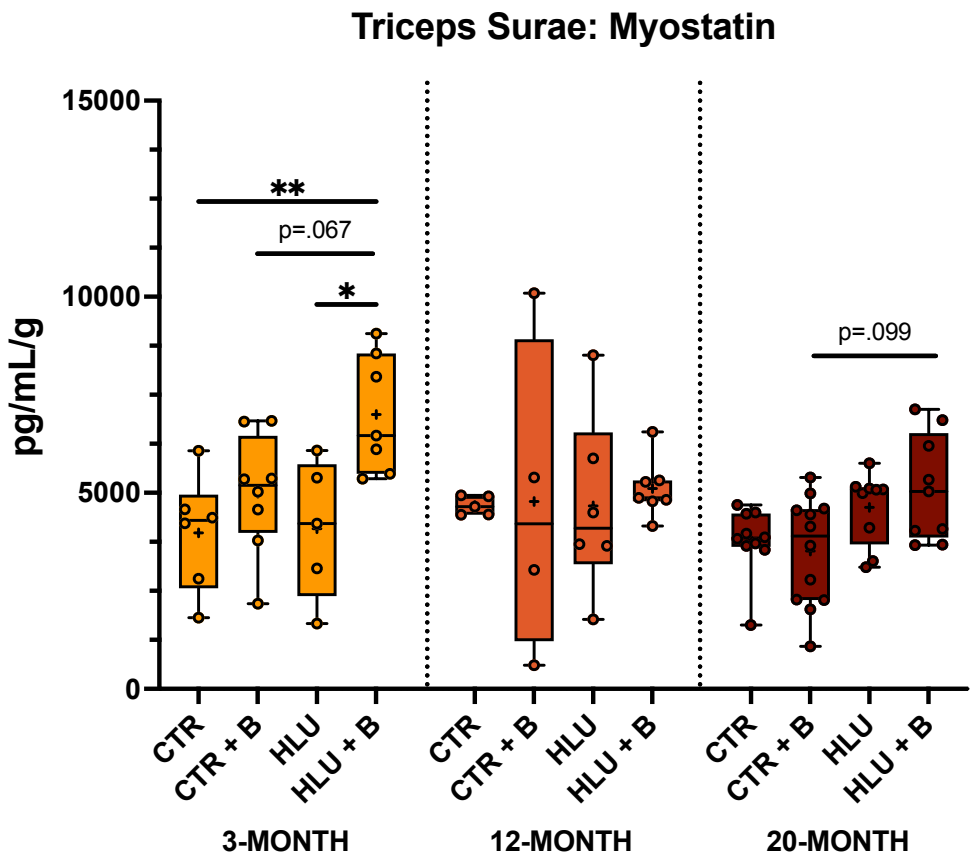

Source of Variation	% of total variation	P value	P value summary
Age	5.737	0.0400	*
(Loaded vs Unloaded)	8.693	0.0021	**
(Saline vs Bisphosphonate)	8.251	0.0027	**
Age x (Loaded vs Unloaded)	0.03767	0.9782	ns
Age x (Saline vs Bisphosphonate)	4.649	0.0722	ns
(Loaded vs Unloaded) x (Saline vs Bisphosphonate)	4.541	0.0239	*
Age x (Loaded vs Unloaded) x (Saline vs Bisphosphonate)	0.7781	0.6356	ns

*Figure 2.5. ELISA analysis of triceps surae myostatin concentration during hindlimb unloading (HLU) and bisphosphonate (alendronate) treatment (+B) in 3-,12-, and 20-month-old mice. Significance values of 3-way ANOVA with Tukey's post-hoc analysis: * p-value < 0.05, ** p-value <0.01, *** p-value < 0.001, **** p-value < 0.0001.*

3.3.2 TGF-β in Serum

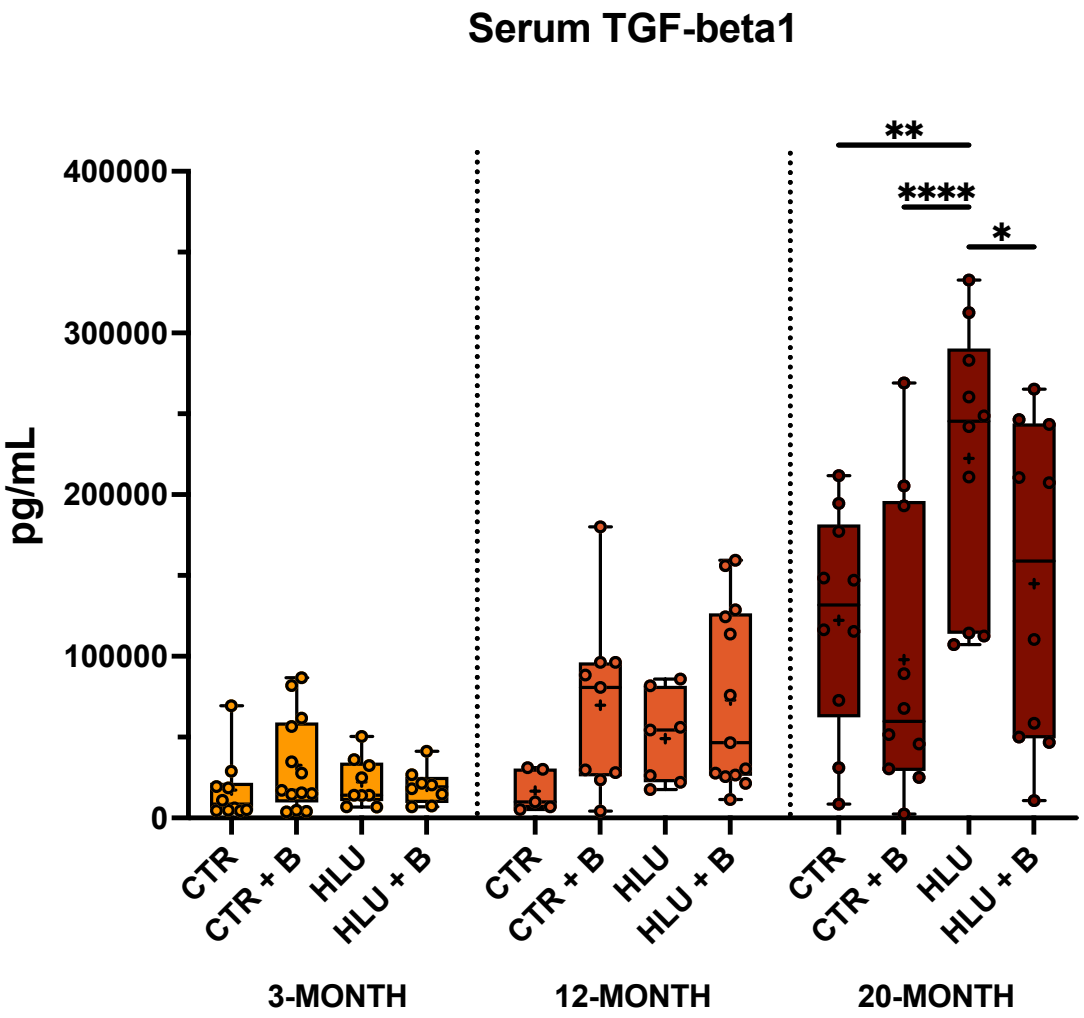

Source of Variation	% of total variation	P value	P value summary
Age	42.33	<0.0001	****
(Loaded vs Unloaded)	2.946	0.0116	*
(Saline vs Bisphosphonate)	0.01441	0.8577	ns
Age x (Loaded vs Unloaded)	4.055	0.0128	*
Age x (Saline vs Bisphosphonate)	4.736	0.0064	**
(Loaded vs Unloaded) x (Saline vs Bisphosphonate)	0.9727	0.1427	ns
Age x (Loaded vs Unloaded) x (Saline vs Bisphosphonate)	0.2061	0.7940	ns

*Figure 2.6. ELISA analysis of serum TGF-β1 concentration during hindlimb unloading (HLU) and bisphosphonate (alendronate) treatment (+B) in 3-,12-, and 20-month-old mice. Significance values of 3-way ANOVA with Tukey's post-hoc analysis: * p-value < 0.05, ** p-value <0.01, *** p-value < 0.001, **** p-value < 0.0001.*

3.4 Tendon Analysis

Tendon mechanical responses to unloading are most pronounced in older mice.

Achilles tendons were mechanically tested to determine mechanical adaptations to unloading and alendronate treatment. Force at MTL was increased in 12-month-old mice undergoing alendronate treatment in both loaded and unloaded conditions (Fig. 2.7A). Achilles tendons of 20-month-old mice had higher Young's Modulus with alendronate treatment during HLU compared to control loaded and control HLU animals (Fig. 2.7B). Similarly, tensile stress at failure was reduced by alendronate treatment during HLU (Fig. 2.7C). Age and the interactions of Age and alendronate treatment significantly impacted these tendon mechanical properties.

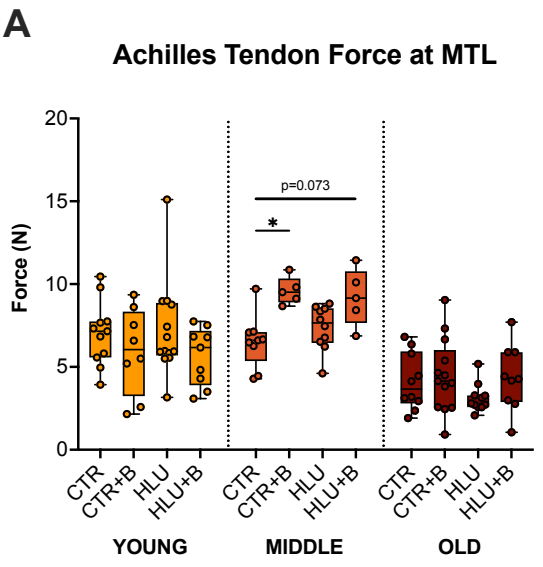

Source of Variation	% of total variation	P value	P value summary
Age	40.55	<0.0001	****
HLU	0.04026	0.7820	ns
Bisphosphonate Treatment	1.341	0.1125	ns
Age x HLU	0.4052	0.6798	ns
Age x Bisphosphonate Treatment	7.763	0.0010	***
HLU x Bisphosphonate Treatment	0.09107	0.6773	ns
Age x HLU x Bisphosphonate Treatment	0.7359	0.4972	ns

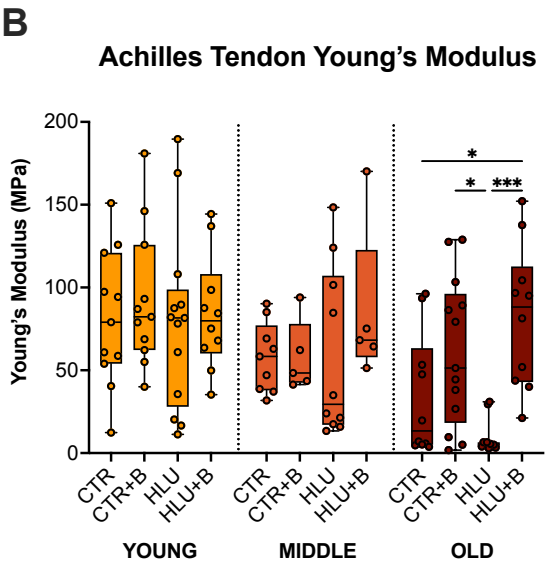

Source of Variation	% of total variation	P value	P value summary
Age	13.05	0.0001	***
HLU	0.07476	0.7403	ns
Bisphosphonate Treatment	6.425	0.0026	**
Age x HLU	0.6861	0.6040	ns
Age x Bisphosphonate Treatment	4.479	0.0404	*
HLU x Bisphosphonate Treatment	1.380	0.1564	ns
Age x HLU x Bisphosphonate Treatment	1.581	0.3152	ns

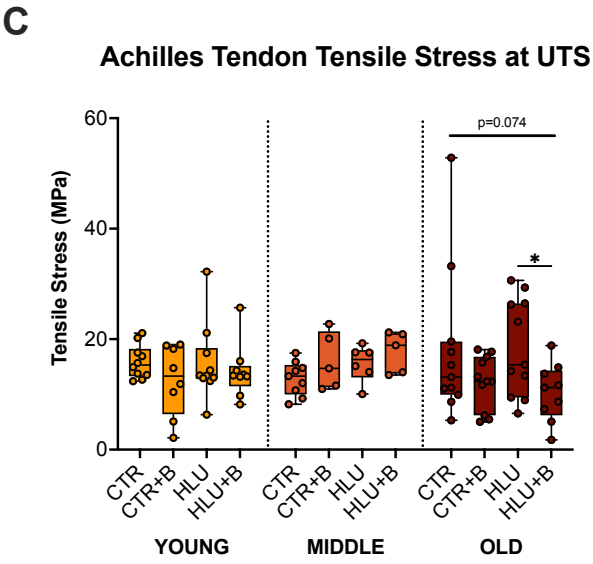

Source of Variation	% of total variation	P value	P value summary
Age	0.2929	0.8566	ns
HLU	0.2602	0.6010	ns
Bisphosphonate Treatment	2.403	0.1142	ns
Age x HLU	0.6296	0.7175	ns
Age x Bisphosphonate Treatment	6.951	0.0291	*
HLU x Bisphosphonate Treatment	0.03609	0.8455	ns
Age x HLU x Bisphosphonate Treatment	0.4387	0.7933	ns

*Figure 2.7. Mechanical testing of Achilles tendon after hindlimb unloading (HLU) and bisphosphonate (alendronate) treatment (+B) in 3-,12-, and 20-month-old mice. Achilles tendon mechanical properties: A) force at maximal tensile load; B) Young's Modulus; C) tensile stress at ultimate tensile strength. Significance values of 3-way ANOVA with Tukey's post-hoc analysis: * p-value < 0.05, ** p-value <0.01, *** p-value < 0.001, **** p-value < 0.0001.*

4. Discussion

In this study, we investigated differences in bone, muscle, and tendon responses to mechanical unloading with bisphosphonate use in young, middle-aged, and old mice. In contrast to our hypothesis, muscle mass was not maintained with the use of bisphosphonates as a bone mass-maintenance treatment. We did, however, observe changes in musculoskeletal adaptation across the lifespan and in important crosstalk-related cytokine concentrations.

Bone

Our results were partially consistent with our previous studies of systemic bone loss following hindlimb unloading in male mice [260]. The trabecular bone loss in young and old mice was consistent, with estimated reductions in metaphyseal trabecular bone between 30 and 45%. We noted a decrease in trabecular BV/TV between control and unloaded mice in young (-33.2%) and old (-33.6%), though the loss was not statistically significant in old animals. However, middle-aged mice had a less pronounced reduction in BV/TV than expected (-18.1%). We observed less loss of cortical bone (BV/TV) than previously observed (10-15%)[260], with a further reduction in decrease for middle-aged mice (young: -9.1%, middle-aged: -2.6%, old: -5.1%). We noted similar changes to cortical thickness (young: -8.9%, middle-aged: -3.4 %, old: -6.2%). The differences between bone loss in middle-aged and young and old mice demonstrate an interesting resistance to unloading in middle-aged and older animals compared to their young counterparts. This is consistent with rat models, where older animals also demonstrate reduced response to unloading (e.g., nonsignificant loss) in trabecular bone during unloading compared to young animals[244, 261]. This underscores the importance of utilizing different age groups in unloading research with future clinical applications in mind.

Muscle

Whole body weight loss during HLU was consistent with the literature of young and old mice [262] (young: -14.4%, middle-aged: -14.9%, old: -11.2%). However, our young and old mice lost significantly more triceps surae muscle mass than reported by other researchers (10.6% gastric and soleus, [262] young: -19.3%, middle-aged: -11.6%, old: -17.5%). Loss of tibialis anterior mass was more consistent with (young: -12.9%, middle-aged: -7.5%, old: -13.1%).

Muscle force production was significantly lower than observed in the literature, but activation methods differed (tibial nerve excitation [262] vs gastrocnemius excitation). Our contractile force measurements demonstrated a loss of muscle force production of plantar flexor muscles in young mice, but no change in middle-aged mice and an increase in force production in old mice (young: -26.4%, middle-aged: +1%, old: +26.9%). However, several cohorts of our mice could not be tested due to equipment availability, so these old mice results are incomplete, as only an n=2 is available for the old HLU mice group. The percentage of soleus Type I fibers decreased with age, but the size of fibers increased. In the gastrocnemius, type I and type IIa fibers were reduced with age and unloading but not with alendronate treatment. This reduction in fiber type size does not explain the increase in muscle force production in the triceps surae in older mice. An additional mechanism must be at play, such as increased specific force or an increase in type IIb fibers.

Bone-Muscle Crosstalk: Myostatin

Myostatin concentrations did not support that bone mass maintenance influences muscle volume. In young mice, myostatin concentrations increased with alendronate treatment during unloading, indicating increased muscle resorption during bone mass maintenance. No changes in myostatin concentration with unloading or treatment were apparent in middle-aged or old animals except for

a trend with alendronate treatment in older animals undergoing unloading (Fig. 2.6). However, the interaction of age, loading, and alendronate treatment were all visible, as well as the interactions of with unloading and alendronate treatment. The reduction of myostatin across the lifespan is consistent with the literature[263]. However, we did not see a decrease in muscle mass, and our results are based on the muscle unit used for analysis, not serum concentration, so the claim that a reduction of muscle causes a loss of circulating myostatin does not directly apply to this observation.

Bone-Muscle Crosstalk: TGF-β1

Observed TGF-β1 bone-muscle crosstalk was age-dependent. Our study does not support the implication that increased circulating TGF-β1 concentration caused by bone resorption impacts muscle growth in young and middle-aged mice. While unloading was implicated as an important main effect in increased circulating TGF-β1 concentrations (Fig. 2.6), alendronate treatment did not reduce circulating TGF-β1 in these age groups. However, a possible connection was found in older mice, where hindlimb unloading increased circulating TGF-β, and alendronate treatment significantly reduced it. These results corroborate the main effects identified by ANOVA. Muscle atrophy did not align with the levels of circulating TGF-β1. These results do not support the current consensus in the literature that TGF-β1 is an important bone-to-muscle crosstalk agent [94, 101, 264, 265]. It is possible that TGF-β1 release from bone plays a role in muscle atrophy, with the greatest effect seen in old animals.

Future Investigations

Several other cytokines and forms of bone-mass maintenance could be investigated. RANKL, osteocalcin, BAIBA, and IL6, 7, and 15 all have the potential to modulate atrophy in bone and

muscle tissue[94, 95, 102, 105, 107, 109, 110, 131, 266, 267]. Additionally, alendronate treatment could mask normal crosstalk channels due to the reported effects on muscle[268] . Alendronate may upregulate SIRT3 expression in muscle, which can also inhibit myostatin production, leading to muscle mass maintenance [269]. Whether myostatin inhibition influences bone-muscle crosstalk should also be determined. However, we found that alendronate increases muscle myostatin concentration overall while decreasing muscle fiber size in the gastrocnemius. There was an increase in type I muscle fiber size in the soleus with treatment, so the selective impact of this treatment could also be investigated.

5. Conclusion

This study used young, middle-aged, and old mice treated with alendronate to identify key differences in musculoskeletal adaptation to unloading across the lifespan. Notably, we identified that alendronate treatment contributes to reduced body and muscle mass across the lifespan. The potential crosstalk osteokine TGF-β was an effective indicator of bone loss in old animals, but not young or middle-aged animals. Further, TGF-β did not correlate with muscle loss caused by alendronate treatment.

Acknowledgements

This research was supported by the NIH NIAMS (R01 AR071459). Sophie V Orr was supported by a NIAMS funded training program in Musculoskeletal Health Research (T32 AR079099). Natalie Kori Gilmore was supported by the UC Davis T32 in Pharmacology (T32 GM144303).

Chapter 3: Semaglutide Treatment During Mechanical Unloading & Reloading

Abstract

Semaglutide, A GLP-1 receptor agonist, is being prescribed to a growing number of patients for the treatment of type 2 diabetes and for weight loss. This weight loss may also result in bone and muscle loss due to reduced load bearing and insufficient nutrition. Periods of mechanical unloading (disuse) also lead to bone and muscle tissue atrophy, but it is unclear if unloading and Semaglutide treatment have a synergistic effect that would exacerbate bone and muscle loss. We hypothesized that Semaglutide would exacerbate the loss of bone and muscle mass with unloading due to confounding factors of weight loss and disuse. We also hypothesized that Semaglutide would diminish bone and muscle recovery during reloading. Female C57BL/6J mice (14 weeks, n=40) were surgically implanted with Alzet osmotic pumps 14 days prior to unloading. The pumps delivered either Semaglutide in 0.9% saline at a rate of 10mg/kg/day (n=20) or 0.9% saline (n=20). All mice were unloaded for 14 days via a single-limb cast on their left hindlimb. After 14 days, n=20 mice were euthanized (n=10 vehicle and n=10 Semaglutide), and the remaining mice had their casts removed and were reloaded via regular cage activity for 14 days. Body composition and femur bone mineral content were measured weekly via dual x-ray absorptiometry (DEXA). Mice were fed standard chow, and their food intake and body weight were monitored biweekly. After euthanasia, gastrocnemius and Soleus muscles were dissected out and weighed. Femurs were imaged with micro-computed tomography (μCT 35, SCANCO Medical AG) with a 6 μm nominal voxel size; cortical bone was analyzed at the mid-diaphysis, and trabecular bone was examined at the distal femur to determine bone microstructural outcomes. Serum samples were analyzed via ELISA for circulating bone formation marker PINP and bone resorption marker CTX-1 concentrations. Bulk RNAseq was performed on the unloaded legs' proximal tibias and soleus muscles to identify differentially expressed genes. Gene Ontology analysis was conducted on significantly differentially expressed genes to identify biological pathways being altered

by Semaglutide treatment. 14 days of unloading did not cause different magnitudes of bone loss between treatment groups. Serum CTX-1 concentrations were significantly increased in Semaglutide-treated animals (but not vehicle-treated animals) after 14 days of unloading. Serum PINP concentrations were not modified in either group. During unloading, Semaglutide-treated mice lost significantly more leg muscle mass in their unloaded leg (gastrocnemius, plantaris, soleus) compared to their loaded leg. Comparatively, vehicle-treated mice only lost significant mass from the gastrocnemius. Semaglutide-treated mice did not lose weight or reduce chow consumption compared to the vehicle-treated groups. Therefore, muscle and bone loss cannot be attributed to weight loss-related factors. Differentially expressed genes in the tibia include downregulation of Zbtb16, a gene that counteracts osteoporosis. Gene Ontology analysis identified several key biological pathways that Semaglutide treatment affects, including bone and skeletal system development. Understanding the impact of this medication on musculoskeletal tissue will help clarify the treatment of patients who require periods of unloading while using Ozempic, Wegovy, and other GLP-1 receptor agonists to prevent adverse side effects and secondary morbidity of these medications.

1. Introduction

Semaglutide, initially prescribed as the effective type 2 diabetes mellitus (T2D) medication Ozempic®, has become popular due to its prominent weight loss effects. Branded as Wegovy® for weight loss, Semaglutide and other glucagon-like peptide-1 receptor agonists (GLP-1RAs) work by increasing insulin secretion, slowing gastric emptying, and reducing cravings. These medications have also been reported to directly and indirectly (e.g., through weight loss) reduce the severity of cardiovascular disease [218-221, 270], kidney disease [218, 220, 222, 223], osteoarthritis [224, 225, 271], and even substance abuse [272-274]. Impacts on musculoskeletal tissues have also been investigated, though clinical implications are less conclusive than *in vitro* and *in vivo* murine study results [206, 207, 275-278].

GLP-1RAs have been shown to have direct and indirect effects on bone and muscle. Clinical studies have shown both positive and negative impacts of GLP-1RA usage. GLP-1 is secreted from endothelial L-cells of the intestine during digestion to modulate blood glucose levels[279] through the GLP-1 receptor, which is active on several musculoskeletal cell types. Unlike GLP-1, which has a half-life of 1-7 minutes[156], these analogs can remain active for up to 168 hours (1 week) due to their designed resistance to the enzyme dipeptidyl-peptidase IV (DPP-4), which breaks down excess GLP-1[156, 157]. Semaglutide has the highest half-life, with other well-studied examples, such as liraglutide and exendin-4, having half-lives of only 13 hours and 2.4 hours, respectively[157]. The exponential increase of biological availability compared to GLP-1 and other GLP-1RAs is likely biologically relevant. For example, a clinical trial of liraglutide used with associated weight loss prevented bone mineral content loss and increased bone formation

markers[206]. However, other studies have suggested that Semaglutide treatment increases bone resorption markers in patients at risk of fracture [207].

In human patients, decoupling the direct effects of Semaglutide treatment from the secondary weight loss-related effects on musculoskeletal tissue is difficult. While GLP-1s may positively impact bone growth, rapid weight loss causes a reduction in bone quality and quantity[173, 280-283], especially in older adults [281-283]. The loss of even 5-10% of body mass results in substantial bone loss [171, 172]. Higher weight protects against osteoporosis and fractures due to higher bone mineral density (BMD) and bone mineral content (BMC)[284, 285]. Additionally, muscle volume and strength can be reduced due to weight loss[286-288]. Given that Ozempic was FDA-approved for T2D treatment in 2017 and Wegovy was approved for weight loss treatment in 2021, the long-term impacts of Semaglutide-induced weight, bone, and muscle loss are yet to be discovered.

Periods of unloading, such as during bed rest or immobilization, also leads to muscle and bone loss through reductions in mechanical stimuli [238, 239]. Preventing this loss in at-risk populations, such as patients with T2D, older adults, or those undergoing rapid weight loss due to GLP-1RA usage, could be of extreme clinical importance. However, the interaction between Semaglutide and clinically relevant periods of unloading has not yet been addressed. This study aims to identify additive effects of Semaglutide treatment and related weight loss on bone and muscle atrophy and recovery during periods of mechanical unloading and subsequent reloading. We hypothesize that unloading will cause increased bone and muscle loss in animals treated with Semaglutide. Additionally, we hypothesize that this treatment will negatively affect bone and

muscle recovery during subsequent reloading due to weight loss. The study aims to determine the effects of unloading and Semaglutide on:

1) bone, muscle, and tendon morphology and mechanics;

2) whole body composition and bone mineral density (BMD);

and 3) bone and muscle gene expression.

2. Methods

2.1 Animals & experimental design:

Female mice (C57BL/6J, n=40) were purchased from Jackson Laboratory (Sacramento, CA). Mice were obtained at 14 weeks of age and allowed to acclimate to the vivarium for 14 days before surgery. Alzet pumps were surgically inserted, and the mice were given 14 days post-operative to recover. Mice were randomly assigned to one of four groups (n=10 per group): Unloaded Control, Unloaded Treated, Reloaded Control, Reloaded Treated. Treatment groups (2, n=20) received Semaglutide, while control groups (2, n=20) received a vehicle solution. Next, mice were unloaded via single hindlimb casting for 14 days. After 14 days of unlaoding, the Unloaded condition mice (UL, n=20) were euthanized, and the remaining Reloaded condition mice (RL, n=20) were unloaded by removal of the cast. RL mice resumed normal cage movement for 14 days, after which they were euthanized. Standard chow was available *ad libitum* (chow # 2918, Teklad Global, West Lafayette, Indiana, USA), All animals were maintained and used in accordance with National Institutes of Health guidelines on the care and use of laboratory animals. All procedures were approved by the UC Davis Institutional Animal Care and Use Committee.

2.2 Semaglutide Treatment

Alzet osmotic pumps (Model 2006, ALZET, Cupertino, CA, US) were loaded with Semaglutide (CAS:910463-68-2, Adipogen Life Sciences, San Diego, CA, US) in a vehicle (5% AcOH in 0.9% Sterile Saline Solution, USP (VetOne, Paris, France)). Treated mice were dosed with 10 nmol/kg/day of Semaglutide in the vehicle solution. Control mouse pumps contained only the vehicle solution. Pumps were surgically inserted subcutaneously, per manufacturer instructions, under aseptic conditions . Briefly, animals were anesthetized, and the fur was removed from their backs. An incision in the skin was made near the lumbar spine, and a sterile surgical tool was used to elongate the subcutaneous space to accommodate the pump. The pumps were then inserted, and the incision site was sutured closed. 3-days of post-op care was administered, including twice daily buprenorphine injections and wound site and condition monitoring. Any remaining sutures were removed 7 days post-operatively.

2.3 Casting

Fourteen days after Alzet pump insertion, mice had a cast placed on their left hind limb as previously described[289]. Briefly, the hindlimb was shaved and loosely taped with medical tape to restrict knee and ankle joint movement without restricting blood flow. A 1.5 mL Eppendorf tube was applied over the leg and secured with additional medical tape. The tube was modified by removing the cap and cutting a large hole in the conical section to ensure proper airflow. Casts were monitored daily to ensure fit and reapplied as necessary.

2.4 Muscle and Body Mass

Mouse body weights and average chow consumption per cage were measured biweekly. Mice were cohoused with 3 or 4 animals per cage. Chow consumption was then averaged among animals in each cage for analysis. Therefore, mouse treatment groups were separated during housing. After euthanasia, gastrocnemius, plantaris, soleus, and tibialis anterior muscles were dissected and weighed before being flash-frozen and stored at -80°C.

2.5 Dual-energy X-ray absorptiometry (DEXA)

Mice were scanned weekly to track body composition, BMD, and BMC longitudinally. Mice were anesthetized and scanned at 40kV/1000uA on a Kubtec PARAMETER^{TM} 3-D Cabinet X-ray System (Kubtec Scientific, Stratford, CT, US). BMD and BMC data were collected for femur midshafts and lumbar spine. Whole body composition (lean tissue percentage and fatty tissue percentage) was also collected.

2.6 Micro-Computed Tomography (μCT) Analysis of Bone Microstructure:

Femurs were collected and placed in 4% paraformaldehyde (PFA) on a rocker for 3 days at 4°C, after which the femurs were stored in 70% EtOH until scanning. Femurs were scanned using micro-computed tomography (SCANCO μCT 35, Brüttisellen, Switzerland) with a 6 μm nominal voxel size. Trabecular bone was analyzed in the distal femoral metaphysis and epiphysis, and cortical bone was examined at the femoral diaphysis. After μCT, bones were returned to 70% EtOH and stored at 4°C.

2.7 Mechanical Properties Testing: 3-Point Bending

Femurs were rehydrated in PBS for at least 5 minutes in preparation for 3-point bending. The center of the rehydrated femurs was measured and marked with a permanent marker. Femurs were placed condyle size down in a 3-point bending apparatus with an 8mm span, with the center mark lined up with the force-applying point of the apparatus. Stiffness, yield_displacement, yield_load, post-yield displacement, fracture displacement, fracture load, max load, work-to-yield, and work-to-fracture were calculated based on existing literature[290]. Young's modulus was calculated with the addition of μCT results as $E=KL^3/(48\ I_{min})$ [290].

2.8 Serum PINP and CTX-1 Analysis

Immediately prior to euthanasia, mice were anesthetized, and 0.5-1 ml of blood was collected via cardiac puncture and allowed to coagulate. Serum was separated via centrifuge, and these samples were analyzed via enzyme-linked immunosorbent assay (ELISA) for PINP and CTX-1 following the manufacturer's guidelines: Rat/Mouse PINP EIA ELISA kit (Cat# AC-33F1, Immunodiagnostic Systems Limited, East Boldon, UK). And RatLaps™ ELISA (CTX-I) kit (Cat# AC-06F, Immunodiagnostic Systems Limited, East Boldon, UK).

2.9 Tendon mechanical analysis

Achilles tendons were removed during dissection, and the mechanical properties (stress-strain curves, maximal tensile load) were quantified as previously described [257, 258]. Briefly, the width and thickness of each tendon were determined with spectral-domain optical coherence tomography (OCT) using an OQ Labscope (Lumedica, Durham, NC). Cross-sectional area was

calculated by measuring the width and thickness at the narrowest point and assuming the tendons have a rectangular shape. Tendons were stretched to failure using a Model 68SC-1 single-column tensile tester with a BioPuls Body Temperature Bath and BioPuls Submersible Pneumatic Side Action Grips (Instron, Norwood, MA) with a 100-Newton (N) load cell. During testing, tissues were submerged in 0.9% saline at 37°C. Grip tension was held at 80 lb./in^2 (56245.57 kg/m^2). The mechanical testing protocol included 10 preconditioning cycles (0.10-0.25 N) at a rate of 0.25 mm/s before loading to failure at a constant rate of 0.25 mm/s until the force dropped 80% from the maximum.

2.10 Bulk RNA sequencing

Soleus Muscles were flash-frozen after dissection in liquid nitrogen and stored at -80 °C. Tibias were cut in half and centrifuged to remove bone marrow, then stored in RNAprotect Tissue Reagent (Quiagen, Hilden, Germany) overnight at 4°C before being transferred to -80 °C. Muscle and bone tissues were processed using a Qiagen RNeasy Mini Kit. The RNase-Free DNase Set (Qiagen, Hilden, Germany) was also used to remove DNA components during processing. RNA isolation was performed as described in the product manuals. Briefly, samples were homogenized in Trizol until no chunks were visible. Chloroform was added and the tubes were shaken for 15 seconds, rested for 2 minutes, then centrifuged at 1200 RPM at 4°C. RNA lysate was then carefully collected and run through several filtration steps via the provided kit columns under centrifugation. Final filtered contents were added to 50 mL RNase-free water, and RNA concentration and quality were quantified using the NanoDrop One (Waltham, MA, US).

RNA samples were processed via bulk RNAseq by Novogene (Sacramento, CA, US). Results were aligned to the Mus musculus genome (GRCm39/mm39) with the Spliced Transcripts Alignment to a Reference (STAR) algorithm [291] using RStudio software (Boston, MA, US). Gene expression variance was calculated separately for tibia and soleus samples. Soleus sample counts were normalized to tissue weights. Only tissue from the casted legs of 14-day unloaded mouse samples was analyzed. Data visualization was completed using DeSeq2[292] in RStudio.

Known genes with significant differences in expression (adjusted $p < 0.05$) were run through the Gene Ontology Enrichment Analysis tool utilizing the PANTHER Classification System. Analysis was performed using the following settings:

- Analysis Type: PANTHER Overrepresentation Test (Released 20240807)
- Annotation Version and Release Date: GO Ontology database DOI: 10.5281/zenodo.14861039 Released 2025-02-06
- Reference List: Mus musculus (all genes in database)
- Annotated data sets:
    - GO biological process complete
    - GO cellular component complete
- Test Type: Fisher's Exact
- Correction: Calculate False Discovery Rate (FDR)

2.11 Immunoblotting

Immunoblotting protocol was followed as described previously [293]: Frozen plantaris muscles were powdered and homogenized via vortexer in 200 µL sucrose lysis buffer (SLB; 50 mM Tris pH 7.5, 250 mM sucrose, 1 mM EDTA, 1 mM EGTA, 1% Triton X-100, 1% protease inhibitor complex) for 60 min at 4 °C. Following centrifugation at 10,000 *g* for 10 min, the supernatant was collected. Protein concentrations were determined in triplicate using the DC protein assay (Bio-Rad, Hercules, CA, USA). Sample concentrations were adjusted using SLB. Following dilution in Laemmli sample buffer (LSB), samples were denatured for 5 min at 100 °C. Protein (10–30 µg per lane) was loaded on 4–15% Criterion TGX Stain-free gels (Bio-Rad), run for 45 min at 200 V, and visualized after a UV-induced 1-minute reaction to produce fluorescence.

Following quantification, proteins were transferred to nitrocellulose or polyvinylidene difluoride (PVDF) membrane for 30-60 min at 100 V, depending on the size of the protein of interest. Efficient transfer was confirmed using Ponceau S staining of the membrane. Membranes were then air dried and directly incubated with the primary antibody, or washed and blocked in 1% fish skin gelatin dissolved in Tris-buffered saline with 0.1% Tween-20 (TBST) for 1 hour, rinsed, and then incubated with the primary antibody (1:1000 in TBST) overnight at 4 °C. The next day, membranes were washed and incubated with HRP-conjugated secondary antibodies at 1:5000 (goat) (catalog #31402, Pierce, Rockford, IL) to 1:10 000 (mouse, rabbit) (catalog #7076 and 7074, Cell Signaling Technology, Danvers, MA) in 1% skim milk-TBST for 1 hour at room temperature. Immobilon Western Chemiluminescent HRP substrate (Millipore, Hayward, CA, USA) was then applied to the membranes for protein visualization by chemiluminescence. Image acquisition and band quantification were performed using the ChemiDoc MP System and Image Lab 5.0 software (Bio-

Rad). Protein levels of each sample were calculated as band intensities relative to total protein as described previously [294]. All samples of both groups (i.e., plantaris from cast and contralateral controls) were run on the same gel for each protein probed; images of the bands in the figures are representative, with biological replicates shown for each treatment.

The following antibodies were used in this study at a concentration of 1 to 1000:

- phospho S6 (Proteintech 67898-1-Ig)
- phospho eEF2 (Cell Signaling #2331),
- phospho AMPK (Cell Signaling #2535),
- REDD1 (Proteintech 10638-1-AP),
- MuRF1 (Santa Cruz, sc-398608)
- Phospho P38 (T180) (Cell Signaling #9211)
- Phospho AKT (Proteintech #81232-10-RR)

2.14 Statistical Analysis

Statistically significant differences were identified at $p < 0.05$, and trends were noted at $p \leq 0.10$. All statistical tests (excluding bulk RNA seq data analysis and Gene Ontology analysis) were performed using Prism 10.4.1 for Mac (Graphpad Software, San Diego, CA). Main effects of Semaglutide treatment, unloading, and their interactions were identified where applicable.

For paired analysis, when data from the casted and contralateral leg of the same mouse is available, statistical analysis was performed with 2-way repeated-measure analysis of variance (ANOVA) stratified by treatment (vehicle vs Semaglutide) and loading condition (loading vs unloading).

When data were missing (which prevented ANOVA analysis), a Restricted Maximum Likelihood (REML) analysis was run. Post hoc Tukey's multiple comparisons tests were performed after ANOVA and REML analysis.

For unpaired single-timepoint analysis, such as serum ELISAs, a 2-way ANOVA stratified by treatment (vehicle vs. Semaglutide) and loading condition (loading vs. unloading) was performed. Post hoc analysis was performed using Tukey's Honest Significant Difference (HSD) test.

For non-paired longitudinal analysis, including food consumption and body weight, 2-way repeated measures ANOVA stratified by treatment (vehicle or Semaglutide) and time point (weeks post-pump insertion) with Šídák post hoc test.

Bulk RNA seq statistical analysis was performed as part of either the STAR analysis pipeline on RStudio or the Gene Ontology (GO) analysis using the Gene Ontology Enrichment Analysis tool, utilizing the PANTHER Classification System. Statistically significant differences were identified at adjusted p values (STAR) or False Discovery Rates (FDR, GO) of < 0.05, and trends were noted at $p \leq 0.10$.

3. Results

Body mass, composition, and chow consumption were not changed in Semaglutide-treated mice fed with standard chow during mechanical unloading.

No changes in body weight were observed between the vehicle and Semaglutide-treated groups (Fig.3.1), and no changes in food consumption were observed between groups. Food consumption increased the week after cast removal in both groups. Throughout the study, we used weekly Dual-energy X-ray absorptiometry (DEXA) scans to monitor body composition. Whole-body fat percentage increased during unloading (week 2 to 4, p=0.0077) and decreased after reloading (week 4 to 6, p=0.0161), with an overall reduction in fatty tissue throughout the study (Fig. 3.2). Lean percentage increased during unloading (weeks 2 to 4, p=0.0225) and trended towards an increase overall (week 0 to 6, p=0.067). Neither Whole-body fatty tissue nor lean tissue percentages were affected by Semaglutide treatment.

3.1 Muscle and Body Mass

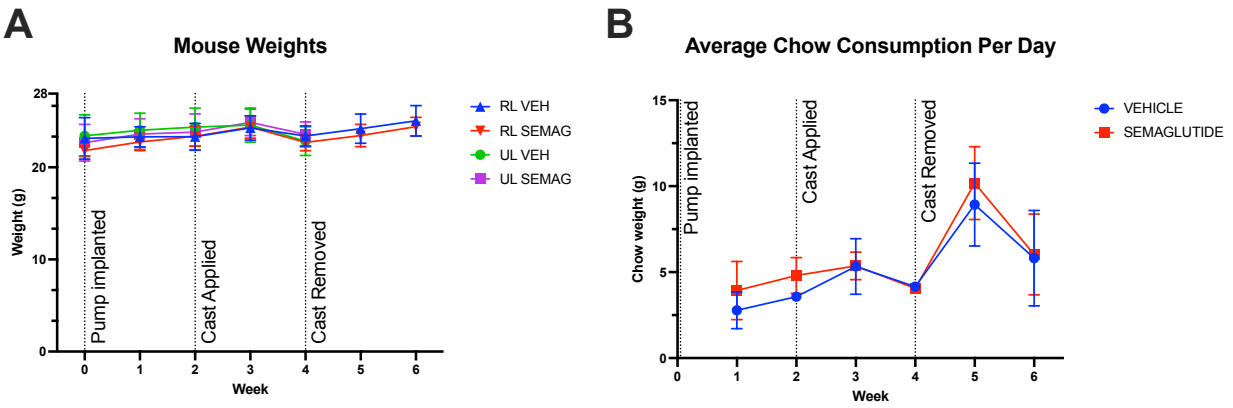

Figure 3.1. Weekly monitoring of mouse body weights and chow consumption during and after single-limb immobilization via cast and Semaglutide treatment in female mice. All body weights (A) include osmotic pump weights; weeks 2 and 3 include cast weights (approx. 1.4g). Chow weights (B) are based on weekly cage consumption divided by the number of animals housed in the cage. No significant differences were observed between control and Semaglutide-treated mice.

3.2 Dual-energy X-ray absorptiometry (DEXA)

A

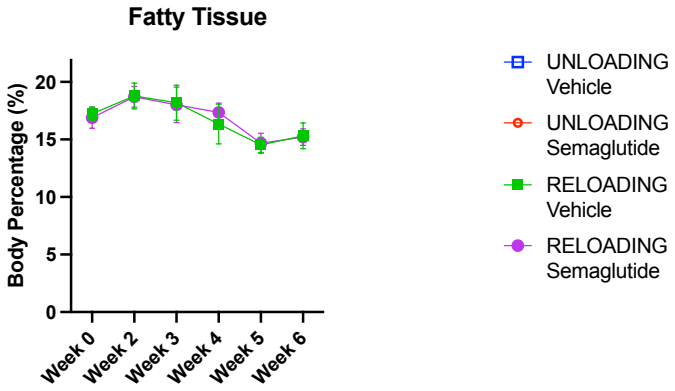

Source of Variation	% of total variation	P value	P value summary
Time x Semaglutide	1.495	0.4653	ns
Time	64.42	<0.0001	****
Semaglutide	0.04685	0.7288	ns

B

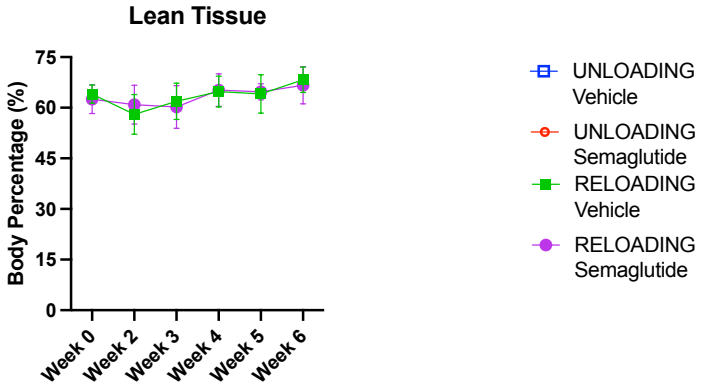

Source of Variation	% of total variation	P value	P value summary
Time x Semaglutide	2.328	0.4928	ns
Time	23.32	<0.0001	****
Semaglutide	0.02179	0.9118	ns

*Figure 3.2. Weekly DEXA Analysis of whole-body tissue composition during and after single-limb immobilization via cast and Semaglutide treatment in female mice. Body percentage of A) fatty tissue and B)lean tissue. Significance values of 2-way ANOVA with Tukey's post-hoc analysis: * p-value < 0.05, ** p-value <0.01, *** p-value < 0.001, **** p-value < 0.0001.*

A

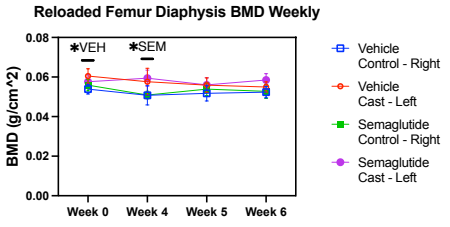

Source of Variation	% of total variation	P value	P value summary	Significant?
Time	5.239	0.0076	**	Yes
Semaglutide	0.9541	0.2172	ns	No
Cast	26.95	<0.0001	****	Yes
Time x Semaglutide	0.8676	0.5181	ns	No
Time x Cast	3.493	0.0313	*	Yes
Semaglutide x Cast	0.07252	0.7310	ns	No
Time x Semaglutide x Cast	2.865	0.0625	ns	No

B

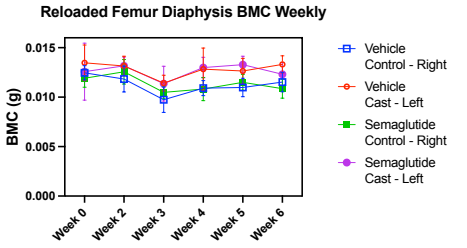

Source of Variation	% of total variation	P value	P value summary	Significant?
Time	15.91	<0.0001	****	Yes
Semaglutide	0.01458	0.8738	ns	No
Cast	19.89	<0.0001	****	Yes
Time x Semaglutide	2.991	0.0265	*	Yes
Time x Cast	1.798	0.1712	ns	No
Semaglutide x Cast	0.2292	0.5301	ns	No
Time x Semaglutide x Cast	0.3740	0.8965	ns	No

C

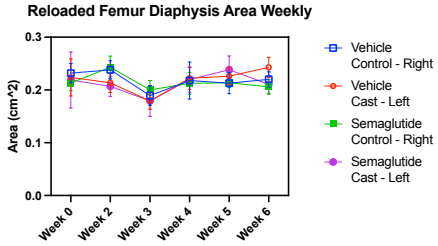

Source of Variation	% of total variation	P value	P value summary
Time	22.31	<0.0001	****
Semaglutide	0.6985	0.2703	ns
Cast	0.06865	0.7275	ns
Time x Semaglutide	3.453	0.0228	*
Time x Cast	9.425	<0.0001	****
Semaglutide x Cast	0.03680	0.7985	ns
Time x Semaglutide x Cast	1.175	0.4722	ns

*Figure 3.3. Weekly DEXA Analysis of femur diaphysis during and after single-limb immobilization via cast and Semaglutide treatment in female mice. Cortical bone A) bone mineral density; B) bone mineral content; and C) bone area. Significance values of 3-way ANOVA with Tukey's post-hoc analysis: * p-value < 0.05, ** p-value <0.01, *** p-value < 0.001, **** p-value < 0.0001.*

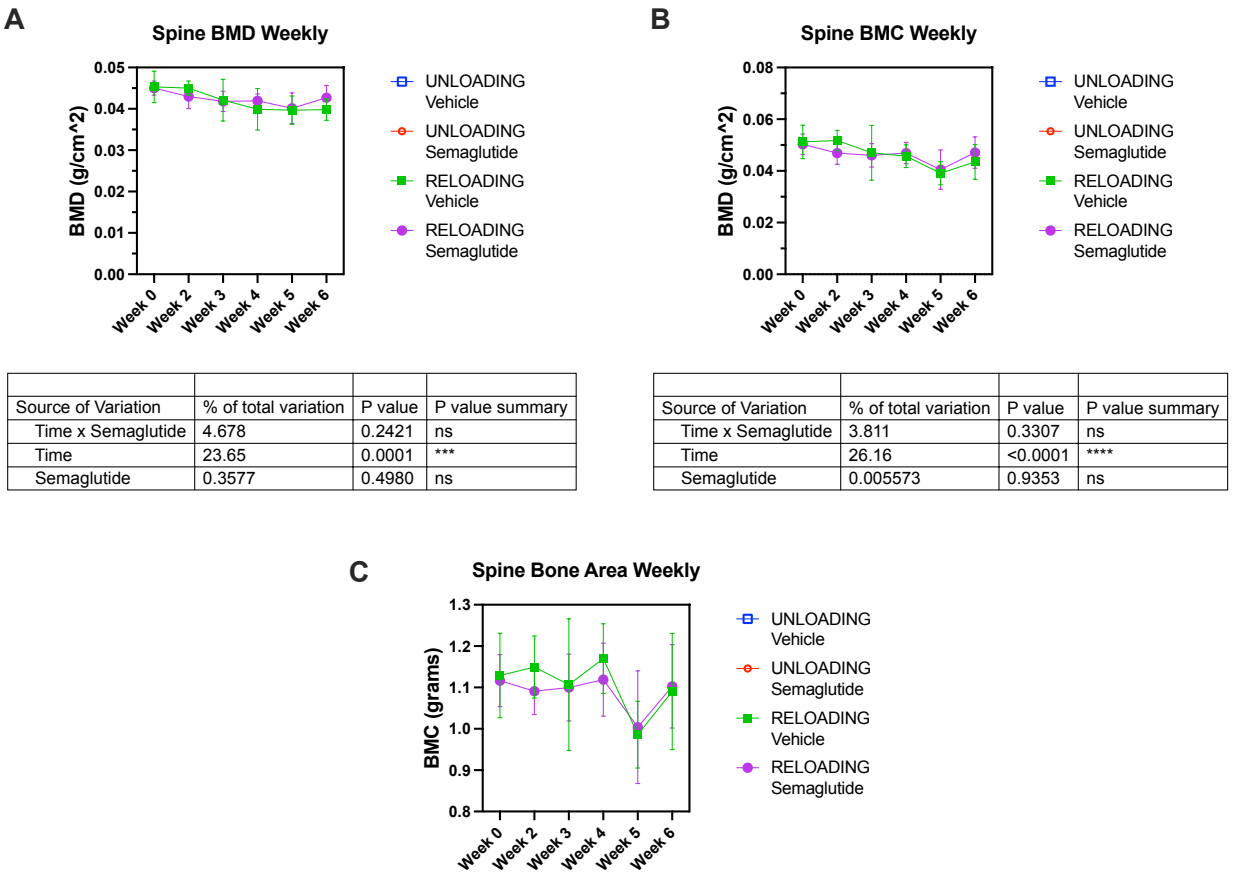

Source of Variation	% of total variation	P value	P value summary
Time x Semaglutide	4.678	0.2421	ns
Time	23.65	0.0001	***
Semaglutide	0.3577	0.4980	ns

Source of Variation	% of total variation	P value	P value summary
Time x Semaglutide	3.811	0.3307	ns
Time	26.16	<0.0001	****
Semaglutide	0.005573	0.9353	ns

Source of Variation	% of total variation	P value	P value summary
Time x Semaglutide	1.738	0.7597	ns
Time	19.07	0.0006	***
Semaglutide	0.5633	0.5129	ns

*Figure 3.4. DEXA analysis of lumbar spine during and after single-limb immobilization via cast and Semaglutide treatment in female mice. Trabecular bone A) bone mineral density (BMD); B) bone mineral content (BMC); and C) bone area. Significance values of 3-way ANOVA with Tukey's post-hoc analysis: * p-value < 0.05, ** p-value <0.01, *** p-value < 0.001, **** p-value < 0.0001.*

3.3 Micro-Computed Tomography (μCT) Analysis of Bone Microstructure

Semaglutide treatment interactions modify bone microstructure during unloading without weight loss.

Semaglutide treatment did not affect lumbar spine bone metrics assessed by DEXA analysis (Fig. 3.4). However, unloading (week 2-4) caused losses in BMD and BMC assessed by DEXA, with possible increases after 14 days of reloading. Casting significantly increased BMD in the femoral diaphysis ($p<0.0001$), but changes were not significant after reloading (Fig. 3.3A). The interaction of week x Semaglutide treatment was evident for femur BMD, BMC, and area.

No changes within or between groups were identified in the cortical bone of the femoral mid-diaphysis (Fig. 3.5). However, the main effect of the interaction between cast x reloading was significant for both Ct.Th ($p=0.0334$) and Ct.Ar/T.Ar (0.0154). A significant interaction of reloading x Semaglutide treatment caused reductions in TMD compared to reloaded controls and unloaded Semaglutide-treated mice.

Trabecular bone was relatively more responsive to casting. Bone changes and main effects were noted in the distal femoral metaphysis(Fig. 3.6). Semaglutide-treated mice had reductions in bone volume fraction(BV/TV, $p=0.023$) and bone mineral density (BMD, $p=0.011$) with casting (Fig. 3.6A, B). BMD was reduced in vehicle-treated mice with casting ($p=0.041$, Fig. 3.6B). No significant changes in trabecular number (Tb.N) or trabecular separation (Tb.Sp) of the metaphysis were identified between groups (Fig. 3.6C, E). Significant reductions in trabecular thickness (Tb.Th) were observed between cast and uncast legs in unloaded groups (vehicle $p=0.008$,

Semaglutide p=0.0008) and reloaded vehicle-treated mice (p=0.004, Fig. 3.6D). Reloading recovered the Tb.Th lost in vehicle-treated mouse limbs (uncast p<0.0001, cast p<0.0001) and cast legs of Semaglutide-treated mice (p<0.0001). Casting significantly reduced all microstructure parameters in the metaphysis and Tb.Th was modified by reloading (p<0.0001), cast x reloading (p=0.042), and Cast x unloading/reloading x Semaglutide (p =0.038).

Trabecular bone responses and main effects were most visible in the distal femoral epiphysis (Fig.3.7). Casting caused significant loss in BV/TV, BMD, Tb.N, Tb.Th, and an increase in Tb.Sp. Reloading recovered this loss in all cases except for Tb.N and Tb.Sp. Legs that had been casted showed significant increases in BV/TV, BMD, and Tb.Th with reloading compared to uncasted limbs. The interaction of Semaglutide with reloading increased both leg BMD values compared to mice that had only undergone unloading (p=0.042). No other changes linked to Semaglutide were present in the distal epiphysis.

No significant changes were noted between groups in mechanical testing (Figs. 3.8 & 3.9). However, main effects and/or trends were noted for casting and Semaglutide treatment. Casting increased post-yield displacement, fracture displacement, fracture load, and work to fracture. Semaglutide reduced yield load and max load and trended towards decreasing yield-displacement and fracture load. An increase in fracture displacement due to all three variables is also possible (p=0.098). elastic modulus, yield stress, and ultimate stress were not affected by casting, reloading, or Semaglutide treatment (Fig. 3.9).

Circulating concentrations of bone homeostasis markers were quantified in serum using ELISAs. The serum concentration of bone formation marker PINP did not increase compared to vehicle controls in unloaded or reloaded conditions (Fig. 3.10A). However, when both unloading and reloading groups were assesed together, the main effect of Semaglutide treatment ($p=0.025$) and trending effects of loading condition ($p=0.0834$) were observed. In contrast, the bone resorption marker CTX-1 concentrations were elevated in unloaded mice treated with Semaglutide ($p=0.022$) but not in reloaded mice (Fig. 3.10B). The main effect of Semaglutide treatment ($p=0.021$) and trending effects of unloading/reloading ($p=0.075$) and Semaglutide x reloading interaction ($p=0.070$) were observed.

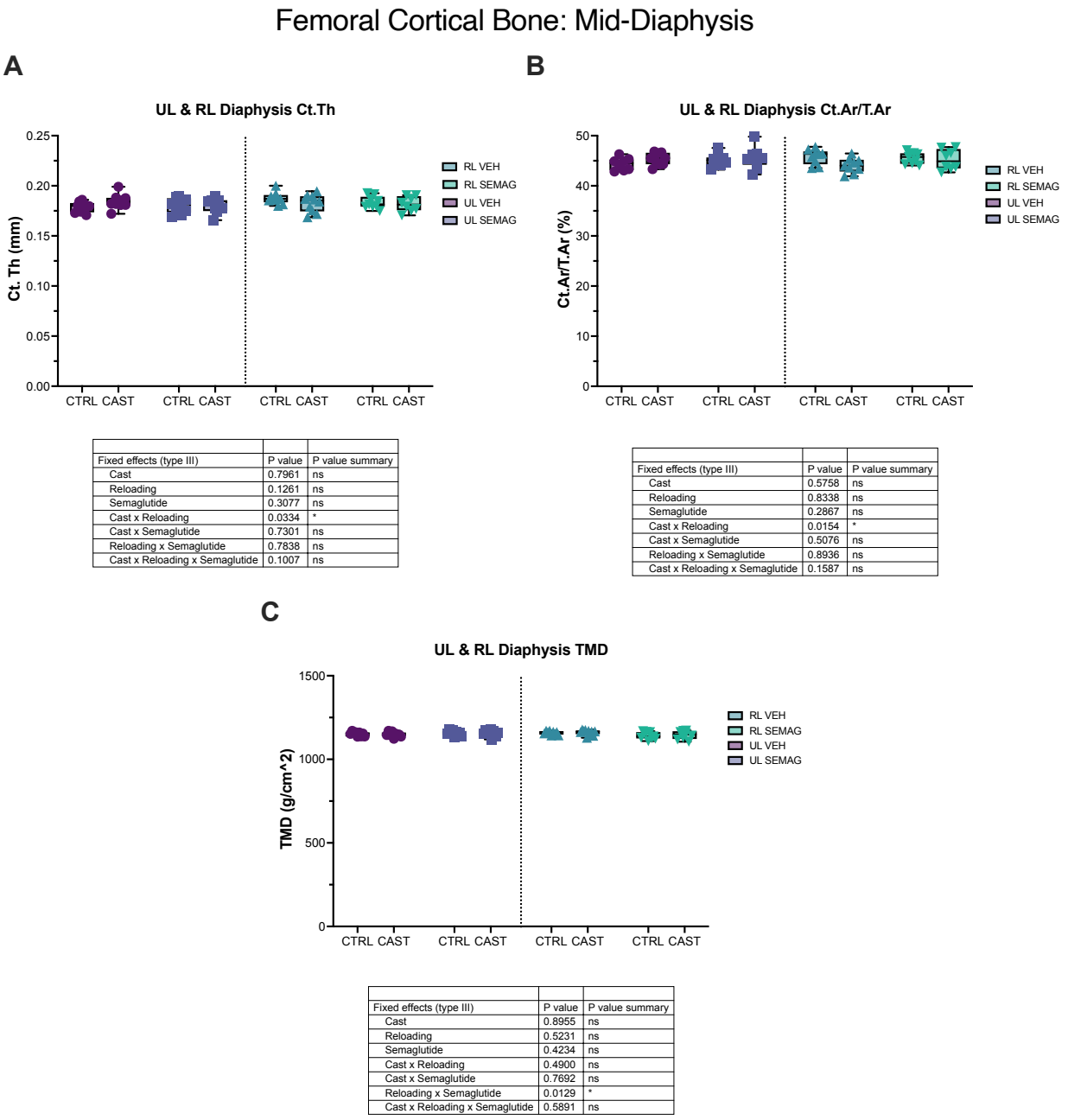

Fixed effects (type III)	P value	P value summary
Cast	0.7961	ns
Reloading	0.1261	ns
Semaglutide	0.3077	ns
Cast x Reloading	0.0334	*
Cast x Semaglutide	0.7301	ns
Reloading x Semaglutide	0.7838	ns
Cast x Reloading x Semaglutide	0.1007	ns

Fixed effects (type III)	P value	P value summary
Cast	0.5758	ns
Reloading	0.8338	ns
Semaglutide	0.2867	ns
Cast x Reloading	0.0154	*
Cast x Semaglutide	0.5076	ns
Reloading x Semaglutide	0.8936	ns
Cast x Reloading x Semaglutide	0.1587	ns

Fixed effects (type III)	P value	P value summary
Cast	0.8955	ns
Reloading	0.5231	ns
Semaglutide	0.4234	ns
Cast x Reloading	0.4900	ns
Cast x Semaglutide	0.7692	ns
Reloading x Semaglutide	0.0129	*
Cast x Reloading x Semaglutide	0.5891	ns

*Figure 3.5. µCT analysis of cortical bone at the femoral mid-diaphysis during single-limb immobilization via cast and Semaglutide treatment in female mice. Cortical bone microarchitecture: A) cortical thickness (Ct.Th); B) bone volume fraction (Ct.Ar/T.Ar); C) Tissue mineral density. Significance values of 3-way ANOVA with Tukey's post-hoc analysis: * p-value < 0.05, ** p-value <0.01, *** p-value < 0.001, **** p-value < 0.0001.*

.

Femoral Trabecular Bone: Distal Metaphysis

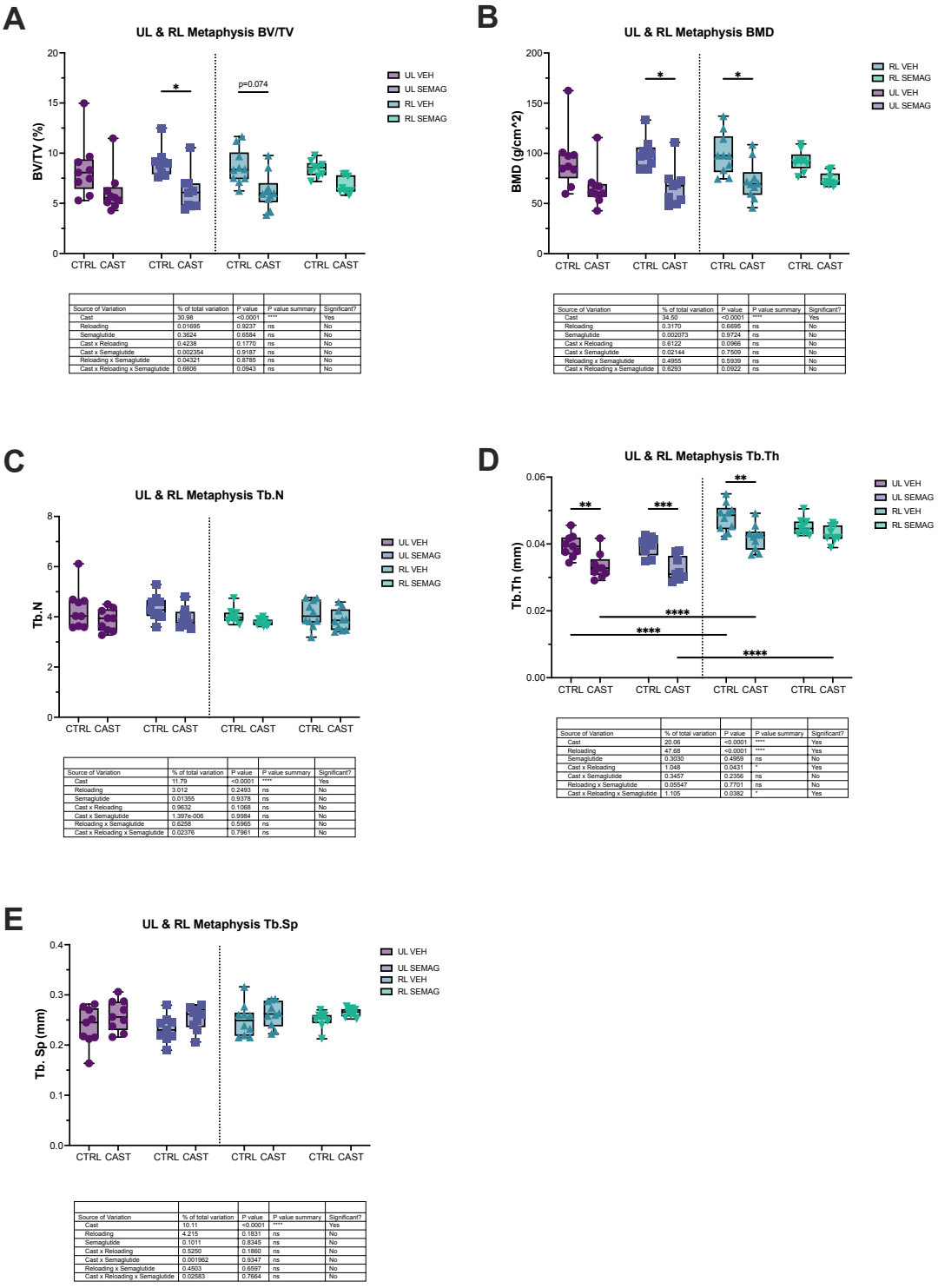

Source of Variation	% of total variation	P value	P value summary	Significant?
Cast	30.98	<0.0001	****	Yes
Reloading	0.01695	0.9237	ns	No
Semaglutide	0.3624	0.6584	ns	No
Cast x Reloading	0.4238	0.1770	ns	No
Cast x Semaglutide	0.002354	0.9187	ns	No
Reloading x Semaglutide	0.04321	0.8785	ns	No
Cast x Reloading x Semaglutide	0.6606	0.0943	ns	No

Source of Variation	% of total variation	P value	P value summary	Significant?
Cast	34.50	<0.0001	****	Yes
Reloading	0.3170	0.6695	ns	No
Semaglutide	0.002073	0.9724	ns	No
Cast x Reloading	0.6122	0.0966	ns	No
Cast x Semaglutide	0.02144	0.7509	ns	No
Reloading x Semaglutide	0.4955	0.5939	ns	No
Cast x Reloading x Semaglutide	0.6293	0.0922	ns	No

Source of Variation	% of total variation	P value	P value summary	Significant?
Cast	11.79	<0.0001	****	Yes
Reloading	3.012	0.2493	ns	No
Semaglutide	0.01355	0.9378	ns	No
Cast x Reloading	0.9632	0.1068	ns	No
Cast x Semaglutide	1.397e-006	0.9984	ns	No
Reloading x Semaglutide	0.6258	0.5965	ns	No
Cast x Reloading x Semaglutide	0.02376	0.7961	ns	No

Source of Variation	% of total variation	P value	P value summary	Significant?
Cast	20.06	<0.0001	****	Yes
Reloading	47.68	<0.0001	****	Yes
Semaglutide	0.3030	0.4959	ns	No
Cast x Reloading	1.048	0.0431	*	Yes
Cast x Semaglutide	0.3457	0.2356	ns	No
Reloading x Semaglutide	0.05547	0.7701	ns	No
Cast x Reloading x Semaglutide	1.105	0.0382	*	Yes

Source of Variation	% of total variation	P value	P value summary	Significant?
Cast	10.11	<0.0001	****	Yes
Reloading	4.215	0.1831	ns	No
Semaglutide	0.1011	0.8345	ns	No
Cast x Reloading	0.5250	0.1860	ns	No
Cast x Semaglutide	0.001962	0.9347	ns	No
Reloading x Semaglutide	0.4503	0.6597	ns	No
Cast x Reloading x Semaglutide	0.02583	0.7664	ns	No

*Figure 3.6. µCT analysis of trabecular bone at the distal femoral metaphysis during single-limb immobilization via cast and Semaglutide treatment in female mice. Trabecular bone microarchitecture: A) bone volume (BV); B) bone volume fraction (BV/TV); C) trabecular number (Tb.N); D) trabecular thickness (Tb.Th); E) Trabecular Separation (Tb.Sp). Significance values of 3-way ANOVA with Tukey's post-hoc analysis: * p-value < 0.05, ** p-value <0.01, *** p-value < 0.001, **** p-value < 0.0001.*

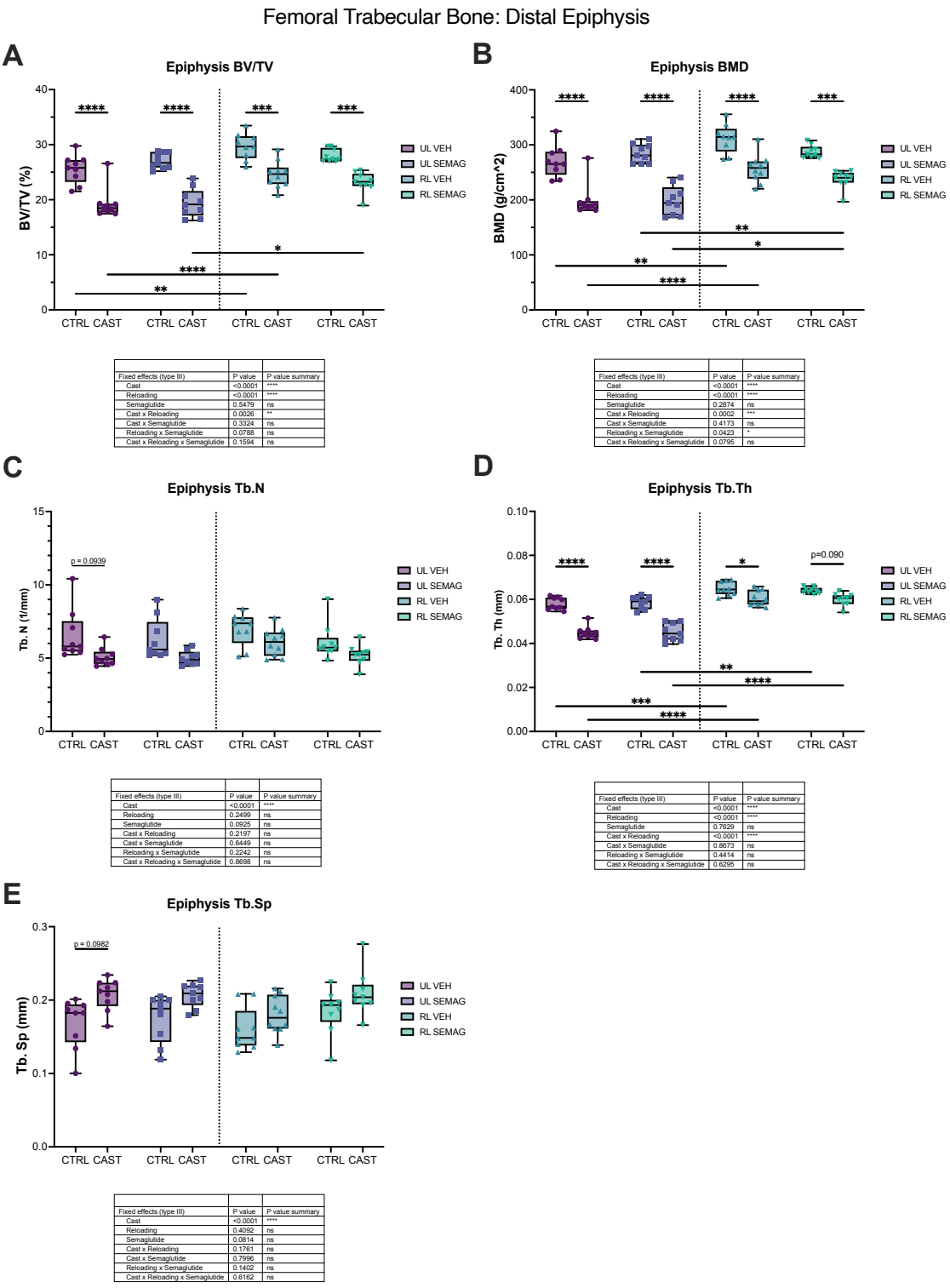

Fixed effects (type III)	P value	P value summary
Cast	<0.0001	****
Reloading	<0.0001	****
Semaglutide	0.5479	ns
Cast x Reloading	0.0026	**
Cast x Semaglutide	0.3324	ns
Reloading x Semaglutide	0.0788	ns
Cast x Reloading x Semaglutide	0.1594	ns

Fixed effects (type III)	P value	P value summary
Cast	<0.0001	****
Reloading	<0.0001	****
Semaglutide	0.2874	ns
Cast x Reloading	0.0002	***
Cast x Semaglutide	0.4173	ns
Reloading x Semaglutide	0.0423	*
Cast x Reloading x Semaglutide	0.0795	ns

Fixed effects (type III)	P value	P value summary
Cast	<0.0001	****
Reloading	0.2499	ns
Semaglutide	0.0925	ns
Cast x Reloading	0.2197	ns
Cast x Semaglutide	0.6449	ns
Reloading x Semaglutide	0.2242	ns
Cast x Reloading x Semaglutide	0.8698	ns

Fixed effects (type III)	P value	P value summary
Cast	<0.0001	****
Reloading	<0.0001	****
Semaglutide	0.7629	ns
Cast x Reloading	<0.0001	****
Cast x Semaglutide	0.8673	ns
Reloading x Semaglutide	0.4414	ns
Cast x Reloading x Semaglutide	0.6295	ns

Fixed effects (type III)	P value	P value summary
Cast	<0.0001	****
Reloading	0.4092	ns
Semaglutide	0.0814	ns
Cast x Reloading	0.1761	ns
Cast x Semaglutide	0.7996	ns
Reloading x Semaglutide	0.1402	ns
Cast x Reloading x Semaglutide	0.6162	ns

*Figure 3.7. µCT analysis of trabecular bone of the distal femoral epiphysis during single-limb immobilization via cast and Semaglutide treatment in female mice. Trabecular bone microarchitecture: A) bone volume (BV); B) bone volume fraction (BV/TV); C) trabecular number (Tb.N); D) trabecular thickness (Tb.Th); E) Trabecular Separation (Tb.Sp). Significance values of repeat measures linear model (RMLM) with Tukey's post-hoc analysis: * p-value < 0.05, ** p-value <0.01, *** p-value < 0.001, **** p-value < 0.0001.*

3.4 Mechanical Properties Testing: 3-Point Bending

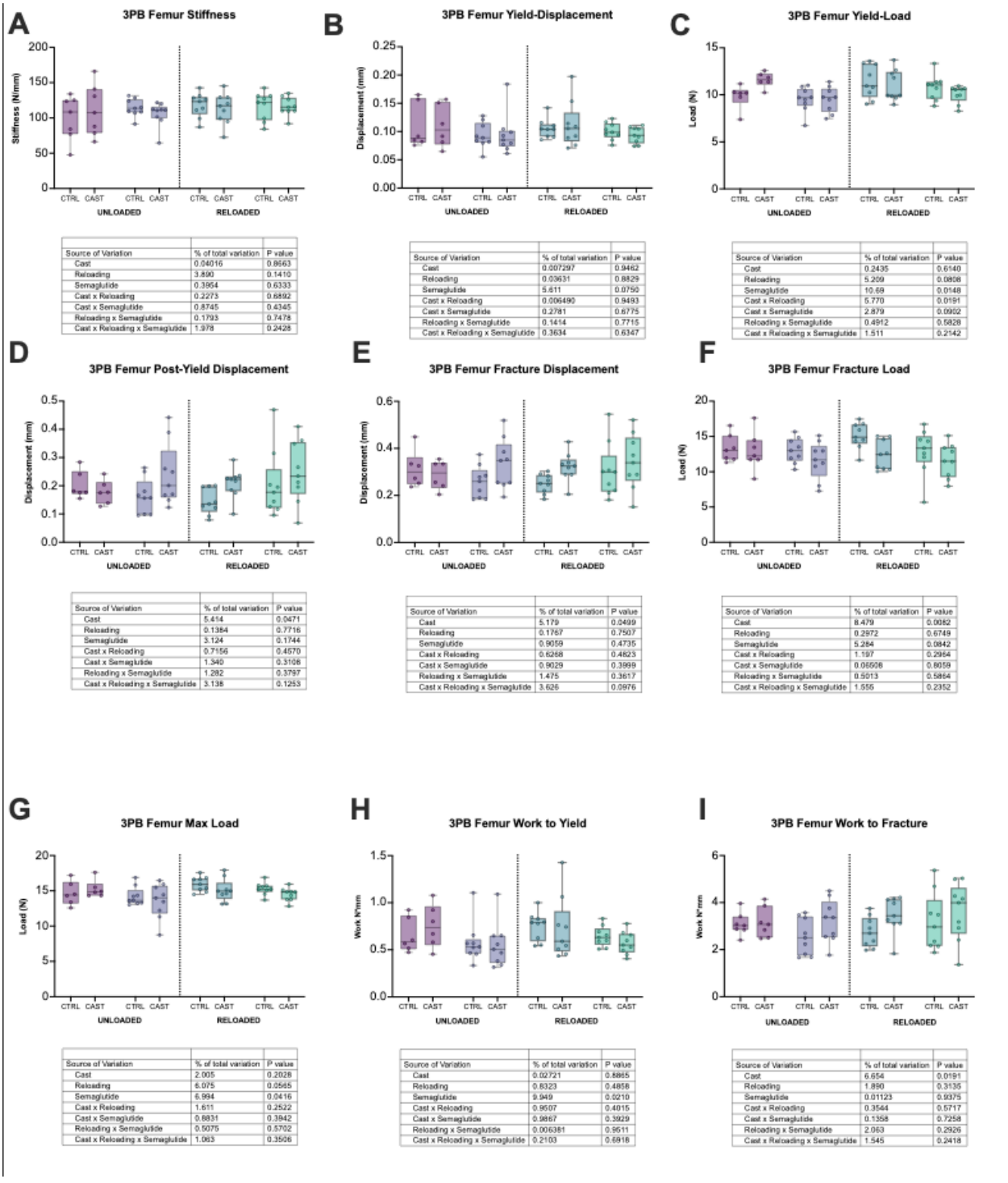

Source of Variation	% of total variation	P value
Cast	0.04016	0.8663
Reloading	3.890	0.1410
Semaglutide	0.3954	0.6333
Cast x Reloading	0.2273	0.6892
Cast x Semaglutide	0.8745	0.4345
Reloading x Semaglutide	0.1793	0.7478
Cast x Reloading x Semaglutide	1.978	0.2428

Source of Variation	% of total variation	P value
Cast	0.007297	0.9462
Reloading	0.03631	0.8829
Semaglutide	5.611	0.0750
Cast x Reloading	0.006490	0.9493
Cast x Semaglutide	0.2781	0.6775
Reloading x Semaglutide	0.1414	0.7715
Cast x Reloading x Semaglutide	0.3634	0.6347

Source of Variation	% of total variation	P value
Cast	0.2435	0.6140
Reloading	5.209	0.0808
Semaglutide	10.69	0.0148
Cast x Reloading	5.770	0.0191
Cast x Semaglutide	2.879	0.0902
Reloading x Semaglutide	0.4912	0.5828
Cast x Reloading x Semaglutide	1.511	0.2142

Source of Variation	% of total variation	P value
Cast	5.414	0.0471
Reloading	0.1384	0.7716
Semaglutide	3.124	0.1744
Cast x Reloading	0.7156	0.4570
Cast x Semaglutide	1.340	0.3108
Reloading x Semaglutide	1.282	0.3797
Cast x Reloading x Semaglutide	3.138	0.1253

Source of Variation	% of total variation	P value
Cast	5.179	0.0499
Reloading	0.1767	0.7507
Semaglutide	0.9059	0.4735
Cast x Reloading	0.6268	0.4823
Cast x Semaglutide	0.9029	0.3999
Reloading x Semaglutide	1.475	0.3617
Cast x Reloading x Semaglutide	3.626	0.0976

Source of Variation	% of total variation	P value
Cast	8.479	0.0082
Reloading	0.2972	0.6749
Semaglutide	5.264	0.0842
Cast x Reloading	1.197	0.2964
Cast x Semaglutide	0.06508	0.8059
Reloading x Semaglutide	0.5013	0.5864
Cast x Reloading x Semaglutide	1.555	0.2352

Source of Variation	% of total variation	P value
Cast	2.005	0.2028
Reloading	6.075	0.0565
Semaglutide	6.994	0.0416
Cast x Reloading	1.611	0.2522
Cast x Semaglutide	0.8831	0.3842
Reloading x Semaglutide	0.5075	0.5702
Cast x Reloading x Semaglutide	1.063	0.3506

Source of Variation	% of total variation	P value
Cast	0.02721	0.8865
Reloading	0.8323	0.4858
Semaglutide	9.949	0.0210
Cast x Reloading	0.9507	0.4015
Cast x Semaglutide	0.9867	0.3929
Reloading x Semaglutide	0.006381	0.9511
Cast x Reloading x Semaglutide	0.2103	0.6918

Source of Variation	% of total variation	P value
Cast	6.654	0.0191
Reloading	1.890	0.3135
Semaglutide	0.01123	0.9375
Cast x Reloading	0.3544	0.5717
Cast x Semaglutide	0.1358	0.7258
Reloading x Semaglutide	2.063	0.2926
Cast x Reloading x Semaglutide	1.545	0.2418

*Figure 3.8. 3-Point bending analysis of femurs after single-limb immobilization via cast and Semaglutide treatment in female mice. Femur structural properties: A) stiffness; B) yield-displacement; C) yield load; D) post-yield displacement; E) fracture displacement; F) fracture load; G) max load; H) work to yield; and I) work to fracture. Significance values of 3-way ANOVA with Tukey's post-hoc analysis: * p-value < 0.05, ** p-value <0.01, *** p-value < 0.001, **** p-value < 0.0001.*

A

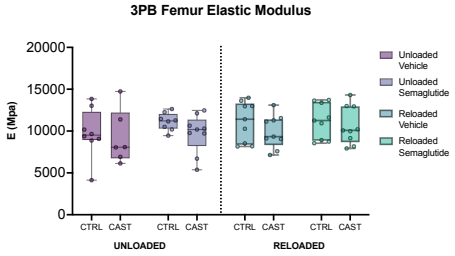

Fixed effects (type III)	P value	P value summary	Statistically significant (P < 0.05)?
Cast	0.1112	ns	No
Reloading	0.2007	ns	No
Semaglutide	0.2738	ns	No
Cast x Reloading	0.9568	ns	No
Cast x Semaglutide	0.8828	ns	No
Reloading x Semaglutide	0.6574	ns	No

B

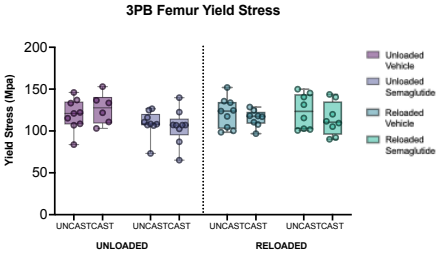

Fixed effects (type III)	P value	P value summary	Statistically significant (P < 0.05)?
Cast	0.4482	ns	No
Reloading	0.4985	ns	No
Semaglutide	0.1282	ns	No
Cast x Reloading	0.2467	ns	No
Cast x Semaglutide	0.3763	ns	No
Reloading x Semaglutide	0.0940	ns	No

C

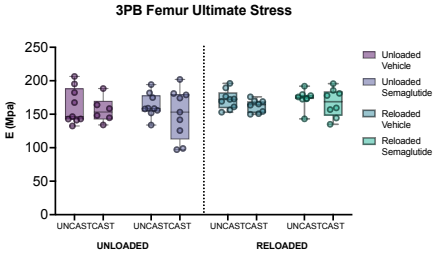

Fixed effects (type III)	P value	P value summary	Statistically significant (P < 0.05)?
Cast	0.0965	ns	No
Reloading	0.0684	ns	No
Semaglutide	0.9304	ns	No
Cast x Reloading	0.8732	ns	No
Cast x Semaglutide	0.8719	ns	No
Reloading x Semaglutide	0.6546	ns	No

*Figure 3.9. Analysis of femur material properties after single-limb immobilization via cast and Semaglutide treatment in female mice. Material properties: A) Elastic Modulus; B) yield stress; C) ultimate stress. Significance values of 3-way ANOVA with Tukey's post-hoc analysis: * p-value < 0.05, ** p-value <0.01, *** p-value < 0.001, **** p-value < 0.0001.*

3.5 PINP and CTX-1 Analysis

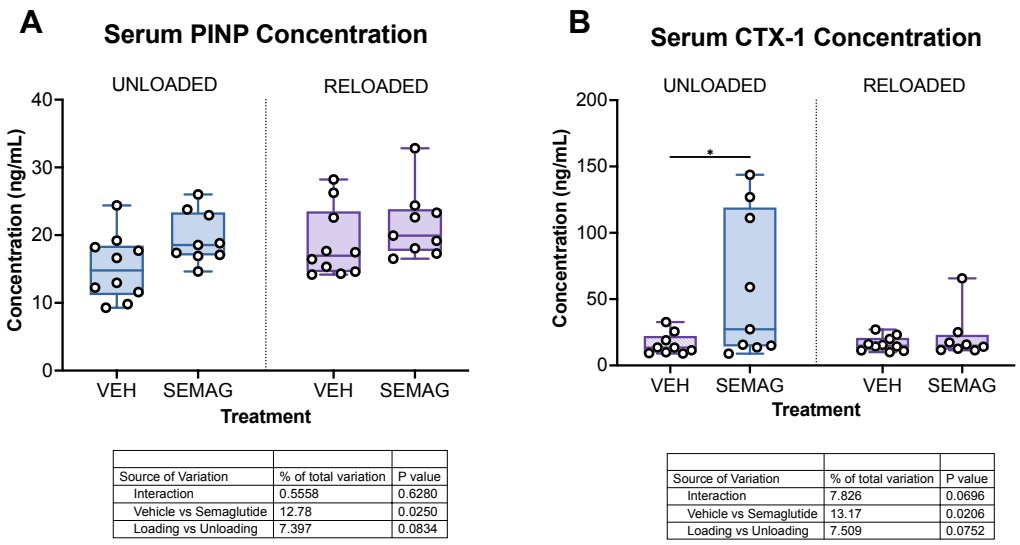

Source of Variation	% of total variation	P value
Interaction	0.5558	0.6280
Vehicle vs Semaglutide	12.78	0.0250
Loading vs Unloading	7.397	0.0834

Source of Variation	% of total variation	P value
Interaction	7.826	0.0696
Vehicle vs Semaglutide	13.17	0.0206
Loading vs Unloading	7.509	0.0752

Figure 3.10. ***Serum bone formation and resorption markers after single-limb immobilization via cast and Semaglutide treatment in female mice.*** *Serum concentrations of A) PINP and B) CTX-1. Main effect of semaglutide treatment was observed in both markers ($p<0.05$), with trending effect of unloading ($p<0.1$) and interaction ($p=0.0696$) in CTX-1 concentration. Significance values of 2-way ANOVA with Tukey's post-hoc analysis: * p-value < 0.05, ** p-value <0.01, *** p-value < 0.001, **** p-value < 0.0001.*

3.6 Tendon mechanical analysis

Tendons are less responsive to Semaglutide treatment than to unloading and reloading.

Casting increased Achilles tendon thickness and force at MTL and reduced Young's Modulus (Fig. 3.11 B, D, E). Reloading decreased CSA and increased force at MTL, Young's modulus, and Ultimate stress. Semaglutide treatment trended towards increasing force at MTL after reloading ($p=0.090$), but had no other apparent impacts on Achilles tendon mechanics at these timepoints.

Figure 3.11.

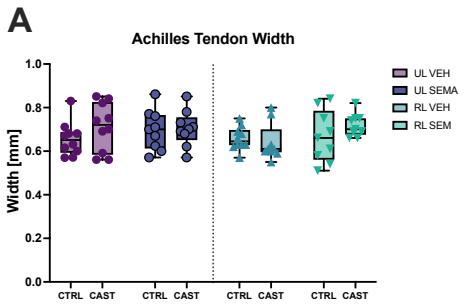

Fixed effects (type III)	P value	P value summary
Cast	0.2385	ns
Reloading	0.2923	ns
Semaglutide	0.1400	ns
Cast x Reloading	0.7167	ns
Cast x Semaglutide	0.7842	ns
Reloading x Semaglutide	0.5115	ns
Cast x Reloading x Semaglutide	0.1526	ns

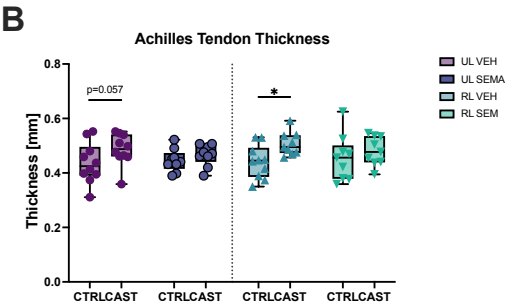

Fixed effects (type III)	P value	P value summary
Cast	0.0043	**
Reloading	0.3896	ns
Semaglutide	0.6666	ns
Cast x Reloading	0.6713	ns
Cast x Semaglutide	0.1853	ns
Reloading x Semaglutide	0.9781	ns
Cast x Reloading x Semaglutide	0.8617	ns

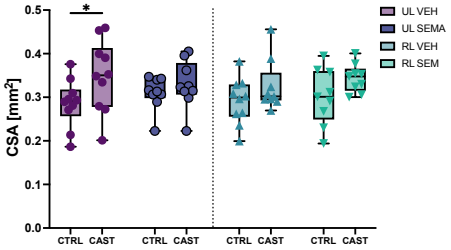

Fixed effects (type III)	P value	P value summary
Cast	0.5517	ns
Reloading	<0.0001	****
Semaglutide	0.6985	ns
Cast x Reloading	0.8535	ns
Cast x Semaglutide	0.1267	ns
Reloading x Semaglutide	0.1166	ns
Cast x Reloading x Semaglutide	0.2098	ns

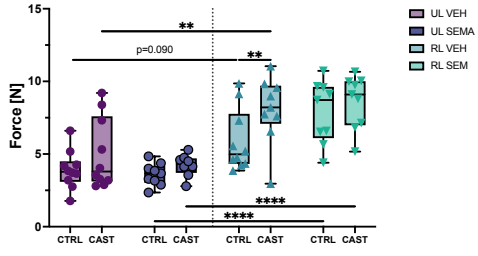

Fixed effects (type III)	P value	P value summary
Cast	0.0060	**
Reloading	<0.0001	****
Semaglutide	0.4387	ns
Cast x Reloading	0.4615	ns
Cast x Semaglutide	0.2334	ns
Reloading x Semaglutide	0.0607	ns
Cast x Reloading x Semaglutide	0.5315	ns

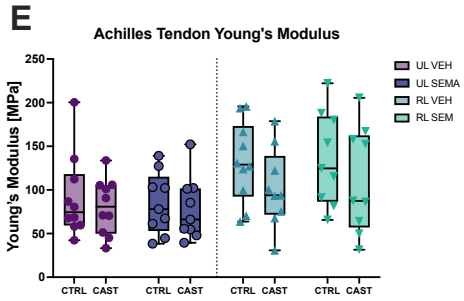

Fixed effects (type III)	P value	P value summary
Cast	0.0443	*
Reloading	0.0046	**
Semaglutide	0.8991	ns
Cast x Reloading	0.2626	ns
Cast x Semaglutide	0.7400	ns
Reloading x Semaglutide	0.6164	ns
Cast x Reloading x Semaglutide	0.9206	ns

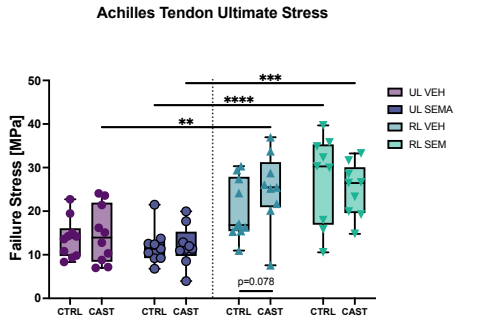

Fixed effects (type III)	P value	P value summary
Cast	0.5517	ns
Reloading	<0.0001	****
Semaglutide	0.6985	ns
Cast x Reloading	0.8535	ns
Cast x Semaglutide	0.1267	ns
Reloading x Semaglutide	0.1166	ns
Cast x Reloading x Semaglutide	0.2098	ns

*Mechanical testing of the Achilles tendon after single-limb immobilization via cast and Semaglutide treatment in female mice. Achilles tendon structural and mechanical properties: A) width; B) thickness; C)cross-sectional area; D) force at maximal tensile Load; E) Young's Modulus; and F) ultimate stress. Significance values of Repeat Measures Linear mixed-methods model (RMLM) with Tukey's post-hoc analysis: * p-value < 0.05, ** p-value <0.01, *** p-value < 0.001, **** p-value < 0.0001.*

3.7 Muscle

Semaglutide significantly decreases muscle mass during unloading.

Significant loss of muscle mass was observed between the cast and contralateral control legs of Semaglutide-treated mice (Fig. 3.12). Gastrocnemius muscles were also reduced in vehicle-treated mice ($p<0.001$). Reloading did not recover lost gastrocnemius mass with or without Semaglutide treatment. Semaglutide was not an independent factor for muscle loss, but it had significant interactions with reloading in the soleus ($p=0.036$), gastrocnemius ($p=0.004$), and plantaris ($p=0.008$). Casting x Reloading interactions were substantial in the soleus ($p=0.004$) and gastrocnemius ($p=0.041$) muscles.

Anabolic and catabolic muscle protein concentrations are impacted by unloading, reloading, and Semaglutide treatment.

Semaglutide significantly affected MURF1 and pAKT abundance in plantaris muscles during unloading, with trending changes in REDD1 (32kDa and 36kDa) and peEF2 concentrations (Fig. 3.13). Casting increased pS6 and decreased MURF1. Interactions of casting and Semaglutide treatment caused decreases in plantaris MURF 1 concentrations and trending increases in pAMPK and peEF2. Reloading greatly affected protein concentrations in casted legs of vehicle and Semaglutide-treated animals, including decreased pS6 and pP38, as well as increased REDD1 (32kDa and 36kDa) and peEF2 (Fig. 3.14). Semaglutide x reloading effects increased REDD1(36kDa) concentrations and decreased and pAKT concentrations, with trending decreases in peEF2 and pP38.

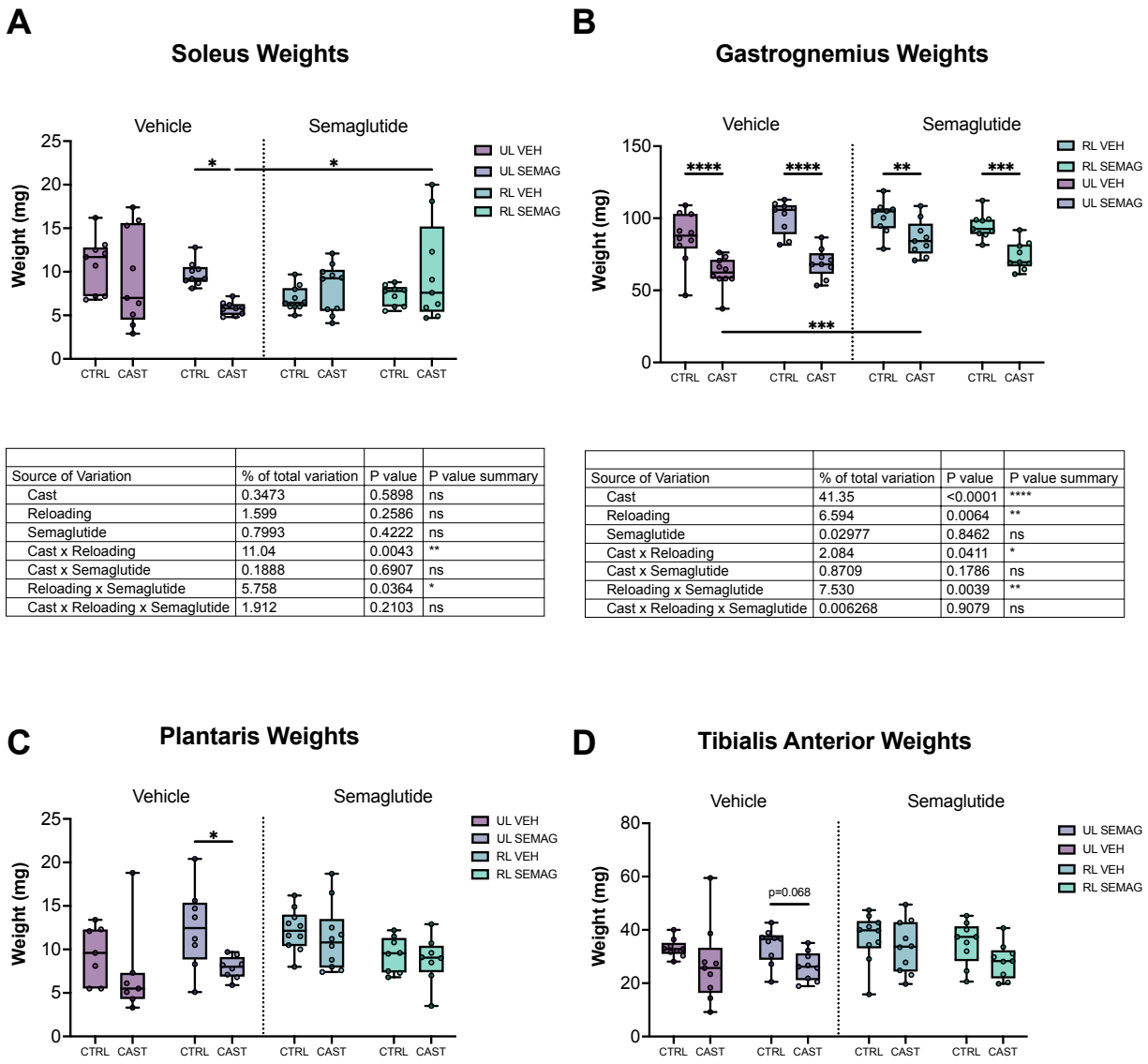

Source of Variation	% of total variation	P value	P value summary
Cast	0.3473	0.5898	ns
Reloading	1.599	0.2586	ns
Semaglutide	0.7993	0.4222	ns
Cast x Reloading	11.04	0.0043	**
Cast x Semaglutide	0.1888	0.6907	ns
Reloading x Semaglutide	5.758	0.0364	*
Cast x Reloading x Semaglutide	1.912	0.2103	ns

Source of Variation	% of total variation	P value	P value summary
Cast	41.35	<0.0001	****
Reloading	6.594	0.0064	**
Semaglutide	0.02977	0.8462	ns
Cast x Reloading	2.084	0.0411	*
Cast x Semaglutide	0.8709	0.1786	ns
Reloading x Semaglutide	7.530	0.0039	**
Cast x Reloading x Semaglutide	0.006268	0.9079	ns

Source of Variation	% of total variation	P value	P value summary
Cast	8.075	0.0256	*
Reloading	2.476	0.1503	ns
Semaglutide	0.3188	0.6000	ns
Cast x Reloading	3.224	0.1477	ns
Cast x Semaglutide	0.4239	0.5938	ns
Reloading x Semaglutide	9.190	0.0080	**
Cast x Reloading x Semaglutide	0.7506	0.4787	ns

Source of Variation	% of total variation	P value	P value summary
Cast	10.97	0.0053	**
Reloading	3.410	0.1122	ns
Semaglutide	1.003	0.3824	ns
Cast x Reloading	0.2189	0.6758	ns
Cast x Semaglutide	0.4426	0.5526	ns
Reloading x Semaglutide	1.028	0.3766	ns
Cast x Reloading x Semaglutide	0.04364	0.8517	ns

*Figure 3.12. Muscle mass after single-limb immobilization via cast and Semaglutide treatment in female mice. Measured mass: A) soleus; B) gastrocnemius; C) plantaris; and D) Tibialis anterior. Significance values of 3-way ANOVA with Tukey's post-hoc analysis: * p-value < 0.05, ** p-value <0.01, *** p-value < 0.001, **** p-value < 0.0001.*

3.8 Immunoblot

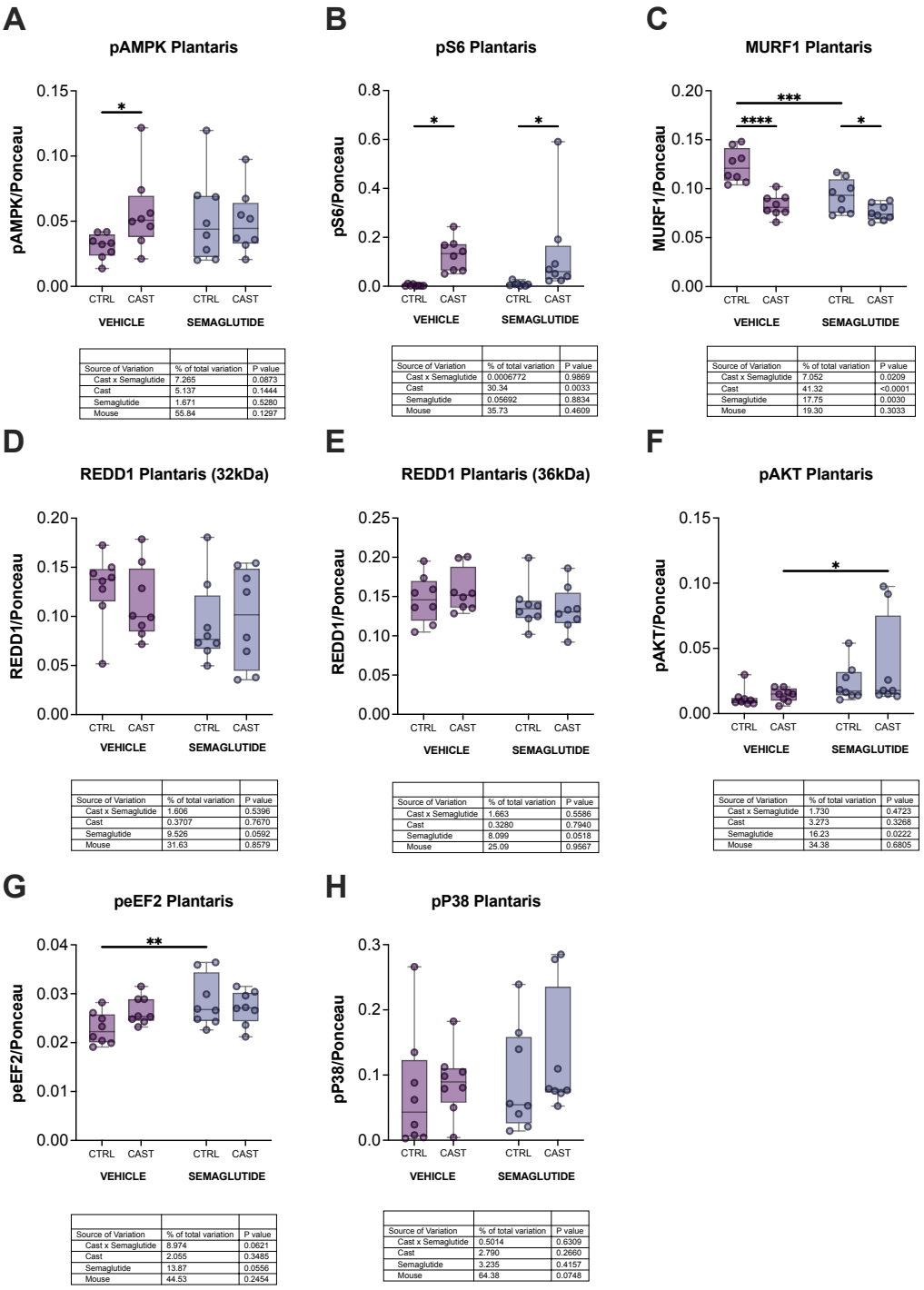

*Figure 3.13. Immunoblot Analysis of Plantaris muscle after single-limb immobilization via cast and Semaglutide treatment in female mice. Measured proteins: A) pAMPK; B) pS6; C) MURPH 1; D) REDD1 (32kDa); E) REDD1. (36kDa); F) pAKT; G) peEF2;and H) pP38 . Significance values of 2-way ANOVA with Tukey's post-hoc analysis: : * p-value < 0.05, ** p-value <0.01, *** p-value < 0.001, **** p-value < 0.0001.*

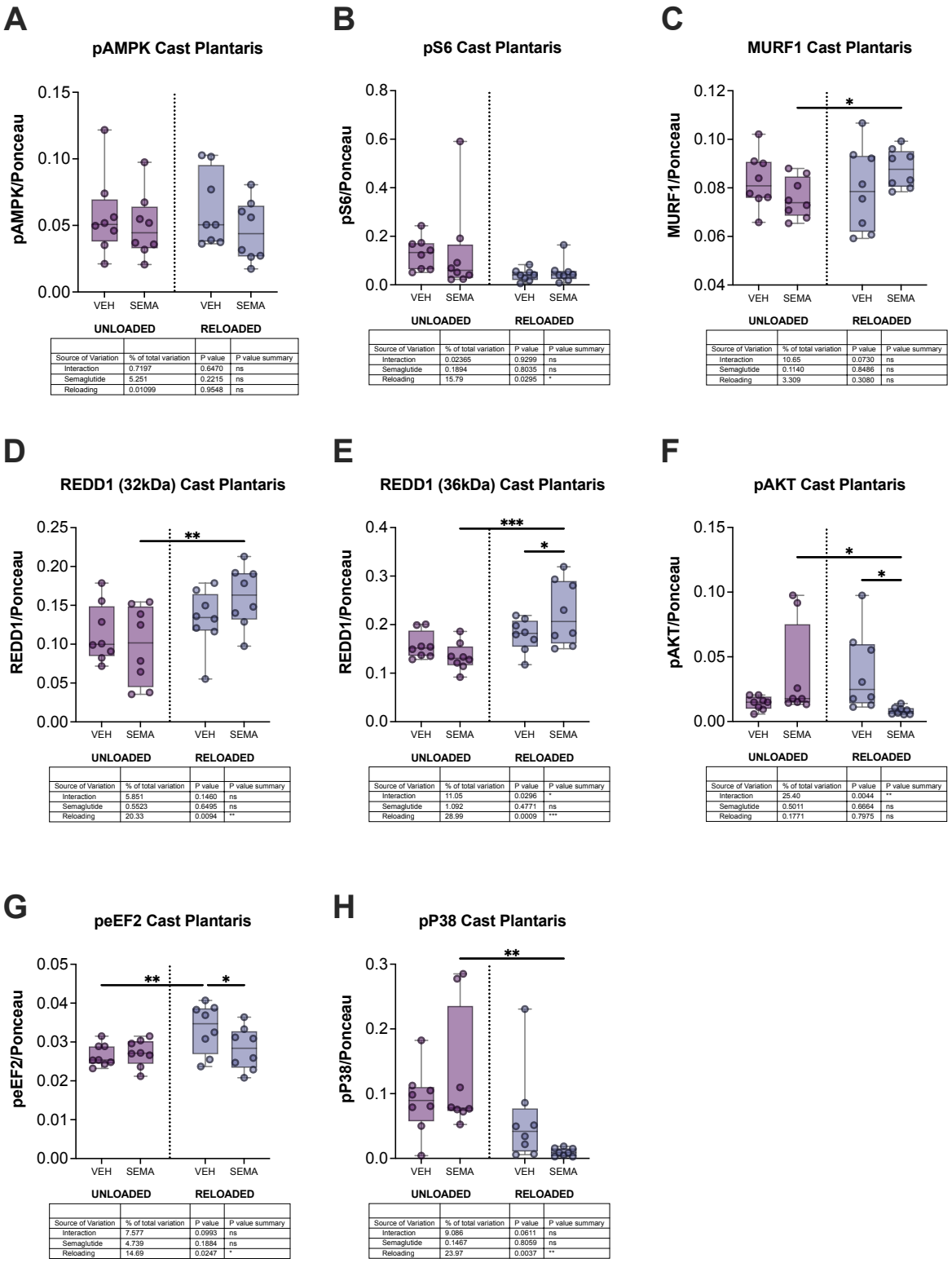

*Figure 3.14 Immunoblot Analysis of Plantaris muscle after single-limb immobilization via cast and subsequent reloading with Semaglutide treatment in female mice. Measured proteins: A) pAMPK; B) pS6; C) MURPH 1; D) REDD1 (32kDa); E) REDD1. (36kDa); F) pAKT; G) peEF2;and H) pP38 . Significance values of 2-way ANOVA with Tukey's post-hoc analysis: : * p-value < 0.05, ** p-value <0.01, *** p-value < 0.001, **** p-value < 0.0001.*

3.9 Bulk RNA Sequencing & Gene Ontology

Semaglutide treatment significantly modifies the expression of genes critical to bone & skeletal system development.

Bulk RNA sequencing found that 15 unique Ensembl IDs were identified as differentially expressed in the unloaded tibia between Semaglutide and vehicle-treated mice (see Appendix 2 for complete list). 13 have been assigned a gene symbol; of those, 5 were noted as having a significant effect size (log2 fold change ±1, Table 1, Fig. 3.15). No significant changes in the expression of biological processes were identified through Gene Ontology analysis. Additionally, 148 unique Ensembl IDs were identified as differentially expressed in the unloaded soleus muscle between Semaglutide and vehicle-treated mice (see Appendix 3 for complete list). 128 have been assigned a gene symbol; of those, 45 were noted as having a significant effect size (log2 fold change ±1, Table 2). Gene Ontology analysis indicated significant changes in various biological processes, including neutrophil aggregation, bone development, regulation of monoatomic ion transport, cell migration, positive regulation of multicellular process, and several subcategories of these processes (Tables 3 & 4). These genes have been noted in tables and heat maps (Fig. 3.16) to indicate differential expression. Notably, downregulation of Zbtb16 was observed in both tibia and soleus datasets.

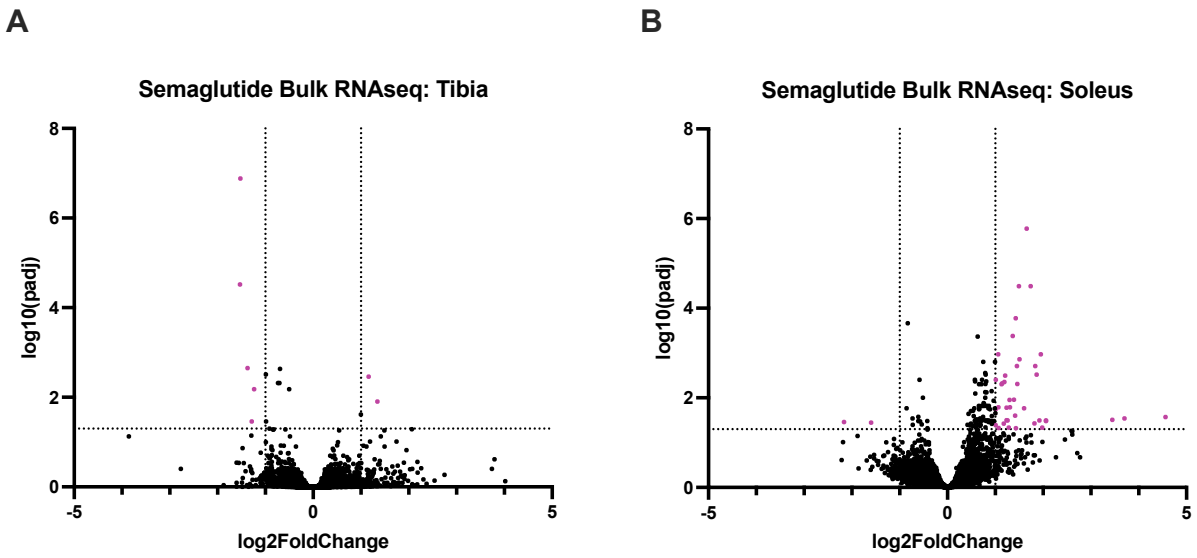

Figure 3.15. Bulk RNA Seq analysis of unloaded tibia and soleus after single-limb immobilization via cast and Semaglutide treatment in female mice. Volcano plot of significantly upregulated genes (pink) in A) tibia and B) soleus muscles. Significance is defined as an adjusted p value <0.05. Significant change in log2 fold change denoted by dashed lines at x= ± 1.

Table 3.1. Differential gene expression of the tibia during unloading via a cast.

Ensembl ID	baseMean	log2FoldChange	lfcSE	stat	pvalue	padj	symbol
ENSMUSG00000059824	130.803727	-1.5224962	0.22245952	-6.8439246	7.71E-12	1.31E-07	Dbp
ENSMUSG00000008874	432.126679	-1.5315917	0.25949292	-5.9022486	3.59E-09	3.05E-05	Clec3a
ENSMUSG00000026574	84.6325984	-1.2358126	0.26724476	-4.6242723	3.76E-06	0.00660539	Dpt
ENSMUSG00000066687	80.1998874	1.34487995	0.30128684	4.46378584	8.05E-06	0.01243511	Zbtb16
ENSMUSG00000037406	89.8072545	-1.2867991	0.30759294	-4.183448	2.87E-05	0.034838	Htra4

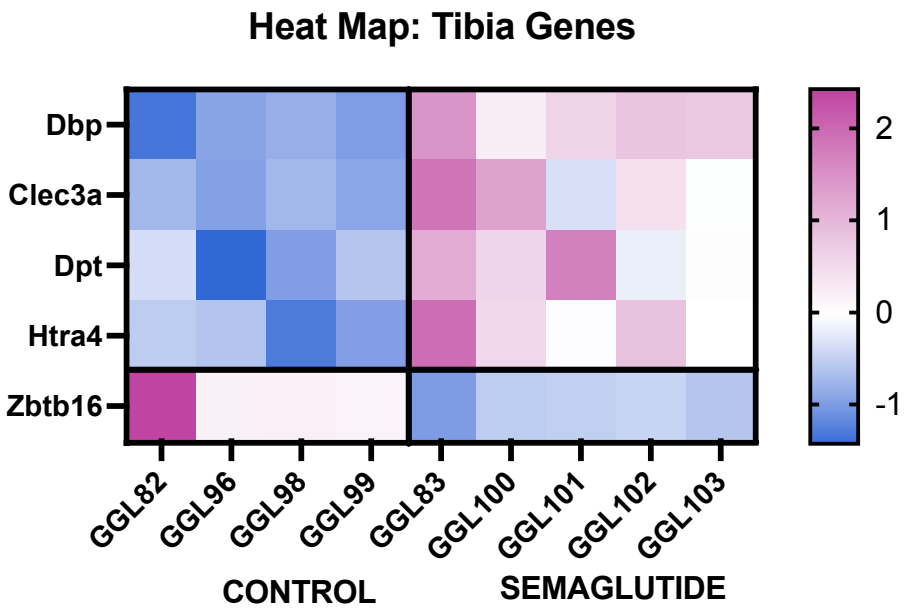

Figure 3.16. Heat map of differentially expressed genes in Semaglutide vs vehicle-treated mouse tibias after single-limb immobilization via cast in female mice. Expression is denoted as relative Z-score for upregulation (pink) and downregulation(blue) genes.

Table3.2.Differentially expressed genes in the unloaded soleus (bulk RNAseq)

	baseMean	log2FoldChange	lfcSE	stat	pvalue	padj	symbol
ENSMUSG00000066687	66.9582806	-1.65612819	0.26015398	6.36595362	1.9408E-10	1.6844E-06	Zbtb16
ENSMUSG00000033124	28.3977905	-1.49527447	0.26403183	5.66323571	1.4854E-08	3.2356E-05	Atg9a
ENSMUSG00000033624	18.3117907	-1.73933437	0.30191459	5.76101461	8.361E-09	3.2356E-05	Pdpr
ENSMUSG00000114382	126.706682	-1.4257837	0.27036593	5.27353312	1.3382E-07	0.00016796	Gm4814
ENSMUSG00000120539	22.2766691	-1.36276304	0.27072108	5.03382677	4.8078E-07	0.00041727	Gm56507
ENSMUSG00000109017	153.709618	-1.06221107	0.22207267	4.7831689	1.7255E-06	0.00106971	Gm38979
ENSMUSG00000114968	22.1161428	-1.95142467	0.40695515	4.79518364	1.6253E-06	0.00106971	A630019I02Rik
ENSMUSG00000087530	53.5958438	-1.5070964	0.31951187	4.71687137	2.395E-06	0.00138574	Gm15533
ENSMUSG00000110711	95.7656979	-1.45159192	0.3164542	4.58705212	4.4955E-06	0.00195082	Gm45760
ENSMUSG00000087253	27.5927736	-1.83528373	0.39938032	4.59532841	4.3207E-06	0.00195082	Gm12043
ENSMUSG00000112841	36.2768348	-1.86306787	0.41816786	4.45531099	8.3772E-06	0.00302939	Gm48752
ENSMUSG00000056071	35.3938028	-5.38940655	1.21404319	4.43922143	9.0285E-06	0.00313433	S100a9
ENSMUSG00000033400	314.362194	-1.20582204	0.27240701	4.42654564	9.5754E-06	0.00319635	Agl
ENSMUSG00000073375	75.4863103	-1.00846822	0.23175084	4.35151918	1.352E-05	0.00396808	Lrrc30
ENSMUSG00002076463	21.9433113	-1.18771996	0.27603177	4.30283794	1.6862E-05	0.00443482	Gm55944
ENSMUSG00000025006	70.1393175	-1.14560373	0.2676879	4.27962469	1.8721E-05	0.00477878	Sorbs1

ENSMUSG00000120290	14.0814816	-1.45981677	0.34257705	4.26128018	2.0326E-05	0.00490024	Gm56959
ENSMUSG00000020634	44.3616878	-1.13081227	0.26706343	4.23424612	2.2932E-05	0.00497566	Ubxn2a
ENSMUSG00000032484	27.6372515	-6.68968525	1.60266157	4.17410973	2.9915E-05	0.00633257	Ngp
ENSMUSG00000028766	12.465005	-1.39093648	0.34736841	4.00421122	6.2225E-05	0.0110214	Alpl
ENSMUSG00000067279	243.723512	-1.29837385	0.32488213	3.99644588	6.4301E-05	0.01116129	Ppp1r3c
ENSMUSG00000121052	139.469893	-1.06635151	0.27688561	3.85123483	0.00011752	0.01619029	Gm56551
ENSMUSG00000034055	326.990252	-1.30621722	0.33960478	3.84628632	0.00011992	0.0162625	Phka1
ENSMUSG00000120274	43.1260795	-1.23721297	0.3222967	3.83873916	0.00012367	0.01651249	Gm56882
ENSMUSG00000090990	179.545301	-1.60127426	0.41841611	3.82699	0.00012972	0.01705815	Gm17197
ENSMUSG00000120133	90.7748026	-1.00455403	0.26517888	3.78821277	0.00015173	0.01798552	Gm56945
ENSMUSG00000026229	103.605864	-1.00226618	0.26940864	3.7202452	0.00019903	0.02214585	Psmd1
ENSMUSG00000086297	14.0355711	-1.41598788	0.38517737	3.67619696	0.00023674	0.02505657	Gm15632
ENSMUSG00000056054	28.8226381	-4.56158733	1.25159438	3.64462114	0.00026779	0.02671396	S100a8
ENSMUSG00000026822	21.9216741	-3.70237676	1.02405292	3.61541548	0.00029987	0.02891711	Lcn2
ENSMUSG00000034472	14.0021782	-3.44932827	0.96158843	3.58711498	0.00033436	0.0308711	Rasd2
ENSMUSG00000092596	14.1465424	-1.23598633	0.34633991	3.56870889	0.00035874	0.03177088	Gm20490
ENSMUSG00000020169	12.3433664	-1.25486098	0.35211188	3.5638132	0.00036551	0.03182313	Best3
ENSMUSG00000041329	88.5004442	-1.92209663	0.5407347	3.55460197	0.00037855	0.03182313	Atp1b2
ENSMUSG00000025161	47.0383711	-2.05968596	0.58123176	3.54365697	0.00039462	0.03200834	Slc16a3
ENSMUSG00000106375	71.7202272	-2.05928986	0.58395927	3.5264272	0.00042121	0.03302715	Gm43361
ENSMUSG00000022371	14.1972082	2.1630211	0.61991529	-3.4892205	0.00048443	0.03463473	Col14a1
ENSMUSG00000021390	50.6638703	1.5993967	0.45979466	-3.4785021	0.00050422	0.03557858	Ogn
ENSMUSG00000026827	60.3028654	-1.81975462	0.52585812	3.46054298	0.00053909	0.0374299	Gpd2
ENSMUSG00000030730	17020.1396	-1.1766713	0.34053761	3.45533435	0.00054961	0.03755368	Atp2a1
ENSMUSG00000028518	102.949188	-1.00515651	0.29406339	3.41816264	0.00063045	0.04023318	Prkaa2
ENSMUSG00000079278	30.907969	-1.98271203	0.58905096	3.3659431	0.00076282	0.04627236	Tmem233
ENSMUSG00000021451	35.2670494	-1.28219276	0.3811319	3.36417066	0.00076774	0.04627236	Sema4d
ENSMUSG00000058975	52.9469104	-1.06808184	0.31837463	3.35479574	0.00079424	0.04721353	Kcnc1
ENSMUSG00000030089	28.2131427	-1.42939098	0.42672919	3.34964423	0.00080915	0.04764291	Slc41a3

Table 3.3. Gene Ontology Analysis Results

	Mus musculus (REF)						
GO biological process complete	MM REF #	Actual #	Expected #	Fold Enrichment	+/-	raw P value	FDR
Neutrophil Aggregation	3	2	0	> 100	+	4.75E-06	0.0362
Neutrophil Aggregation Subset: Leukocyte Aggregation	14	3	0.02	> 100	+	6.81E-07	0.0104
Bone Development	229	5	0.29	17.03	+	9.80E-06	0.0498

Table 3.4. Genes Identified in GO Analysis

Biological Process Class and Subclass	Gene ID/Symbol	Gene Name
Neutrophil aggregation	Gene ID/Symbol	Gene Name
	S100a9	Protein S100-A9
	S100a8	Protein S100-A8
Neutrophil aggregation: Leucocyte aggregation	Gene ID/Symbol	Gene Name
	S100a9	Protein S100-A9
	Sema4d	Semaphorin-4D
	S100a8	Protein S100-A8
Bone development	Gene ID/Symbol	Gene Name
	Sema4d	Semaphorin-4D
	Zbtb16	Zinc finger and BTB domain containing 16
	Atg9a	Autophagy-related protein 9A
	Alpl	Alkaline phosphatase, tissue-nonspecific isozyme
	Ogn	Osteoglycin/ Mimecan

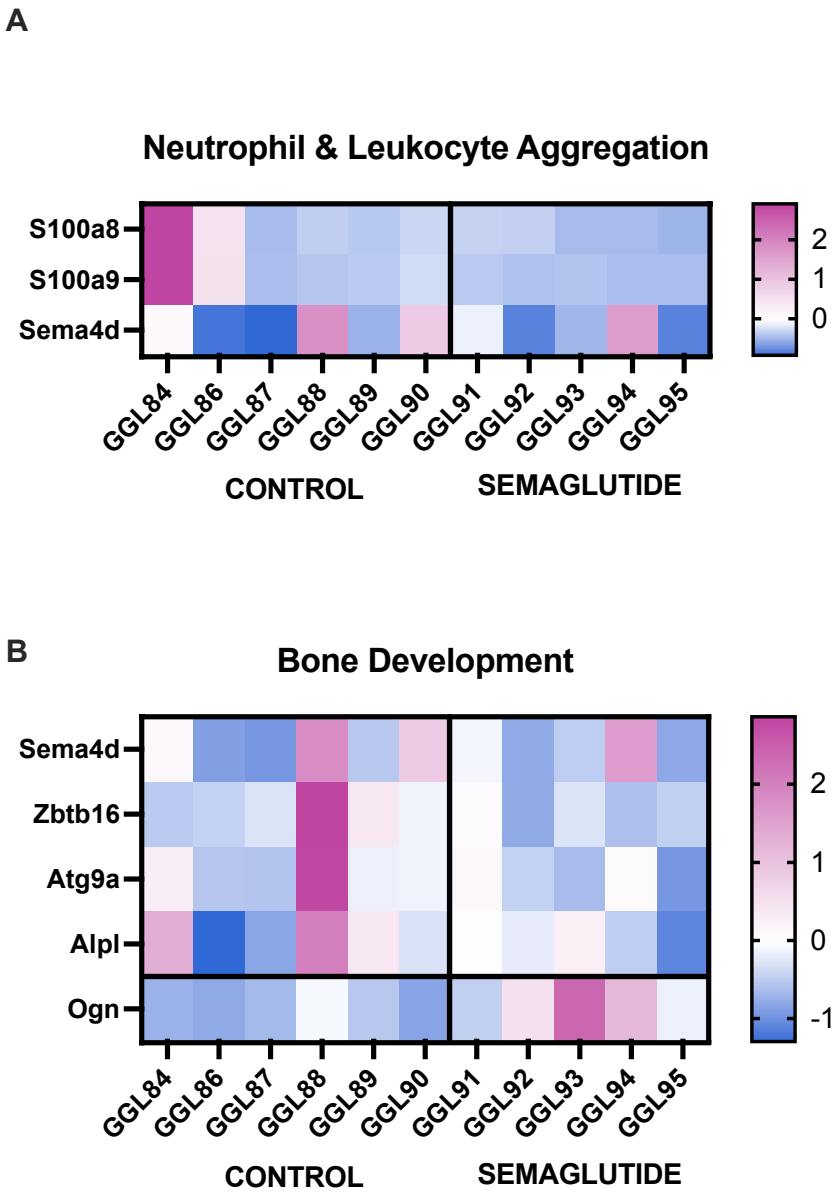

Figure 3.17. Heat map of differentially expressed genes in Semaglutide vs vehicle-treated mouse soleus muscles after single-limb immobilization via cast in female mice. Differently expressed genes have been organized into Gene Ontology biological process categories: A) neutrophil and leukocyte aggregation; B) bone development. Values are normalized to processed muscle mass. Expression is denoted as a relative Z-score for upregulated (pink) and downregulated (blue) genes.

4. Discussion

In this study, we investigated bone, muscle, and tendon responses to unloading and reloading during treatment with the GLP-RA Semaglutide. We originally hypothesized that Semaglutide-related weight loss would exacerbate bone and muscle loss during periods of unloading. However, contrary to our initial hypothesis, mice weight and body composition did not change due to the GLP-1RA dosage and method we used to administer the treatment. This led to an unexpected but interesting investigation into the effect of Semaglutide treatment without weight loss in wild-type female mice fed with a regular diet. We discovered differences in muscle responses to unloading with Semaglutide treatment associated with various differentially expressed genes.

Our selected dosage of Semaglutide was based on effective weight loss available in current literature when delivered subcutaneously [295-297]([47] is a preprint). However, our mice did not lose weight, decrease food intake, and continued to gain weight normally as they grew. Observed feeding habits were consistent between control and treatment groups, contrary to food reductions in studies where the animals lost weight [295, 296]. It is possible that there was a difference in weight loss because of the use of an Alzet osmotic pump instead of daily or twice daily injections or gavage. Alzet osmotic pumps are designed to continuously release a dosage from a reservoir capsule, while injections and gavage deliver an entire daily dose of the drug at once. The adverse gastrointestinal side effects of Semaglutide medication likely occur at these higher concentrations, which are never reached when using a slow-release osmotic pump. Continuous administration of GLP-1 RAs in healthy human males also reduced changes to gastric emptying compared to intermittent dosing and reduced the ability of these medications to decrease post-meal blood glucose levels[298]. However, continuous administration maintains insulin levels after meals

compared to intermittent dosing, which significantly reduces blood insulin levels compared to placebo controls. These differences could result in reduced weight loss.

Other reasons for weight maintenance include the size, diet, and sex of the mice. Animals in this study had not been fed the high-fat chow commonly used to induce extreme weight gain in mouse models. Higher weight and different nutritional intake could be required for Semaglutide to cause weight loss in mice. Other rodent Semaglutide studies looking at weight loss often use diet-induced obesity (DIO) or diet-restricted obesity (DRO) models, where rodents are fed a high-fat diet consisting of 45 or 60% fat chow[295, 299]. Our mice were not explicitly fed to increase their weight, but rather were fed standard chow with approximately 5% fat, as a normal rodent chow contains 4-6% fat,[300]. Other studies with normal weight, standard chow, and similar Semaglutide dosage did not show long-term weight loss [301]. Higher doses in normal weight rodents resulted in either 12% weight loss in 2 days that was sustained over the 12-day study with reduced food and water intake [297](preprint) or a weight loss of 4-6% that was attenuated with voluntary sucralose intake, indicating that caloric restrictions could be due to solid food intake versus overall intake, though the mechanism isn't well defined[302]. Sex could also be a factor, as many studies were performed using male mice that tend to eat more and gain more weight per gram of food eaten, despite similar feeding patterns [303]. However, female mice also lost weight in at least one study [296]. We chose to use normal weight female mice for a biologically relevant investigation into the effects of Semaglutide on individuals who were being prescribed GLP-1RA medications without confounding medical conditions. We therefore chose to administer a standard chow diet and refrained from adding additional fat to increase their weight. Finally, using an

osmotic pump reduces animal handling; handling animals twice daily for injections may result in stress-induced weight loss and other side effects[304, 305].

In murine Semaglutide studies involving mice fed a high fat diet, weight loss is as high as 10% in 2 days after starting twice daily injections [295]. With higher Semaglutide dosages (30 and 100 nmol/kg/day), animals reach a 20-30% weight reduction in 14-21 days[295, 306]. The UC Davis IACUC lists 20% weight loss in skeletally mature laboratory mice as a condition for a humane endpoint, where an animal is humanely euthanized based on animal health decline. Indeed, other experiments conducted by Novo Nordisk utilizing mouse models noted that excess weight loss is a risk factor for Semaglutide treatment [307]. A treatment that consistently causes this weight loss in a short time frame may not be ethical if not for the potential of weight loss in humans.

Bone Response

We did not expect an increase in femoral mid-shaft BMD due to casting during mechanical unloading, but this may have been a result of initial significant differences between left and right leg in the vehicle group. Femoral mid-shaft bone mineral content (BMC) reductions were expected, as were increases in BMC upon reloading[308, 309]. Semaglutide did not affect BMD or BMC of the spine, though unloading induced small magnitude reductions of both measures. Human studies have shown decreased aBMD in the lumbar spine, but this occurred in conjunction with substantial weight loss[207]. Given the lack of weight loss, our BMD and BMC results are

consistent with our current understanding of systemic bone loss during unloading, which is unlikely to induce significant changes in the lumbar spine over 14 days of partial unloading.

MicroCT analysis of the mid-femur diaphysis yielded conflicting results compared to the current literature using the same model. Cortical bone of the casted leg was not as affected by unloading as seen in a previous study on casting, though that study used 3 weeks of unloading[289]. Our study also had a larger sample size (n=9-10 vs n=3-5), so it is possible there was an issue with the statistical power of the previous research. We also saw the main effects of casting x reloading on Ct. Th and Ct.Ar/T.Ar, which both increased after reloading. This is consistent with the mechanical loading of tissue. TMD was affected by the interaction between casting x Semaglutide treatment.

MicroCT analysis of trabecular bone was consistent with our expectations, with responses to unloading consistent with previous studies: BV/TV, BMD, Tb.N, and Tb.Th were significantly reduced due to the main effect of casting in the distal femoral metaphysis and epiphysis due to casting [289]. Tb.Sp was also significantly increased in both regions, consistent with previous literature [289]. Surprisingly, only Tb.Th was fully recovered with subsequent reloading in the metaphysis, though BV/TV, BMD, Tb.Th, recovered via reloading in the epiphysis. Meng et al. found that bone mass and strength were increased in GPL-1RA-treated rats and suspected the PKA/beta-catenin pathway. This could be rat-specific, or because of ex-4 vs Semaglutide. They also unloaded for 28 days, while we only unloaded for 14 days [192]. We also saw no changes in expression of PKA-regulating genes (Prkc, Prkar1a, etc.) [310] or other Wnt/beta-catenin-related genes in the tibias of Semaglutide-treated mice versus controls.

Mechanical Properties of Cortical Bone

Casting affected the femur's mechanical properties, increasing post-yield and fracture displacement and reducing fracture load. This is expected due to the reduction in BMC measured in the DEXA analysis. Semaglutide reduced the yield load and energy to yield, as well as the max load and trends in fracture load, which was surprising given the lack of BMD or BMC reduction attributed to Semaglutide treatment in our DEXA analysis.

Circulating Markers

Serum bone formation and resorption markers were consistent with previous studies [259] and unloading literature [239, 311, 312]. However, current understanding of the effect of GLP-1RAs on bone formation and resorption is conflicting in rodent and human studies [206, 207, 313]. Human studies on patients with high fracture risk resulted in no bone formation marker changes and an increase in bone resorption markers[207], which is consistent with our study. Studies that note bone maintenance involve diabetic models or are used in conjunction with weight loss, which is not consistent with our model or results, therefore it is not possible to make a direct comparison. A study performed on a diabetic rat model cites anabolic effects of liraglutide on bone[313]. Iepsen et. al discussed increased bone formation and decreased bone loss in humans, but focused on BMC, not BMD, in patients undergoing weight loss and liraglutide treatment [206]. These studies also use liraglutide, which may affect bone growth and resorption differently than Semaglutide, given its much shorter half-life. The possible interaction between unloading and Semaglutide use on increasing bone resorption markers warrants further exploration.

Bone Gene Expression

Only five genes were differentially expressed in the tibias from unloaded legs of Semaglutide-treated mice compared to unloaded vehicle-treated mice. Four were upregulated: Dbp, Clec3a, Dpt, and HtrA4. Dbp stabilizes vitamin D availability, allowing for consistent vitamin D utilization required for bone homeostasis [314]. Clec3a is involved in chondrogenesis and osteogenesis and may be upregulated in osteosarcoma tissue [315, 316]. Dpt upregulation may repress papillary thyroid cancers [317], though Semaglutide treatment is contraindicated explicitly in those at risk for these cancers, given their high occurrence in rodent models [231, 232]. Dpt also triggers osteogenic differentiation in human periodontal ligament stem cells [318], and could have a similar effect in MSCs. Dpt gene silencing has also been suggested to treat osteosarcoma [319], so whether upregulation is beneficial or detrimental is yet to be seen. HtrA4 expression in mice has not been specifically identified[320]. However, HtrA4 is significantly elevated in the placentas of women with pre-eclampsia [321]. Pregnancy is contraindicated with GLP-1RA treatment, given the adverse effects on fetal growth [231, 232], but this is another possible adverse side effect that could be explored to better understand the role of HtrA4.

Zbtb16 was downregulated in the bone tissue from unloaded legs in Semaglutide-treated mice. Zbtb16 regulates many stages of bone development, including the osteogenesis of MSCs [322, 323]. Reductions in Zbtb16 expression reduces osteogenic differentiation, resulting in osteoporosis [324]. As such, Zbtb16 has seen interest as a target to prevent and reverse osteoporosis [324]. Therefore, downregulation of this gene expression is worrying, as patients taking Semaglutide for T2D and weight loss are already at risk of reduced bone mass. This must be thoroughly investigated to protect patients from this life-altering bone disease.

Tendon Response

Tendon mechanics were altered during unloading, which is in contrast with our previous study investigating the effects of alendronate during unloading, which did not show a change in Young's modulus or force at MTL in Achilles tendons during mechanical unloading. Our study using alendronate during unloading did not indicate a change in Young's modulus or force at MTL in Achilles tendons during mechanical unloading. However, these changes are apparent in human tendons during disuse [325-327]. Our aforementioned study used a tail suspension hindlimb unloading model (HLU) instead of a single-leg casting immobilization model. The position or restraint of the ankle may have restricted both load and movement of the tendon when compared the freedom of ankle movement without load in the HLU model. This could explain the decrease in E during casting due to casting and subsequent increase in E and ultimate stress in reloaded mouse groups, attributed to the main effects of casting and reloading. Increases in Achilles tendon cross-sectional area (CSA) during unloading were expected, as observed previously [326].

Muscle Response

We were somewhat surprised to see increased muscle loss with Semaglutide treatment and casting without concurrent treatment-induced weight loss. Additionally, it was unexpected to see the interaction of reloading and Semaglutide treatment resulting in an increase in muscle mass in reloaded animals compared to unloaded animals. Though we initially expected weight loss to reduce muscle size during and after unloading, the noted anabolic effects of Semaglutide on muscle are supported by our observations [213, 328-330]. We identified decreased levels of myostatin gene expression in Semaglutide-treated mice during immobilization, a trend that may have continued after the cast was removed. Myostatin is a key regulator of muscle mass [247, 248], so

a decreased expression in Semaglutide treatment could contribute to heightened muscle growth after reloading. However, this expression is paradoxical for our unloading results. Therefore, other factors must play into the muscle atrophy caused by Semaglutide treatment during mechanical unloading.

The observed changes in plantaris muscle protein concentrations somewhat align with previous research regarding protein concentrations during muscle growth and atrophy. Notably, it supports the counterintuitive finding in current studies that upregulation in catabolic proteins occurs during muscle maintenance and downregulation in anabolic proteins occurs during muscle regrowth [331-334]. For example, REDD1 is traditionally thought of as a driver of muscle atrophy[335] with glucocorticoid-dependent expression that may have increased during the stress of casting. However, REDD1 may also act as a regulator of muscle mass based on energy availability. In this case, the increase in REDD1 expression during casting-induced muscle loss could be due to adaptations meant to maintain muscle mass by reducing in energy requirements[336]. These counterintuitive responses could be due to increased muscle remodeling as a response to changes in mechanical stimulus during unloading and reloading.

Gene ontology analysis identified several critical biological processes with significant levels of differentially expressed genes. Of these, the regulation of bone development is of particular interest given the scope of this study. In addition to Zbtb16, which has been discussed previously, the following factors are negatively expressed in Semaglutide-treated soleus muscles from casted limbs:

Sema4d is a pro-inflammatory regulator [337] that also plays a role in bone homeostasis [338] and is highly expressed in tumor cells[339]. Downregulation of this gene could result in beneficial musculoskeletal outcomes. Atg9a is necessary for autophagy, or the removal of damaged organelles and proteins [340]. This is required for proper tissue remodeling. Atg9a expression is increased as lean and fat mass increase, so it may also be reduced in periods of weight or tissue loss, including the reductions observed in the soleus muscle tissue [341]. However, this study did not observe weight loss, so the mechanism must be different. ALPL encodes for tissue-nonspecific alkaline phosphatase (TNSALP), a key component for proper mineralization of bone[342]. Decreased ALPL expression can cause Hypophosphatasia, characterized by bone weakness and fragility, stunted bone growth, muscle weakness, seizures, and other effects from vitamin B6 deficiency [343, 344]. Reductions in ALPL could cause long-term musculoskeletal complications, especially where reduced dietary intake due to GLP-1RA-related hunger suppression may have already decreased vitamin B6 intake and absorption. Finally, we observed an increase in Ogn expression. Ogn encodes for osteoglycin, or mimecan, which is produced by myoblastic cells and regulates osteoblast differentiation[345]. It is a potent muscle-bone crosstalk agent for osteoblast differentiation through the RUNX2 pathway [345]. Interestingly, downregulation of Ogn has also been implicated in glucose-induced T2D osteoporosis[346], so this increase in osteoglycin crosstalk may explain why reduced Zbtb16 downregulation does not result in short-term bone loss. The altered expression of these essential musculoskeletal genes could pose long-term issues for patients taking Semaglutide, with or without weight loss. However, given the beneficial and negative effects that likely occur from these alterations, more research will need to be conducted to assess overall positive or negative impacts of these changes on musculoskeletal health during long-term treatment.

5. Conclusions

This study established the adverse effects of Semaglutide treatment on musculoskeletal tissue during mechanical unloading and reloading without weight loss. More investigation into the impacts of Semaglutide treatment on relevant bone and muscle gene expression changes, especially Zbtb16, needs to be conducted. Additionally, weight loss must still be investigated with unloading studies, especially given the muscle loss without weight loss seen in this study. These investigations will help prevent long-term bone and muscle degradation issues associated with Semaglutide treatment in a growing population of GLP-1RA-treated patients.

Acknowledgements

This research was supported by the NIH NIAMS (R01 AR071459). Sophie V Orr was supported by the UC Davis Graduate Research Mentorship Fellowship. Natalie Kori Gilmore was supported by the UC Davis T32 in Pharmacology (T32 GM144303).

Chapter 4: Dissertation Summary

Periods of mechanical unloading remains a concern for musculoskeletal health across the lifespan. The occurrence of unloading can happen to patients of all ages, many of whom are taking medications for other conditions. This dissertation explored the interactions between mechanical unloading, age, and pharmaceutical usage that impacts these patients.

In the first study, we demonstrated that bone morphology changes in response to 14 days of mechanical unloading and bisphosphonate use changed throughout the lifespan. We also noted differences in bone-muscle crosstalk cytokines across the lifespan. Muscle weights decreased with unloading and were not rescued with bisphosphonate treatment, whereas myostatin concentrations were increased with alendronate in young animals, contradicting our hypothesis that maintaining bone would facilitate muscle maintenance. Myostatin concentrations were most notably modified in young animals, while and TGF-β was modified in older animals. TGF-β may be an important bone-muscle crosstalk driver of muscle atrophy, but only in older animals, where concentrations were negatively correlated with bone volume. These results indicate the importance of different age models for unloading studies depending on the target audience for therapeutics.

In the second study, we found that Semaglutide treatment increased muscle atrophy in limbs that were unloaded for 14 days but did not affect bone morphology. This atrophy occurred without weight loss in female mice fed standard chow. However, circulating bone resorption markers were significantly increased, suggesting a possible long-term effect that was not captured at the observed timepoint. 14 days of mechanical reloading also successfully recovered the observed musculoskeletal atrophy. Bulk RNAseq analysis showed reductions in several bone development

genes, including zbtb16, which is important for preventing osteoporosis. Additionally, we observed an increase in the Ogn gene which encodes for osteoglycin, an important muscle-bone crosstalk myokine that promotes osteoblast differentiation. These findings have interesting implications for the future of Semaglutide use and warrant further research to prevent unintended harm to musculoskeletal tissues during treatment.

Together these studies show a need for further investigation into the effect of pharmaceutical use during periods of mechanical unloading, especially in at-risk populations, such as older adults and those undergoing rapid weight loss. They also show that biological bone-muscle crosstalk may influence tissue health during unloading differently as a function of pharmaceutical use and age. Further investigation into these topics will be needed to reduce unintended harms of pharmaceutical treatments on musculoskeletal health.

References

1. Qin, L., et al., *Molecular mechanosensors in osteocytes.* Bone Research, 2020. **8**(1): p. 23.
2. Bonewald, L.F., *The amazing osteocyte.* Journal of Bone and Mineral Research, 2011. **26**(2): p. 229-238.
3. Yellowley, C.E., et al., *Functional gap junctions between osteocytic and osteoblastic cells.* J Bone Miner Res, 2000. **15**(2): p. 209-17.
4. Maciel, G.B.M., R.M. Maciel, and C.C. Danesi, *Bone cells and their role in physiological remodeling.* Molecular Biology Reports, 2023. **50**(3): p. 2857-2863.
5. Roodman, G.D., *Cell biology of the osteoclast.* Experimental Hematology, 1999. **27**(8): p. 1229-1241.
6. Boyle, W.J., W.S. Simonet, and D.L. Lacey, *Osteoclast differentiation and activation.* Nature, 2003. **423**(6937): p. 337-342.
7. Väänänen, H.K., et al., *The cell biology of osteoclast function.* Journal of Cell Science, 2000. **113**(3): p. 377-381.
8. Ainola, M., *Pannus invasion into cartilage and bone in rheumatoid arthritis.*
9. HADJIDAKIS, D.J. and I.I. ANDROULAKIS, *Bone Remodeling.* Annals of the New York Academy of Sciences, 2006. **1092**(1): p. 385-396.
10. Eriksen, E.F., *Cellular mechanisms of bone remodeling.* Reviews in Endocrine and Metabolic Disorders, 2010. **11**: p. 219-227.
11. van Bezooijen, R.L., et al., *Sclerostin is an osteocyte-expressed negative regulator of bone formation, but not a classical BMP antagonist.* J Exp Med, 2004. **199**(6): p. 805-14.
12. Winkler, D.G., et al., *Osteocyte control of bone formation via sclerostin, a novel BMP antagonist.* Embo j, 2003. **22**(23): p. 6267-76.
13. French, A., *Mechanotransduction.* Annual review of physiology, 1992. **54**(1): p. 135-152.
14. Duncan, R.L. and C.H. Turner, *Mechanotransduction and the functional response of bone to mechanical strain.* Calcified Tissue International, 1995. **57**(5): p. 344-358.
15. Stewart, S., et al., *Mechanotransduction in osteogenesis.* Bone Joint Res, 2020. **9**(1): p. 1-14.
16. Li, M.C.M., et al., *The role of osteocytes-specific molecular mechanism in regulation of mechanotransduction – A systematic review.* Journal of Orthopaedic Translation, 2021. **29**: p. 1-9.
17. Hart, N.H., et al., *Mechanical basis of bone strength: influence of bone material, bone structure and muscle action.* J Musculoskelet Neuronal Interact, 2017. **17**(3): p. 114-139.
18. Bertram, J.E. and A.A. Biewener, *Bone curvature: sacrificing strength for load predictability?* J Theor Biol, 1988. **131**(1): p. 75-92.
19. Rubin, C.T. and L.E. Lanyon, *Regulation of bone mass by mechanical strain magnitude.* Calcif Tissue Int, 1985. **37**(4): p. 411-7.
20. Hughes, J., et al., *The role of adaptive bone formation in the etiology of stress fracture.* Experimental Biology and Medicine, 2016. **242**.
21. Turner, C.H. and M.R. Forwood, *What role does the osteocyte network play in bone adaptation?* Bone, 1995. **16**(3): p. 283-285.

22. Weinbaum, S., S.C. Cowin, and Y. Zeng, *A model for the excitation of osteocytes by mechanical loading-induced bone fluid shear stresses.* Journal of Biomechanics, 1994. **27**(3): p. 339-360.
23. You, L., et al., *A model for strain amplification in the actin cytoskeleton of osteocytes due to fluid drag on pericellular matrix.* Journal of Biomechanics, 2001. **34**(11): p. 1375-1386.
24. Shapiro, F., et al., *Transmission electron microscopic demonstration of vimentin in rat osteoblast and osteocyte cell bodies and processes using the immunogold technique.* The Anatomical Record, 1995. **241**(1): p. 39-48.
25. Fiori, M.C., et al., *Inhibition by Commercial Aminoglycosides of Human Connexin Hemichannels Expressed in Bacteria.* Molecules, 2017. **22**(12): p. 2063.
26. Genetos, D.C., et al., *Oscillating fluid flow activation of gap junction hemichannels induces ATP release from MLO-Y4 osteocytes.* J Cell Physiol, 2007. **212**(1): p. 207-14.
27. Hoey, D.A., D.J. Kelly, and C.R. Jacobs, *A role for the primary cilium in paracrine signaling between mechanically stimulated osteocytes and mesenchymal stem cells.* Biochem Biophys Res Commun, 2011. **412**(1): p. 182-7.
28. Hoey, D.A., et al., *Primary Cilia-Mediated Mechanotransduction in Human Mesenchymal Stem Cells.* Stem Cells, 2012. **30**(11): p. 2561-2570.
29. Norvell, S.M., et al., *Fluid shear stress induces beta-catenin signaling in osteoblasts.* Calcif Tissue Int, 2004. **75**(5): p. 396-404.
30. Arnsdorf, E.J., P. Tummala, and C.R. Jacobs, *Non-canonical Wnt signaling and N-cadherin related beta-catenin signaling play a role in mechanically induced osteogenic cell fate.* PLoS One, 2009. **4**(4): p. e5388.
31. Duan, P. and L.F. Bonewald, *The role of the wnt/β-catenin signaling pathway in formation and maintenance of bone and teeth.* Int J Biochem Cell Biol, 2016. **77**(Pt A): p. 23-29.
32. Komiya, Y. and R. Habas, *Wnt signal transduction pathways.* Organogenesis, 2008. **4**(2): p. 68-75.
33. Wang, B., et al., *Focal adhesion kinase signaling pathway is involved in mechanotransduction in MG-63 Cells.* Biochemical and Biophysical Research Communications, 2011. **410**(3): p. 671-676.
34. Kusumi, A., et al., *Regulation of synthesis of osteoprotegerin and soluble receptor activator of nuclear factor-kappaB ligand in normal human osteoblasts via the p38 mitogen-activated protein kinase pathway by the application of cyclic tensile strain.* J Bone Miner Metab, 2005. **23**(5): p. 373-81.
35. Adachi, T., et al., *Calcium response in single osteocytes to locally applied mechanical stimulus: Differences in cell process and cell body.* Journal of Biomechanics, 2009. **42**(12): p. 1989-1995.
36. Hung, C.T., et al., *Real-time calcium response of cultured bone cells to fluid flow.* Clin Orthop Relat Res, 1995(313): p. 256-69.
37. Cherian, P.P., et al., *Mechanical strain opens connexin 43 hemichannels in osteocytes: a novel mechanism for the release of prostaglandin.* Mol Biol Cell, 2005. **16**(7): p. 3100-6.
38. L. Harris, A., *Emerging issues of connexin channels: biophysics fills the gap.* Quarterly Reviews of Biophysics, 2001. **34**(3): p. 325-472.
39. Harris, A.L., *Connexin channel permeability to cytoplasmic molecules.* Prog Biophys Mol Biol, 2007. **94**(1-2): p. 120-43.

40. Plotkin, L.I. and T. Bellido, *Beyond gap junctions: Connexin43 and bone cell signaling.* Bone, 2013. **52**(1): p. 157-66.
41. Plotkin, L.I., S.C. Manolagas, and T. Bellido, *Transduction of Cell Survival Signals by Connexin-43 Hemichannels *.* Journal of Biological Chemistry, 2002. **277**(10): p. 8648-8657.
42. Frost, H.M., *A 2003 Update of Bone Physiology and Wolff's Law for Clinicians.* The Angle Orthodontist, 2004. **74**(1): p. 3-15.
43. Frost, H.M., *Bone's mechanostat: A 2003 update.* The Anatomical Record Part A: Discoveries in Molecular, Cellular, and Evolutionary Biology, 2003. **275A**(2): p. 1081-1101.
44. Frost, H.M., *Perspectives: A proposed general model of the "mechanostat" (suggestions from a new skeletal-biologic paradigm).* The Anatomical Record, 1996. **244**(2): p. 139-147.
45. Frost, H.M., *Bone "mass" and the "mechanostat": A proposal.* The Anatomical Record, 1987. **219**(1): p. 1-9.
46. Skedros, J.G., M.W. Mason, and R.D. Bloebaum, *Modeling and remodeling in a developing artiodactyl calcaneus: A model for evaluating Frost's Mechanostat hypothesis and its corollaries.* The Anatomical Record, 2001. **263**(2): p. 167-185.
47. Lanyon, L.E. and C.T. Rubin, *Static vs dynamic loads as an influence on bone remodelling.* Journal of Biomechanics, 1984. **17**(12): p. 897-905.
48. Morey-Holton, E.R. and R.K. Globus, *Hindlimb unloading rodent model: technical aspects.* Journal of Applied Physiology, 2002. **92**(4): p. 1367-1377.
49. Globus, R.K. and E. Morey-Holton, *Hindlimb unloading: rodent analog for microgravity.* J Appl Physiol (1985), 2016. **120**(10): p. 1196-206.
50. Gotti, C., et al., *Hierarchical fibrous structures for muscle-inspired soft-actuators: A review.* Applied Materials Today, 2020. **20**: p. 100772.
51. Mirzoev, T.M., *Mechanotransduction for Muscle Protein Synthesis via Mechanically Activated Ion Channels.* Life (Basel), 2023. **13**(2).
52. Nakamichi, R. and H. Asahara, *The role of mechanotransduction in tendon.* J Bone Miner Res, 2024. **39**(7): p. 814-820.
53. Lavagnino, M., et al., *Tendon mechanobiology: Current knowledge and future research opportunities.* J Orthop Res, 2015. **33**(6): p. 813-22.
54. Burkholder, T.J., *Mechanotransduction in skeletal muscle.* Frontiers in bioscience: a journal and virtual library, 2007. **12**: p. 174.
55. Hill, M.A., et al., *Invited review: arteriolar smooth muscle mechanotransduction: Ca2+ signaling pathways underlying myogenic reactivity.* Journal of applied physiology, 2001. **91**(2): p. 973-983.
56. Yasuda, H., *RANKL, a necessary chance for clinical application to osteoporosis and cancer-related bone diseases.* World J Orthop, 2013. **4**(4): p. 207-17.
57. Ono, T., et al., *RANKL biology: bone metabolism, the immune system, and beyond.* Inflammation and Regeneration, 2020. **40**(1): p. 2.
58. Sobacchi, C., et al., *Osteoclast-poor human osteopetrosis due to mutations in the gene encoding RANKL.* Nat Genet, 2007. **39**(8): p. 960-2.

59. Guerrini, M.M., et al., *Human osteoclast-poor osteopetrosis with hypogammaglobulinemia due to TNFRSF11A (RANK) mutations.* The American journal of human genetics, 2008. **83**(1): p. 64-76.
60. Rahnert, J., et al., *The role of nitric oxide in the mechanical repression of RANKL in bone stromal cells.* Bone, 2008. **43**(1): p. 48-54.
61. Smalt, R., et al., *Induction of NO and prostaglandin E2 in osteoblasts by wall-shear stress but not mechanical strain.* Am J Physiol, 1997. **273**(4): p. E751-8.
62. Rubin, J., et al., *Activation of extracellular signal-regulated kinase is involved in mechanical strain inhibition of RANKL expression in bone stromal cells.* J Bone Miner Res, 2002. **17**(8): p. 1452-60.
63. Kajiya, M., et al., *Role of periodontal pathogenic bacteria in RANKL-mediated bone destruction in periodontal disease.* Journal of oral microbiology, 2010. **2**(1): p. 5532.
64. Khosla, S., *Minireview: The OPG/RANKL/RANK System.* Endocrinology, 2001. **142**(12): p. 5050-5055.
65. Melsen, B., *Biological reaction of alveolar bone to orthodontic tooth movement.* Angle Orthod, 1999. **69**(2): p. 151-8.
66. Melsen, B., *Tissue reaction to orthodontic tooth movement--a new paradigm.* Eur J Orthod, 2001. **23**(6): p. 671-81.
67. Huang, J.C., et al., *PTH differentially regulates expression of RANKL and OPG.* J Bone Miner Res, 2004. **19**(2): p. 235-44.
68. Wijenayaka, A.R., et al., *Sclerostin stimulates osteocyte support of osteoclast activity by a RANKL-dependent pathway.* PLoS One, 2011. **6**(10): p. e25900.
69. Sanchez, C., et al., *Mechanical loading highly increases IL-6 production and decreases OPG expression by osteoblasts.* Osteoarthritis and Cartilage, 2009. **17**(4): p. 473-481.
70. Manolagas, S.C. and R.L. Jilka, *Bone marrow, cytokines, and bone remodeling—emerging insights into the pathophysiology of osteoporosis.* New England journal of medicine, 1995. **332**(5): p. 305-311.
71. Jacobs, C.R., et al., *Differential effect of steady versus oscillating flow on bone cells.* Journal of biomechanics, 1998. **31**(11): p. 969-976.
72. Piekarski, K. and M. Munro, *Transport mechanism operating between blood supply and osteocytes in long bones.* Nature, 1977. **269**(5623): p. 80-82.
73. Kim, C.H., et al., *Oscillatory fluid flow-induced shear stress decreases osteoclastogenesis through RANKL and OPG signaling.* Bone, 2006. **39**(5): p. 1043-1047.
74. Massagué, J., *The transforming growth factor-beta family.* Annu Rev Cell Biol, 1990. **6**: p. 597-641.
75. Chin, D., et al., *What is transforming growth factor-beta (TGF-beta)?* Br J Plast Surg, 2004. **57**(3): p. 215-21.
76. Chaudhury, A. and P.H. Howe, *The tale of transforming growth factor-beta (TGFbeta) signaling: a soigné enigma.* IUBMB Life, 2009. **61**(10): p. 929-39.
77. Gentry, L.E., et al., *Molecular events in the processing of recombinant type 1 pre-pro-transforming growth factor beta to the mature polypeptide.* Mol Cell Biol, 1988. **8**(10): p. 4162-8.
78. Yang, T., et al., *E-selectin ligand 1 regulates bone remodeling by limiting bioactive TGF-β in the bone microenvironment.* Proc Natl Acad Sci U S A, 2013. **110**(18): p. 7336-41.

79. Tang, Y., et al., *TGF-beta1-induced migration of bone mesenchymal stem cells couples bone resorption with formation.* Nat Med, 2009. **15**(7): p. 757-65.
80. Dallas, S.L., et al., *Characterization and autoregulation of latent transforming growth factor beta (TGF beta) complexes in osteoblast-like cell lines. Production of a latent complex lacking the latent TGF beta-binding protein.* J Biol Chem, 1994. **269**(9): p. 6815-21.
81. Kubiczkova, L., et al., *TGF-β – an excellent servant but a bad master.* Journal of Translational Medicine, 2012. **10**(1): p. 183.
82. Bernasconi, P., et al., *Expression of transforming growth factor-beta 1 in dystrophic patient muscles correlates with fibrosis. Pathogenetic role of a fibrogenic cytokine.* J Clin Invest, 1995. **96**(2): p. 1137-44.
83. Shehata, M., et al., *TGF-beta1 induces bone marrow reticulin fibrosis in hairy cell leukemia.* J Clin Invest, 2004. **113**(5): p. 676-85.
84. Campos-Xavier, B., et al., *Phenotypic variability at the TGF-beta1 locus in Camurati-Engelmann disease.* Hum Genet, 2001. **109**(6): p. 653-8.
85. Kinoshita, A., et al., *Domain-specific mutations in TGFB1 result in Camurati-Engelmann disease.* Nat Genet, 2000. **26**(1): p. 19-20.
86. Klein-Nulend, J., et al., *Mechanical loading stimulates the release of transforming growth factor-β activity by cultured mouse calvariae and periosteal cells.* Journal of Cellular Physiology, 1995. **163**(1): p. 115-119.
87. Monteiro, D.A., et al., *Fluid shear stress generates a unique signaling response by activating multiple TGFβ family type I receptors in osteocytes.* Faseb j, 2021. **35**(3): p. e21263.
88. Bravenboer, N., et al., *The effect of exercise on systemic and bone concentrations of growth factors in rats.* Journal of Orthopaedic Research, 2001. **19**(5): p. 945-949.
89. Clarke, K.A., *Differential fore- and hindpaw force transmission in the walking rat.* Physiol Behav, 1995. **58**(3): p. 415-9.
90. Elliott, B., et al., *The central role of myostatin in skeletal muscle and whole body homeostasis.* Acta Physiologica, 2012. **205**(3): p. 324-340.
91. Han, H.Q. and W.E. Mitch, *Targeting the myostatin signaling pathway to treat muscle wasting diseases.* Curr Opin Support Palliat Care, 2011. **5**(4): p. 334-41.
92. Kitajima, Y., K. Yoshioka, and N. Suzuki, *The ubiquitin–proteasome system in regulation of the skeletal muscle homeostasis and atrophy: from basic science to disorders.* The Journal of Physiological Sciences, 2020. **70**(1): p. 40.
93. Khalil, R., *Ubiquitin-Proteasome Pathway and Muscle Atrophy.* Adv Exp Med Biol, 2018. **1088**: p. 235-248.
94. Bonewald, L., *Use it or lose it to age: A review of bone and muscle communication.* Bone, 2019. **120**: p. 212-218.
95. Brotto, M. and L. Bonewald, *Bone and muscle: Interactions beyond mechanical.* Bone, 2015. **80**: p. 109-114.
96. Brotto, M. and M.L. Johnson, *Endocrine crosstalk between muscle and bone.* Current osteoporosis reports, 2014. **12**(2): p. 135-141.
97. He, C., et al., *Bone and Muscle Crosstalk in Aging.* Frontiers in Cell and Developmental Biology, 2020. **8**.

98. Maurel, D.B., K. Jähn, and N. Lara-Castillo, *Muscle-Bone Crosstalk: Emerging Opportunities for Novel Therapeutic Approaches to Treat Musculoskeletal Pathologies.* Biomedicines, 2017. **5**(4): p. 62.
99. Tagliaferri, C., et al., *Muscle and bone, two interconnected tissues.* Ageing Research Reviews, 2015. **21**: p. 55-70.
100. Burks, T.N. and R.D. Cohn, *Role of TGF-β signaling in inherited and acquired myopathies.* Skeletal Muscle, 2011. **1**(1): p. 19.
101. Waning, D.L., et al., *Excess TGF-β mediates muscle weakness associated with bone metastases in mice.* Nat Med, 2015. **21**(11): p. 1262-1271.
102. Pin, F., L.F. Bonewald, and A. Bonetto, *Role of myokines and osteokines in cancer cachexia.* Exp Biol Med (Maywood), 2021. **246**(19): p. 2118-2127.
103. Panizo, S., et al., *RANKL Increases Vascular Smooth Muscle Cell Calcification Through a RANK-BMP4–Dependent Pathway.* Circulation Research, 2009. **104**(9): p. 1041-1048.
104. Dufresne, S.S., et al., *Muscle RANK is a key regulator of Ca2+ storage, SERCA activity, and function of fast-twitch skeletal muscles.* American Journal of Physiology-Cell Physiology, 2016. **310**(8): p. C663-C672.
105. Bonnet, N., et al., *RANKL inhibition improves muscle strength and insulin sensitivity and restores bone mass.* The Journal of clinical investigation, 2019. **129**(8): p. 3214-3223.
106. Hamoudi, D., et al., *An anti-RANKL treatment reduces muscle inflammation and dysfunction and strengthens bone in dystrophic mice.* Human Molecular Genetics, 2019. **28**(18): p. 3101-3112.
107. Xiong, J., et al., *RANKL Mediates Muscle Atrophy and Dysfunction in a Cigarette Smoke–induced Model of Chronic Obstructive Pulmonary Disease.* American Journal of Respiratory Cell and Molecular Biology, 2021. **64**(5): p. 617-628.
108. Lu, W., et al., *The Role of Osteokines in Sarcopenia: Therapeutic Directions and Application Prospects.* Frontiers in Cell and Developmental Biology, 2021. **9**.
109. Marcadet, L., et al., *The Roles of RANK/RANKL/OPG in Cardiac, Skeletal, and Smooth Muscles in Health and Disease.* Front Cell Dev Biol, 2022. **10**: p. 903657.
110. Pin, F., et al., *RANKL Blockade Reduces Cachexia and Bone Loss Induced by Non-Metastatic Ovarian Cancer in Mice.* Journal of Bone and Mineral Research, 2022. **37**(3): p. 381-396.
111. Buehring, B. and N. Binkley, *Myostatin--the holy grail for muscle, bone, and fat?* Curr Osteoporos Rep, 2013. **11**(4): p. 407-14.
112. Lee, S.-J., et al., *Targeting myostatin/activin A protects against skeletal muscle and bone loss during spaceflight.* Proceedings of the National Academy of Sciences, 2020. **117**(38): p. 23942-23951.
113. Omosule, C.L. and C.L. Phillips, *Deciphering Myostatin's Regulatory, Metabolic, and Developmental Influence in Skeletal Diseases.* Frontiers in Genetics, 2021. **12**(453).
114. Chan, A.S.M., et al., *Bone Geometry Is Altered by Follistatin-Induced Muscle Growth in Young Adult Male Mice.* JBMR Plus, 2021. **5**(4): p. e10477.
115. Elkasrawy, M.N. and M.W. Hamrick, *Myostatin (GDF-8) as a key factor linking muscle mass and bone structure.* J Musculoskelet Neuronal Interact, 2010. **10**(1): p. 56-63.

116. Barreto, R., et al., *ACVR2B/Fc counteracts chemotherapy-induced loss of muscle and bone mass.* Sci Rep, 2017. **7**(1): p. 14470.
117. Porras, A.G., S.D. Holland, and B.J. Gertz, *Pharmacokinetics of Alendronate.* Clinical Pharmacokinetics, 1999. **36**(5): p. 315-328.
118. Rodan, G.A., *Bone mass homeostasis and bisphosphonate action.* Bone, 1997. **20**(1): p. 1-4.
119. Sato, M., et al., *Bisphosphonate action. Alendronate localization in rat bone and effects on osteoclast ultrastructure.* The Journal of Clinical Investigation, 1991. **88**(6): p. 2095-2105.
120. Essex, A.L., et al., *Bisphosphonate Treatment Ameliorates Chemotherapy-Induced Bone and Muscle Abnormalities in Young Mice.* Front Endocrinol (Lausanne), 2019. **10**: p. 809.
121. Veilleux, L.N., P. Trejo, and F. Rauch, *Muscle abnormalities in osteogenesis imperfecta.* J Musculoskelet Neuronal Interact, 2017. **17**(2): p. 1-7.
122. Leblanc, A., et al., *Bisphosphonates as a supplement to exercise to protect bone during long-duration spaceflight.* Osteoporos Int, 2013. **24**(7): p. 2105-14.
123. Hughes, D.E., et al., *Bisphosphonates promote apoptosis in murine osteoclasts in vitro and in vivo.* J Bone Miner Res, 1995. **10**(10): p. 1478-87.
124. Fisher, J.E., et al., *Alendronate mechanism of action: geranylgeraniol, an intermediate in the mevalonate pathway, prevents inhibition of osteoclast formation, bone resorption, and kinase activation in vitro.* Proc Natl Acad Sci U S A, 1999. **96**(1): p. 133-8.
125. Rodan, G., et al., *Bone safety of long-term bisphosphonate treatment.* Current medical research and opinion, 2004. **20**(8): p. 1291-1300.
126. Boyce, B.F., et al., *Apoptosis in bone cells*, in *Principles of bone biology*. 2002, Elsevier. p. 151-X.
127. Castellano, D., et al., *The role of RANK-ligand inhibition in cancer: the story of denosumab.* Oncologist, 2011. **16**(2): p. 136-45.
128. Tu, K.N., et al., *Osteoporosis: A Review of Treatment Options.* P t, 2018. **43**(2): p. 92-104.
129. Aditya, S. and A. Rattan, *Sclerostin Inhibition: A Novel Target for the Treatment of Postmenopausal Osteoporosis.* J Midlife Health, 2021. **12**(4): p. 267-275.
130. Tipton, D.A., B.A. Seshul, and M. Dabbous, *Effect of bisphosphonates on human gingival fibroblast production of mediators of osteoclastogenesis: RANKL, osteoprotegerin and interleukin-6.* J Periodontal Res, 2011. **46**(1): p. 39-47.
131. Dobnig, H., et al., *Changes in the RANK ligand/osteoprotegerin system are correlated to changes in bone mineral density in bisphosphonate-treated osteoporotic patients.* Osteoporos Int, 2006. **17**(5): p. 693-703.
132. Verde, M.E., et al., *Effect of Bisphosphonates on the Levels of Rankl and Opg in Gingival Crevicular Fluid of Patients With Periodontal Disease and Post-menopausal Osteoporosis.* Acta Odontol Latinoam, 2015. **28**(3): p. 215-21.
133. Kim, Y.H., G.S. Kim, and B. Jeong-Hwa, *Inhibitory action of bisphosphonates on bone resorption does not involve the regulation of RANKL and OPG expression.* Exp Mol Med, 2002. **34**(2): p. 145-51.
134. Seino, Y., M. Fukushima, and D. Yabe, *GIP and GLP-1, the two incretin hormones: Similarities and differences.* Journal of Diabetes Investigation, 2010. **1**(1-2): p. 8-23.

135. Drucker, D.J., *Biological actions and therapeutic potential of the glucagon-like peptides.* Gastroenterology, 2002. **122**(2): p. 531-544.
136. Giacco, F. and M. Brownlee, *Mechanisms of hyperglycemic damage in diabetes.* Atlas of Diabetes: Fourth Edition, 2011: p. 217-231.
137. Giugliano, D., A. Ceriello, and K. Esposito, *Glucose metabolism and hyperglycemia.* The American journal of clinical nutrition, 2008. **87**(1): p. 217S-222S.
138. Ryu, T.Y., J. Park, and P.E. Scherer, *Hyperglycemia as a risk factor for cancer progression.* Diabetes & metabolism journal, 2014. **38**(5): p. 330.
139. Laakso, M., *Hyperglycemia and cardiovascular disease in type 2 diabetes.* Diabetes, 1999. **48**(5): p. 937-942.
140. Schrijvers, B.F., A.S. De Vriese, and A. Flyvbjerg, *From hyperglycemia to diabetic kidney disease: the role of metabolic, hemodynamic, intracellular factors and growth factors/cytokines.* Endocrine reviews, 2004. **25**(6): p. 971-1010.
141. Sharma, K. and F.N. Ziyadeh, *Hyperglycemia and Diabetic Kidney Disease: The Case for Transforming Growth Factor–β as a Key Mediator.* Diabetes, 1995. **44**(10): p. 1139-1146.
142. Malone, J.I., *Diabetic central neuropathy: CNS damage related to hyperglycemia.* Diabetes, 2016. **65**(2): p. 355-357.
143. Sima, A.A., H. Kamiya, and Z.G. Li, *Insulin, C-peptide, hyperglycemia, and central nervous system complications in diabetes.* European journal of pharmacology, 2004. **490**(1-3): p. 187-197.
144. Chiu, C.-J. and A. Taylor, *Dietary hyperglycemia, glycemic index and metabolic retinal diseases.* Progress in retinal and eye research, 2011. **30**(1): p. 18-53.
145. Garvey, W.T., et al., *The effect of insulin treatment on insulin secretion and insulin action in type II diabetes mellitus.* Diabetes, 1985. **34**(3): p. 222-234.
146. Matthaei, S., et al., *Pathophysiology and pharmacological treatment of insulin resistance.* Endocrine reviews, 2000. **21**(6): p. 585-618.
147. McCall, A.L., *Insulin therapy and hypoglycemia.* Endocrinology and Metabolism Clinics, 2012. **41**(1): p. 57-87.
148. Malouf, R. and J.C. Brust, *Hypoglycemia: causes, neurological manifestations, and outcome.* Annals of Neurology: Official Journal of the American Neurological Association and the Child Neurology Society, 1985. **17**(5): p. 421-430.
149. Arieff, A.I., et al., *Mechanisms of Seizures and Coma in Hypoglycemia Evidence for a direct effect of insulin on electrolyte transport in brain.* The Journal of Clinical Investigation, 1974. **54**(3): p. 654-663.
150. Ben-Ami, H., et al., *Drug-induced hypoglycemic coma in 102 diabetic patients.* Archives of internal medicine, 1999. **159**(3): p. 281-284.
151. Auer, R.N., *Hypoglycemic brain damage.* Forensic science international, 2004. **146**(2-3): p. 105-110.
152. Cryer, P.E., *Hypoglycemia, functional brain failure, and brain death.* The Journal of clinical investigation, 2007. **117**(4): p. 868-870.
153. Zoungas, S., et al., *Severe hypoglycemia and risks of vascular events and death.* New England Journal of Medicine, 2010. **363**(15): p. 1410-1418.
154. Unger, J. and C. Parkin, *Hypoglycemia in insulin-treated diabetes: a case for increased vigilance.* Postgraduate medicine, 2011. **123**(4): p. 81-91.

155. Verspohl, E.J., *Novel therapeutics for type 2 diabetes: Incretin hormone mimetics (glucagon-like peptide-1 receptor agonists) and dipeptidyl peptidase-4 inhibitors.* Pharmacology & Therapeutics, 2009. **124**(1): p. 113-138.
156. MENTLEIN, R., B. GALLWITZ, and W.E. SCHMIDT, *Dipeptidyl-peptidase IV hydrolyses gastric inhibitory polypeptide, glucagon-like peptide-1(7–36)amide, peptide histidine methionine and is responsible for their degradation in human serum.* European Journal of Biochemistry, 1993. **214**(3): p. 829-835.
157. Zheng, Z., et al., *Glucagon-like peptide-1 receptor: mechanisms and advances in therapy.* Signal Transduction and Targeted Therapy, 2024. **9**(1): p. 234.
158. Lau, J., et al., *Discovery of the once-weekly glucagon-like peptide-1 (GLP-1) analogue semaglutide.* Journal of medicinal chemistry, 2015. **58**(18): p. 7370-7380.
159. West, J., et al., *Are Glucagon-Like Peptide-1 (GLP-1) Receptor Agonists Central Nervous System (CNS) Penetrant: A Narrative Review.* Neurology and Therapy, 2025.
160. Prado, C.M., et al., *Muscle matters: the effects of medically induced weight loss on skeletal muscle.* The Lancet Diabetes & Endocrinology, 2024. **12**(11): p. 785-787.
161. Chaston, T.B., J. Dixon, and P.E. O'Brien, *Changes in fat-free mass during significant weight loss: a systematic review.* International journal of obesity, 2007. **31**(5): p. 743-750.
162. Conte, C., K.D. Hall, and S. Klein, *Is weight loss–induced muscle mass loss clinically relevant?* Jama, 2024. **332**(1): p. 9-10.
163. Uchiyama, S., et al., *Oral Semaglutide Induces Loss of Body Fat Mass Without Affecting Muscle Mass in Patients With Type 2 Diabetes.* J Clin Med Res, 2023. **15**(7): p. 377-383.
164. Severinsen, M.C.K. and B.K. Pedersen, *Muscle–Organ Crosstalk: The Emerging Roles of Myokines.* Endocrine Reviews, 2020. **41**(4): p. 594-609.
165. Rossi, A.P., et al., *Weight Cycling as a Risk Factor for Low Muscle Mass and Strength in a Population of Males and Females with Obesity.* Obesity (Silver Spring), 2019. **27**(7): p. 1068-1075.
166. Prado, C., et al., *Sarcopenic obesity: a critical appraisal of the current evidence.* Clinical nutrition, 2012. **31**(5): p. 583-601.
167. Godziuk, K., et al., *A critical review of weight loss recommendations before total knee arthroplasty.* Joint Bone Spine, 2021. **88**(2): p. 105114.
168. Cruz-Jentoft, A.J. and A.A. Sayer, *Sarcopenia.* The Lancet, 2019. **393**(10191): p. 2636-2646.
169. Morley, J.E., et al., *Sarcopenia With Limited Mobility: An International Consensus.* Journal of the American Medical Directors Association, 2011. **12**(6): p. 403-409.
170. Park, S.W., et al., *Accelerated loss of skeletal muscle strength in older adults with type 2 diabetes: the health, aging, and body composition study.* Diabetes care, 2007. **30**(6): p. 1507-1512.
171. Langlois, J., et al., *Weight loss from maximum body weight among middle-aged and older white women and the risk of hip fracture: the NHANES I epidemiologic follow-up study.* Osteoporosis international, 2001. **12**: p. 763-768.
172. Wing, R.R. and J.O. Hill, *SUCCESSFUL WEIGHT LOSS MAINTENANCE.* Annual Review of Nutrition, 2001. **21**(Volume 21, 2001): p. 323-341.

173. Compston, J.E., et al., *Effect of diet-induced weight loss on total body bone mass.* Clinical Science, 1992. **82**(4): p. 429-432.
174. Andersen, R.E., T.A. Wadden, and R.J. Herzog, *Changes in bone mineral content in obese dieting women.* Metabolism, 1997. **46**(8): p. 857-861.
175. Jensen, L.B., et al., *Bone mineral changes in obese women during a moderate weight loss with and without calcium supplementation.* Journal of Bone and Mineral Research, 2001. **16**(1): p. 141-147.
176. Shapses, S.A. and C.S. Riedt, *Bone, body weight, and weight reduction: what are the concerns?* J Nutr, 2006. **136**(6): p. 1453-6.
177. Shapses, S.A., et al., *Vitamin D supplementation and calcium absorption during caloric restriction: a randomized double-blind trial.* Am J Clin Nutr, 2013. **97**(3): p. 637-45.
178. Schafer, A.L., *Decline in Bone Mass During Weight Loss: A Cause for Concern?* Journal of Bone and Mineral Research, 2016. **31**(1): p. 36-39.
179. Weitzmann, M.N. and R. Pacifici, *Estrogen deficiency and bone loss: an inflammatory tale.* The Journal of clinical investigation, 2006. **116**(5): p. 1186-1194.
180. Frost, H.M., *On the estrogen–bone relationship and postmenopausal bone loss: a new model.* Journal of Bone and Mineral Research, 1999. **14**(9): p. 1473-1477.
181. Richelson, L.S., et al., *Relative contributions of aging and estrogen deficiency to postmenopausal bone loss.* New England Journal of Medicine, 1984. **311**(20): p. 1273-1275.
182. Liu, L. and C.J. Rosen, *New insights into calorie restriction induced bone loss.* Endocrinology and Metabolism, 2023. **38**(2): p. 203-213.
183. Von Thun, N.L., et al., *Does bone loss begin after weight loss ends? Results 2 years after weight loss or regain in postmenopausal women.* Menopause, 2014. **21**(5): p. 501-508.
184. Gleason, P.P., et al., *Real-world persistence and adherence to glucagon-like peptide-1 receptor agonists among obese commercially insured adults without diabetes.* Journal of Managed Care & Specialty Pharmacy, 2024. **30**(8): p. 860-867.
185. Montero, A.S., Grace; Presiado, Marley; Hamel, Liz, *KFF Health Tracking Poll May 2024: The Public's Use and Views of GLP-1 Drugs*. 2024.
186. Fogelholm, M., et al., *Association between weight cycling history and bone mineral density in premenopausal women.* Osteoporosis International, 1997. **7**: p. 354-358.
187. Beavers, K.M., et al., *Is lost lean mass from intentional weight loss recovered during weight regain in postmenopausal women?123.* The American Journal of Clinical Nutrition, 2011. **94**(3): p. 767-774.
188. Hinton, P.S., et al., *Weight-loss-associated changes in bone mineral density and bone turnover after partial weight regain with or without aerobic exercise in obese women.* European journal of clinical nutrition, 2012. **66**(5): p. 606-612.
189. Villalon, K.L., et al., *A losing battle: weight regain does not restore weight loss-induced bone loss in postmenopausal women.* Obesity, 2011. **19**(12): p. 2345-2350.
190. Mabilleau, G., M. Pereira, and C. Chenu, *Novel skeletal effects of glucagon-like peptide-1 (GLP-1) receptor agonists.* Journal of endocrinology, 2018. **236**(1): p. R29-R42.
191. Mabilleau, G., et al., *Optimal bone mechanical and material properties require a functional glucagon-like peptide-1 receptor.* Journal of Endocrinology, 2013. **219**(1): p. 59-68.

192. Meng, J., et al., *Activation of GLP-1 Receptor Promotes Bone Marrow Stromal Cell Osteogenic Differentiation through β-Catenin.* Stem Cell Reports, 2016. **6**(4): p. 579-591.
193. Li, Z., et al., *Liraglutide, a glucagon-like peptide-1 receptor agonist, suppresses osteoclastogenesis through the inhibition of NF-κB and MAPK pathways via GLP-1R.* Biomedicine & Pharmacotherapy, 2020. **130**: p. 110523.
194. Aoyama, E., et al., *Expression of glucagon-like peptide-1 receptor and glucose-dependent insulinotropic polypeptide receptor is regulated by the glucose concentration in mouse osteoblastic MC3T3-E1 cells.* Int J Mol Med, 2014. **34**(2): p. 475-82.
195. Kim, J.-Y., et al., *Exendin-4 increases bone mineral density in type 2 diabetic OLETF rats potentially through the down-regulation of SOST/sclerostin in osteocytes.* Life Sciences, 2013. **92**(10): p. 533-540.
196. Pereira, M., et al., *Chronic administration of Glucagon-like peptide-1 receptor agonists improves trabecular bone mass and architecture in ovariectomised mice.* Bone, 2015. **81**: p. 459-467.
197. Jeon, Y.K., et al., *Expression of glucagon-like peptide 1 receptor during osteogenic differentiation of adipose-derived stem cells.* Endocrinology and metabolism, 2014. **29**(4): p. 567.
198. Zhai, S., et al., *Glucagon-like peptide-1 receptor promotes osteoblast differentiation of dental pulp stem cells and bone formation in a zebrafish scale regeneration model.* Peptides, 2023. **163**: p. 170974.
199. Ma, X., et al., *Exendin-4, a Glucagon-Like Peptide-1 Receptor Agonist, Prevents Osteopenia by Promoting Bone Formation and Suppressing Bone Resorption in Aged Ovariectomized Rats.* Journal of Bone and Mineral Research, 2013. **28**(7): p. 1641-1652.
200. Yamada, C., et al., *The Murine Glucagon-Like Peptide-1 Receptor Is Essential for Control of Bone Resorption.* Endocrinology, 2008. **149**(2): p. 574-579.
201. Luo, G., H. Liu, and H. Lu, *Glucagon-like peptide-1(GLP-1) receptor agonists: potential to reduce fracture risk in diabetic patients?* Br J Clin Pharmacol, 2016. **81**(1): p. 78-88.
202. Bjerre, K.L., L. Madsen, and S. Andersen, *Glucagon-like peptide-1 receptor agonists activate rodent thyroid C-cells causing calcitonin release and C-cell proliferation. vol. 151.* Endocrinology, 2010: p. 2009-1272.
203. Viggers, R., N.H.h. Rasmussen, and P. Vestergaard, *Effects of Incretin Therapy on Skeletal Health in Type 2 Diabetes—A Systematic Review.* JBMR Plus, 2023. **7**(11).
204. Jespersen, M.J., F.K. Knop, and M. Christensen, *GLP-1 agonists for type 2 diabetes: pharmacokinetic and toxicological considerations.* Expert opinion on drug metabolism & toxicology, 2013. **9**(1): p. 17-29.
205. Cornell, S., *A review of GLP-1 receptor agonists in type 2 diabetes: A focus on the mechanism of action of once-weekly agents.* J Clin Pharm Ther, 2020. **45 Suppl 1**(Suppl 1): p. 17-27.
206. Iepsen, E.W., et al., *GLP-1 Receptor Agonist Treatment Increases Bone Formation and Prevents Bone Loss in Weight-Reduced Obese Women.* The Journal of Clinical Endocrinology & Metabolism, 2015. **100**(8): p. 2909-2917.
207. Hansen, M.S., et al., *Once-weekly semaglutide versus placebo in adults with increased fracture risk: a randomised, double-blinded, two-centre, phase 2 trial.* eClinicalMedicine, 2024. **72**.

208. Green, C.J., et al., *Glucagon like peptide-1-induced glucose metabolism in differentiated human muscle satellite cells is attenuated by hyperglycemia.* PLoS One, 2012. **7**(8): p. e44284.
209. Balteau, M., et al., *AMPK activation by glucagon-like peptide-1 prevents NADPH oxidase activation induced by hyperglycemia in adult cardiomyocytes.* American Journal of Physiology-Heart and Circulatory Physiology, 2014. **307**(8): p. H1120-H1133.
210. Li, R., et al., *GLP-1-Induced AMPK Activation Inhibits PARP-1 and Promotes LXR-Mediated ABCA1 Expression to Protect Pancreatic β-Cells Against Cholesterol-Induced Toxicity Through Cholesterol Efflux.* Front Cell Dev Biol, 2021. **9**: p. 646113.
211. Wang, T., et al., *Current understanding of glucose transporter 4 expression and functional mechanisms.* World journal of biological chemistry, 2020. **11**(3): p. 76.
212. Holliday, A. and A. Blannin, *Appetite, food intake and gut hormone responses to intense aerobic exercise of different duration.* Journal of Endocrinology, 2017. **235**(3): p. 193-205.
213. Wu, L., et al., *GLP-1 regulates exercise endurance and skeletal muscle remodeling via GLP-1R/AMPK pathway.* Biochimica et Biophysica Acta (BBA) - Molecular Cell Research, 2022. **1869**(9): p. 119300.
214. Ayala, J.E., et al., *Glucagon-like peptide-1 receptor knockout mice are protected from high-fat diet-induced insulin resistance.* Endocrinology, 2010. **151**(10): p. 4678-87.
215. Hong, Y., et al., *Amelioration of muscle wasting by glucagon-like peptide-1 receptor agonist in muscle atrophy.* J Cachexia Sarcopenia Muscle, 2019. **10**(4): p. 903-918.
216. *FDA-Approved Drugs*. Available from: https://www.accessdata.fda.gov/scripts/cder/daf/index.cfm.
217. Pantanetti, P., et al., *Oral Semaglutide in Type 2 Diabetes: Clinical-Metabolic Outcomes and Quality of Life in Real-World Practice.* J Clin Med, 2024. **13**(16).
218. Knudsen, L.B. and J. Lau, *The Discovery and Development of Liraglutide and Semaglutide.* Frontiers in Endocrinology, 2019. **10**.
219. Lincoff, A.M., et al., *Semaglutide and Cardiovascular Outcomes in Obesity without Diabetes.* N Engl J Med, 2023. **389**(24): p. 2221-2232.
220. Badve, S.V., et al., *Effects of GLP-1 receptor agonists on kidney and cardiovascular disease outcomes: a meta-analysis of randomised controlled trials.* The Lancet Diabetes & Endocrinology, 2025. **13**(1): p. 15-28.
221. Odigwe, C., et al., *Emerging role of GLP-1 agonists in cardio-metabolic therapy - Focus on Semaglutide.* American Heart Journal Plus: Cardiology Research and Practice, 2025. **52**: p. 100518.
222. Colhoun, H.M., et al., *Long-term kidney outcomes of semaglutide in obesity and cardiovascular disease in the SELECT trial.* Nature Medicine, 2024. **30**(7): p. 2058-2066.
223. Perkovic, V., et al., *Effects of Semaglutide on Chronic Kidney Disease in Patients with Type 2 Diabetes.* N Engl J Med, 2024. **391**(2): p. 109-121.
224. Bliddal, H., et al., *Once-Weekly Semaglutide in Persons with Obesity and Knee Osteoarthritis.* N Engl J Med, 2024. **391**(17): p. 1573-1583.
225. Baser, O., et al., *Impact of semaglutide on osteoarthritis risk in patients with obesity: A retrospective cohort study.* Obesity Science & Practice, 2024. **10**(3): p. e762.

226. Wilding, J.P., et al., *Once-weekly semaglutide in adults with overweight or obesity.* New England Journal of Medicine, 2021. **384**(11): p. 989-1002.
227. Wilding, J.P.H., et al., *Weight regain and cardiometabolic effects after withdrawal of semaglutide: The STEP 1 trial extension.* Diabetes Obes Metab, 2022. **24**(8): p. 1553-1564.
228. Rubino, D.M., et al., *Effect of weekly subcutaneous semaglutide vs daily liraglutide on body weight in adults with overweight or obesity without diabetes: the STEP 8 randomized clinical trial.* Jama, 2022. **327**(2): p. 138-150.
229. Smits, M.M. and D.H. Van Raalte, *Safety of Semaglutide.* Frontiers in Endocrinology, 2021. **Volume 12 - 2021**.
230. Madsen, L.W., et al., *GLP-1 receptor agonists and the thyroid: C-cell effects in mice are mediated via the GLP-1 receptor and not associated with RET activation.* Endocrinology, 2012. **153**(3): p. 1538-47.
231. *OZEMPIC [FDA Label]. Novo Nordisk, 2005.*
232. *WEGOVY [FDA Label]. Novo Nordisk, 2002.*
233. NIH Consensus Development Panel on Osteoporosis Prevention, D. and Therapy, *Osteoporosis Prevention, Diagnosis, and Therapy.* JAMA, 2001. **285**(6): p. 785-795.
234. Dempster, D.W., *Osteoporosis and the burden of osteoporosis-related fractures.* Am J Manag Care, 2011. **17 Suppl 6**: p. S164-9.
235. *Osteoporosis or low bone mass in older adults : United States, 2017–2018*, S. National Center for Health, Editor. 2021, http://dx.doi.org/10.15620/cdc:103477: Hyattsville, MD.
236. Reginster, J.-Y., et al., *Osteoporosis and sarcopenia: two diseases or one?* Current opinion in clinical nutrition and metabolic care, 2016. **19**(1): p. 31-36.
237. Clynes, M.A., et al., *Osteosarcopenia: where osteoporosis and sarcopenia collide.* Rheumatology, 2020. **60**(2): p. 529-537.
238. Burr, D.B., *Muscle strength, bone mass, and age-related bone loss.* J Bone Miner Res, 1997. **12**(10): p. 1547-51.
239. Bikle, D.D. and B.P. Halloran, *The response of bone to unloading.* J Bone Miner Metab, 1999. **17**(4): p. 233-44.
240. Caiozzo, V.J., et al., *Effect of spaceflight on skeletal muscle: mechanical properties and myosin isoform content of a slow muscle.* Journal of Applied Physiology, 1994. **76**(4): p. 1764-1773.
241. Collet, P., et al., *Effects of 1- and 6-month spaceflight on bone mass and biochemistry in two humans.* Bone, 1997. **20**(6): p. 547-51.
242. Adams, G.R., V.J. Caiozzo, and K.M. Baldwin, *Skeletal muscle unweighting: spaceflight and ground-based models.* Journal of Applied Physiology, 2003. **95**(6): p. 2185-2201.
243. Lang, T., et al., *Cortical and Trabecular Bone Mineral Loss From the Spine and Hip in Long-Duration Spaceflight.* Journal of Bone and Mineral Research, 2004. **19**(6): p. 1006-1012.
244. Cunningham, H.C., et al., *Age-dependent bone loss and recovery during hindlimb unloading and subsequent reloading in rats.* BMC Musculoskelet Disord, 2018. **19**(1): p. 223.

245. Czaja, C.A., et al., *Age-Related Differences in Hospitalization Rates, Clinical Presentation, and Outcomes Among Older Adults Hospitalized With Influenza-U.S. Influenza Hospitalization Surveillance Network (FluSurv-NET).* Open Forum Infect Dis, 2019. **6**(7).
246. Russo, C.A. and A. Elixhauser, *Hospitalizations in the Elderly Population, 2003: Statistical Brief #6*, in *Healthcare Cost and Utilization Project (HCUP) Statistical Briefs*. 2006: Rockville (MD).
247. Lee, S.-J. and A.C. McPherron, *Myostatin and the control of skeletal muscle mass: Commentary.* Current Opinion in Genetics & Development, 1999. **9**(5): p. 604-607.
248. Lee, S.-J. and A.C. McPherron, *Regulation of myostatin activity and muscle growth.* Proceedings of the National Academy of Sciences, 2001. **98**(16): p. 9306-9311.
249. Baig, M.H., et al., *Myostatin and its Regulation: A Comprehensive Review of Myostatin Inhibiting Strategies.* Front Physiol, 2022. **13**: p. 876078.
250. Smith, R.C. and B.K. Lin, *Myostatin inhibitors as therapies for muscle wasting associated with cancer and other disorders.* Curr Opin Support Palliat Care, 2013. **7**(4): p. 352-60.
251. Murphy, K.T., et al., *Acute antibody-directed myostatin inhibition attenuates disuse muscle atrophy and weakness in mice.* J Appl Physiol (1985), 2011. **110**(4): p. 1065-72.
252. Rybalka, E., et al., *The Failed Clinical Story of Myostatin Inhibitors against Duchenne Muscular Dystrophy: Exploring the Biology behind the Battle.* Cells, 2020. **9**(12): p. 2657.
253. Khorasani, M.S., et al., *Effect of alendronate on post-traumatic osteoarthritis induced by anterior cruciate ligament rupture in mice.* Arthritis Res Ther, 2015. **17**(1): p. 30.
254. Osipov, B., et al., *Sex differences in systemic bone and muscle loss following femur fracture in mice.* J Orthop Res, 2022. **40**(4): p. 878-890.
255. Bodine, S.C. and K. Baar, *Analysis of Skeletal Muscle Hypertrophy in Models of Increased Loading*, in *Myogenesis: Methods and Protocols*, J.X. DiMario, Editor. 2012, Humana Press: Totowa, NJ. p. 213-229.
256. Smith, L.R. and E.R. Barton, *SMASH – semi-automatic muscle analysis using segmentation of histology: a MATLAB application.* Skeletal Muscle, 2014. **4**(1): p. 21.
257. Lee, C.A., et al., *Estrogen inhibits lysyl oxidase and decreases mechanical function in engineered ligaments.* J Appl Physiol (1985), 2015. **118**(10): p. 1250-7.
258. Avey, A.M., O. Valdez, and K. Baar, *Characterization of an in vitro engineered ligament model.* Matrix Biology Plus, 2024. **21**: p. 100140.
259. Cunningham, H.C., et al., *Differential bone adaptation to mechanical unloading and reloading in young, old, and osteocyte deficient mice.* Bone, 2023. **167**: p. 116646.
260. Cunningham, H., *Bone Adaptation to Disuse in Aging Rodents: Age-Related Differences in Response to Mechanical Unloading and Subsequent Reloading*. 2021, University of California, Davis.
261. Perrien, D.S., et al., *Aging alters the skeletal response to disuse in the rat.* Am J Physiol Regul Integr Comp Physiol, 2007. **292**(2): p. R988-96.
262. Oliveira, J.R.S., et al., *Effects of hindlimb suspension and reloading on gastrocnemius and soleus muscle mass and function in geriatric mice.* Exp Gerontol, 2019. **115**: p. 19-31.
263. Schafer, M.J., et al., *Quantification of GDF11 and Myostatin in Human Aging and Cardiovascular Disease.* Cell Metabolism, 2016. **23**(6): p. 1207-1215.
264. Regan, J.N., et al., *The Role of TGFβ in Bone-Muscle Crosstalk.* Curr Osteoporos Rep, 2017. **15**(1): p. 18-23.

265. Sun, Q., et al., *Transforming growth factor-beta-regulated miR-24 promotes skeletal muscle differentiation.* Nucleic Acids Res, 2008. **36**(8): p. 2690-9.
266. Kitase, Y., et al., *β-aminoisobutyric Acid, l-BAIBA, Is a Muscle-Derived Osteocyte Survival Factor.* Cell Rep, 2018. **22**(6): p. 1531-1544.
267. Hamoudi, D., et al., *Muscle weakness and selective muscle atrophy in osteoprotegerin-deficient mice.* Hum Mol Genet, 2020. **29**(3): p. 483-494.
268. Harada, A., et al., *Effect of alendronate on muscle mass: Investigation in patients with osteoporosis.* Osteoporosis and Sarcopenia, 2015. **1**(1): p. 53-58.
269. Chiu, H.C., et al., *Preventing muscle wasting by osteoporosis drug alendronate in vitro and in myopathy models via sirtuin-3 down-regulation.* J Cachexia Sarcopenia Muscle, 2018. **9**(3): p. 585-602.
270. Marso, S.P., et al., *Liraglutide and Cardiovascular Outcomes in Type 2 Diabetes.* N Engl J Med, 2016. **375**(4): p. 311-22.
271. Meurot, C., et al., *Liraglutide, a glucagon-like peptide 1 receptor agonist, exerts analgesic, anti-inflammatory and anti-degradative actions in osteoarthritis.* Scientific Reports, 2022. **12**(1): p. 1567.
272. Klausen, M.K., et al., *The role of glucagon-like peptide 1 (GLP-1) in addictive disorders.* British Journal of Pharmacology, 2022. **179**(4): p. 625-641.
273. Jerlhag, E., *GLP-1 signaling and alcohol-mediated behaviors; preclinical and clinical evidence.* Neuropharmacology, 2018. **136**: p. 343-349.
274. Eren-Yazicioglu, C.Y., et al., *Can GLP-1 Be a Target for Reward System Related Disorders? A Qualitative Synthesis and Systematic Review Analysis of Studies on Palatable Food, Drugs of Abuse, and Alcohol.* Frontiers in Behavioral Neuroscience, 2021. **Volume 14 - 2020**.
275. Khalid, S.I., et al., *Semaglutide exposure and its association with adverse outcomes in diabetic patients undergoing transforaminal lumbar interbody fusion for lumbar degenerative disc disease: Presented at the 2024 AANS/CNS Joint Section on Disorders of the Spine and Peripheral Nerves.* Journal of Neurosurgery: Spine, 2024. **1**(aop): p. 1-8.
276. Nuche-Berenguer, B., et al., *Effect of GLP-1 Treatment on Bone Turnover in Normal, Type 2 Diabetic, and Insulin-Resistant States.* Calcified Tissue International, 2009. **84**(6): p. 453-461.
277. Bikou, A., et al., *A systematic review of the effect of semaglutide on lean mass: insights from clinical trials.* Expert Opin Pharmacother, 2024. **25**(5): p. 611-619.
278. IKEJIMA, S., et al., *Novel Approach to Sarcopenia in Diabetic Patients Treated with GLP-1 Receptor Agonists (GLP-1RA).* Diabetes, 2018. **67**(Supplement_1).
279. Holst, J.J., *The Physiology of Glucagon-like Peptide 1.* Physiological Reviews, 2007. **87**(4): p. 1409-1439.
280. Salamone, L.M., et al., *Effect of a lifestyle intervention on bone mineral density in premenopausal women: a randomized trial².* The American Journal of Clinical Nutrition, 1999. **70**(1): p. 97-103.
281. Ricci, T.A., et al., *Calcium Supplementation Suppresses Bone Turnover During Weight Reduction in Postmenopausal Women.* Journal of Bone and Mineral Research, 2009. **13**(6): p. 1045-1050.

282. Ryan, A.S., B.J. Nicklas, and K.E. Dennis, *Aerobic exercise maintains regional bone mineral density during weight loss in postmenopausal women.* Journal of Applied Physiology, 1998. **84**(4): p. 1305-1310.
283. Hunter, G.R., E.P. Plaisance, and G. Fisher, *Weight loss and bone mineral density.* Curr Opin Endocrinol Diabetes Obes, 2014. **21**(5): p. 358-62.
284. Ensrud, K.E., et al., *Body size and hip fracture risk in older women: a prospective study.* The American journal of medicine, 1997. **103**(4): p. 274-280.
285. Edelstein, S.L. and E. Barrett-Connor, *Relation between Body Size and Bone Mineral Density in Elderly Men and Women.* American Journal of Epidemiology, 1993. **138**(3): p. 160-169.
286. Zibellini, J., et al., *Effect of diet-induced weight loss on muscle strength in adults with overweight or obesity – a systematic review and meta-analysis of clinical trials.* Obesity Reviews, 2016. **17**(8): p. 647-663.
287. McCarthy, D. and A. Berg, *Weight Loss Strategies and the Risk of Skeletal Muscle Mass Loss.* Nutrients, 2021. **13**(7): p. 2473.
288. Miller, S.L. and R.R. Wolfe, *The danger of weight loss in the elderly.* The Journal of Nutrition Health and Aging, 2008. **12**: p. 487-491.
289. Friedman, M.A., et al., *Single limb immobilization model for bone loss from unloading.* Journal of Biomechanics, 2019. **83**: p. 181-189.
290. Jepsen, K.J., et al., *Establishing biomechanical mechanisms in mouse models: practical guidelines for systematically evaluating phenotypic changes in the diaphyses of long bones.* J Bone Miner Res, 2015. **30**(6): p. 951-66.
291. Dobin, A., et al., *STAR: ultrafast universal RNA-seq aligner.* Bioinformatics, 2013. **29**(1): p. 15-21.
292. Love, M.I., W. Huber, and S. Anders, *Moderated estimation of fold change and dispersion for RNA-seq data with DESeq2.* Genome Biology, 2014. **15**(12): p. 550.
293. Langer, H.T., et al., *Dominant-negative p53-overexpression in skeletal muscle induces cell death and fiber atrophy in rats.* Cell Death Dis, 2022. **13**(8): p. 716.
294. Aldridge, G.M., et al., *The use of total protein stains as loading controls: an alternative to high-abundance single-protein controls in semi-quantitative immunoblotting.* Journal of neuroscience methods, 2008. **172**(2): p. 250-254.
295. Gabery, S., et al., *Semaglutide lowers body weight in rodents via distributed neural pathways.* JCI Insight, 2020. **5**(6).
296. Forny Germano, L., et al., *The GLP-1 medicines semaglutide and tirzepatide do not alter disease-related pathology, behaviour or cognitive function in 5XFAD and APP/PS1 mice.* Mol Metab, 2024. **89**: p. 102019.
297. Moreno, A., et al., *Semaglutide Administration in Healthy Mice Alters Behaviour Related to Stress and Motivation.* bioRxiv, 2024: p. 2024.09.06.611514.
298. Umapathysivam, M.M., et al., *Comparative effects of prolonged and intermittent stimulation of the glucagon-like peptide 1 receptor on gastric emptying and glycemia.* Diabetes, 2014. **63**(2): p. 785-90.
299. Hansen, G., J. Jelsing, and N. Vrang, *Effects of liraglutide and sibutramine on food intake, palatability, body weight and glucose tolerance in the gubra DIO-rats.* Acta Pharmacologica Sinica, 2012. **33**(2): p. 194-200.

300. Knapka, J.J., K.P. Smith, and F.J. Judge, *Effect of Crude Fat and Crude Protein on Reproduction and Weanling Growth in Four Strains of Inbred Mice.* The Journal of Nutrition, 1977. **107**(1): p. 61-69.
301. Ghidewon, M., et al., *Growth differentiation factor 15 (GDF15) and semaglutide inhibit food intake and body weight through largely distinct, additive mechanisms.* Diabetes, Obesity and Metabolism, 2022. **24**(6): p. 1010-1020.
302. Cawthon, C.R., et al., *Chronic Semaglutide Treatment in Rats Leads to Daily Excessive Concentration-Dependent Sucrose Intake.* J Endocr Soc, 2023. **7**(7): p. bvad074.
303. Casimiro, I., et al., *Phenotypic sexual dimorphism in response to dietary fat manipulation in C57BL/6J mice.* J Diabetes Complications, 2021. **35**(2): p. 107795.
304. Maniam, J. and M.J. Morris, *The link between stress and feeding behaviour.* Neuropharmacology, 2012. **63**(1): p. 97-110.
305. Gurfein, B.T., et al., *The calm mouse: an animal model of stress reduction.* Mol Med, 2012. **18**(1): p. 606-17.
306. Martens, M.D., et al., *Semaglutide Reduces Cardiomyocyte Size and Cardiac Mass in Lean and Obese Mice.* JACC: Basic to Translational Science, 2024. **9**(12): p. 1429-1431.
307. Norlin, J., *Animal Model Sharing – NASH, or Non-Alcoholic Steatohepatitis*. Novo Nordisk.
308. Fritton, J., et al., *Loading induces site-specific increases in mineral content assessed by microcomputed tomography of the mouse tibia.* Bone, 2005. **36**(6): p. 1030-1038.
309. Zhang, P., et al., *Lengthening of mouse hindlimbs with joint loading.* J Bone Miner Metab, 2010. **28**(3): p. 268-75.
310. Kirschner, L.S., et al., *Mouse models of altered protein kinase A signaling.* Endocrine-related cancer, 2009. **16**(3): p. 773.
311. Sun, W., et al., *Mechanical stimulation controls osteoclast function through the regulation of Ca(2+)-activated Cl(-) channel Anoctamin 1.* Commun Biol, 2023. **6**(1): p. 407.
312. Zhang, P., K. Hamamura, and H. Yokota, *A brief review of bone adaptation to unloading.* Genomics Proteomics Bioinformatics, 2008. **6**(1): p. 4-7.
313. Sun, H.X., et al., *Liraglutide, the glucagon-like peptide-1 receptor agonist, has anabolic bone effects in diabetic Goto-Kakizaki rats.* J Diabetes, 2015. **7**(4): p. 584-8.
314. Safadi, F.F., et al., *Osteopathy and resistance to vitamin D toxicity in mice null for vitamin D binding protein.* J Clin Invest, 1999. **103**(2): p. 239-51.
315. Ren, C., et al., *Suppression of CLEC3A inhibits osteosarcoma cell proliferation and promotes their chemosensitivity through the AKT1/mTOR/HIF1α signaling pathway.* Mol Med Rep, 2020. **21**(4): p. 1739-1748.
316. Chen, X., et al., *C-type lectin domain-containing protein CLEC3A regulates proliferation, regeneration and maintenance of nucleus pulposus cells.* Cell Mol Life Sci, 2022. **79**(8): p. 435.
317. Guo, Y., et al., *Dermatopontin inhibits papillary thyroid cancer cell proliferation through MYC repression.* Molecular and Cellular Endocrinology, 2019. **480**: p. 122-132.
318. Zhao, X., et al., *Effect of dermatopontin on osteogenic differentiation of periodontal ligament stem cells.* Gene, 2023. **858**: p. 147185.

319. Xi, L.C., et al., *Effects of Dermatopontin gene silencing on apoptosis and proliferation of osteosarcoma MG-63 cells.* Mol Med Rep, 2018. **17**(1): p. 422-427.
320. Liu, J., Y. Li, and J. Hoh, *Generation and characterization of mice with a conditional null allele of the HtrA4 gene.* Mol Med Rep, 2015. **12**(5): p. 6768-74.
321. Inagaki, A., et al., *Upregulation of HtrA4 in the placentas of patients with severe pre-eclampsia.* Placenta, 2012. **33**(11): p. 919-926.
322. Onizuka, S., et al., *ZBTB16 as a downstream target gene of osterix regulates osteoblastogenesis of human multipotent mesenchymal stromal cells.* Journal of cellular biochemistry, 2016. **117**(10): p. 2423-2434.
323. Felthaus, O., M. Gosau, and C. Morsczeck, *ZBTB16 induces osteogenic differentiation marker genes in dental follicle cells independent from RUNX2.* Journal of periodontology, 2014. **85**(5): p. e144-e151.
324. Yu, W., et al., *Super enhancers targeting ZBTB16 in osteogenesis protect against osteoporosis.* Bone Research, 2023. **11**(1): p. 30.
325. Kubo, K., et al., *Measurement of viscoelastic properties of tendon structures in vivo.* Scandinavian journal of medicine & science in sports, 2002. **12**(1): p. 3-8.
326. Kinugasa, R., et al., *Reduction in tendon elasticity from unloading is unrelated to its hypertrophy.* J Appl Physiol (1985), 2010. **109**(3): p. 870-7.
327. Shin, D., et al., *Effect of chronic unloading and rehabilitation on human Achilles tendon properties: a velocity-encoded phase-contrast MRI study.* Journal of Applied Physiology, 2008. **105**(4): p. 1179-1186.
328. Chai, W., et al., *Glucagon-like peptide 1 recruits muscle microvasculature and improves insulin's metabolic action in the presence of insulin resistance.* Diabetes, 2014. **63**(8): p. 2788-99.
329. Abdulla, H., et al., *Glucagon-like peptide 1 infusions overcome anabolic resistance to feeding in older human muscle.* Aging Cell, 2020. **19**(9): p. e13202.
330. Rajagopal, S., et al., *Glucagon-Like Peptide-1 Receptor Agonists in the Treatment of Idiopathic Inflammatory Myopathy: From Mechanisms of Action to Clinical Applications.* Cureus, 2023. **15**(12): p. e51352.
331. Langer, H.T., et al., *Myofibrillar protein synthesis rates are increased in chronically exercised skeletal muscle despite decreased anabolic signaling.* Scientific Reports, 2022. **12**(1): p. 7553.
332. Langer, H.T., et al., *AMPK as a mediator of tissue preservation: time for a shift in dogma?* Nat Rev Endocrinol, 2024. **20**(9): p. 526-540.
333. Langer, H.T., et al., *Restoring adiponectin via rosiglitazone ameliorates tissue wasting in mice with lung cancer.* Acta Physiol (Oxf), 2024. **240**(8): p. e14167.
334. Zhu, W.G., et al., *Identification of a resistance-exercise-specific signalling pathway that drives skeletal muscle growth.* Nature Metabolism, 2025.
335. Kim, J.-Y., Y.-G. Kwon, and Y.-M. Kim, *The stress-responsive protein REDD1 and its pathophysiological functions.* Experimental & Molecular Medicine, 2023. **55**(9): p. 1933-1944.
336. o, F.A., et al., *Glucocorticoid-dependent REDD1 expression reduces muscle metabolism to enable adaptation under energetic stress.* BMC Biology, 2018. **16**(1): p. 65.

337. Maleki, K.T., M. Cornillet, and N.K. Björkström, *Soluble SEMA4D/CD100: a novel immunoregulator in infectious and inflammatory diseases.* Clinical Immunology, 2016. **163**: p. 52-59.
338. Negishi-Koga, T., et al., *Suppression of bone formation by osteoclastic expression of semaphorin 4D.* Nature medicine, 2011. **17**(11): p. 1473-1480.
339. Lontos, K., et al., *The Role of Semaphorin 4D in Bone Remodeling and Cancer Metastasis.* Front Endocrinol (Lausanne), 2018. **9**: p. 322.
340. Imai, K., et al., *Atg9A trafficking through the recycling endosomes is required for autophagosome formation.* Journal of cell science, 2016. **129**(20): p. 3781-3791.
341. Ji, F. and J.-H. Kim, *Muscle Type-Specific Modulation of Autophagy Signaling in Obesity: Effects of Caloric Restriction and Exercise.* bioRxiv, 2024: p. 2024.08.29.610325.
342. Sato, M., et al., *Tissue-Nonspecific Alkaline Phosphatase, a Possible Mediator of Cell Maturation: Towards a New Paradigm.* Cells, 2021. **10**(12).
343. Villa-Suárez, J.M., et al., *Hypophosphatasia: a unique disorder of bone mineralization.* International Journal of Molecular Sciences, 2021. **22**(9): p. 4303.
344. Salles, J.P., *Hypophosphatasia: biological and clinical aspects, avenues for therapy.* The Clinical Biochemist Reviews, 2020. **41**(1): p. 13.
345. Tanaka, K., et al., *Role of osteoglycin in the linkage between muscle and bone.* J Biol Chem, 2012. **287**(15): p. 11616-28.
346. Zhang, Y., et al., *miRNA-seq analysis of high glucose induced osteoblasts provides insight into the mechanism underlying diabetic osteoporosis.* Scientific Reports, 2024. **14**.
347. Craig M. Hales, M.D., Margaret D. Carroll, M.S.P.H., Cheryl D. Fryar, M.S.P.H., and Cynthia L. Ogden, Ph.D., *Prevalence of Obesity Among Adults and Youth: United States, 2015–2016*, in *NCHS Data Brief*. 2020, National Center for Health Statistics.
348. Flegal, K.M., et al., *Prevalence and Trends in Obesity Among US Adults, 1999-2000.* JAMA, 2002. **288**(14): p. 1723-1727.
349. Freedman, D.S., et al., *Trends and Correlates of Class 3 Obesity in the United States From 1990 Through 2000.* JAMA, 2002. **288**(14): p. 1758-1761.
350. *Screening and Interventions for Obesity in Adults: Summary of the Evidence for the U.S. Preventive Services Task Force.* Annals of Internal Medicine, 2003. **139**(11): p. 933-949.
351. *Planned Knee and Hip Replacement Surgeries are on the Rise in the U.S.*, in *The Health of America*, B. BlueShield, Editor. 2019, Blue Health Intelligence.
352. Rullán, P.J., et al., *The Arthroplasty Surgeon Growth Indicator: A Tool for Monitoring Supply and Demand Trends in the Orthopaedic Surgeon Workforce from 2020 to 2050.* J Bone Joint Surg Am, 2023. **105**(13): p. 1038-1045.
353. Singh, J.A., et al., *Rates of Total Joint Replacement in the United States: Future Projections to 2020-2040 Using the National Inpatient Sample.* J Rheumatol, 2019. **46**(9): p. 1134-1140.
354. Ri, M., S. Aikou, and Y. Seto, *Obesity as a surgical risk factor.* Ann Gastroenterol Surg, 2018. **2**(1): p. 13-21.
355. Jämsen, E., et al., *Comorbid diseases as predictors of survival of primary total hip and knee replacements: a nationwide register-based study of 96 754 operations on patients with primary osteoarthritis.* Ann Rheum Dis, 2013. **72**(12): p. 1975-82.

356. Bordini, B., et al., *Relationship between obesity and early failure of total knee prostheses.* BMC Musculoskelet Disord, 2009. **10**: p. 29.
357. Amin, A.K., et al., *Does obesity influence the clinical outcome at five years following total knee replacement for osteoarthritis?* J Bone Joint Surg Br, 2006. **88**(3): p. 335-40.
358. Eaton, C.B., *Obesity as a risk factor for osteoarthritis: mechanical versus metabolic.* Med Health R I, 2004. **87**(7): p. 201-4.
359. Udhaya Nedunchezhiyan, I.V., Antonia RuJia Sun, Xiaoxin Wu, Ross Crawford, Indira Prasadam, *Obesity, Inflammation, and Immune System in Osteoarthritis.* Frontiers in Immunology, 2022. **13-2022**.
360. Eknoyan, G., *Adolphe Quetelet (1796-1874)--the average man and indices of obesity.* Nephrol Dial Transplant, 2008. **23**(1): p. 47-51.
361. Humphreys, S., *The unethical use of BMI in contemporary general practice.* Br J Gen Pract, 2010. **60**(578): p. 696-7.
362. Teicholz, N., *A short history of saturated fat: the making and unmaking of a scientific consensus.* Curr Opin Endocrinol Diabetes Obes, 2023. **30**(1): p. 65-71.
363. Strings, S., *How the Use of BMI Fetishizes White Embodiment and Racializes Fat Phobia.* AMA J Ethics, 2023. **25**(7): p. E535-539.
364. Komaroff, M., *For Researchers on Obesity: Historical Review of Extra Body Weight Definitions.* J Obes, 2016. **2016**: p. 2460285.
365. Sherman, W.F., et al., *Surgeon Decision-Making for Individuals With Obesity When Indicating Total Joint Arthroplasty.* The Journal of Arthroplasty, 2021. **36**(8): p. 2708-2715.e1.
366. *Obesity*. Preoperative Risk Factors [cited 2024 Feb 13, 2024]; Available from: https://www.aaos.org/quality/quality-programs/quality-toolkits/obesity/.
367. Madsen, H.J., et al., *The association between obesity and postoperative outcomes in a broad surgical population: A 7-year American College of Surgeons National Surgical Quality Improvement analysis.* Surgery, 2023. **173**(5): p. 1213-1219.
368. Turcotte, J., et al., *Complication rates and resource utilization after total hip and knee arthroplasty stratified by body mass index.* J Orthop, 2021. **24**: p. 111-120.
369. Aggarwal, V.A., S.N. Sambandam, and D.K. Wukich, *The impact of obesity on total knee arthroplasty outcomes: A retrospective matched cohort study.* J Clin Orthop Trauma, 2022. **33**: p. 101987.
370. Issa, K., et al., *Does obesity affect the outcomes of primary total knee arthroplasty?* J Knee Surg, 2013. **26**(2): p. 89-94.
371. Sloan, M., N. Sheth, and G.C. Lee, *Is Obesity Associated With Increased Risk of Deep Vein Thrombosis or Pulmonary Embolism After Hip and Knee Arthroplasty? A Large Database Study.* Clin Orthop Relat Res, 2019. **477**(3): p. 523-532.
372. Järvenpää, J., et al., *Obesity May Impair the Early Outcome of Total Knee Arthroplasty a Prospective Study of 100 Patients.* Scandinavian Journal of Surgery, 2010. **99**(1): p. 45-49.
373. Waisbren, E., et al., *Percent Body Fat and Prediction of Surgical Site Infection.* Journal of the American College of Surgeons, 2010. **210**(4): p. 381-389.
374. Huttunen, R. and J. Syrjänen, *Obesity and the risk and outcome of infection.* International Journal of Obesity, 2013. **37**(3): p. 333-340.

375. Ayers, D.C., et al., *Using Joint Registry Data from FORCE-TJR to Improve the Accuracy of Risk-Adjustment Prediction Models for Thirty-Day Readmission After Total Hip Replacement and Total Knee Replacement.* JBJS, 2015. **97**(8).
376. Suleiman, L.I., et al., *Does BMI affect perioperative complications following total knee and hip arthroplasty?* J Surg Res, 2012. **174**(1): p. 7-11.
377. Craik, J.D., M.D. Bircher, and M. Rickman, *Hip and knee arthroplasty implants contraindicated in obesity.* Ann R Coll Surg Engl, 2016. **98**(5): p. 295-9.
378. Shohat, N., et al., *Weighing in on Body Mass Index and Infection After Total Joint Arthroplasty: Is There Evidence for a Body Mass Index Threshold?* Clin Orthop Relat Res, 2018. **476**(10): p. 1964-1969.
379. Li, W., et al., *Functional Gain and Pain Relief After Total Joint Replacement According to Obesity Status.* J Bone Joint Surg Am, 2017. **99**(14): p. 1183-1189.
380. Arora, L., S. Sharma, and J.F. Carillo, *Obesity and anesthesia.* Curr Opin Anaesthesiol, 2024.
381. Mehta, J.H., et al., *Assessment of perioperative minute ventilation in obese versus non-obese patients with a non-invasive respiratory volume monitor.* BMC Anesthesiology, 2017. **17**(1): p. 61.
382. Raphael, I.J., et al., *Obesity and operative time in primary total joint arthroplasty.* J Knee Surg, 2013. **26**(2): p. 95-9.
383. Phelan, S.M., et al., *The mixed impact of medical school on medical students' implicit and explicit weight bias.* Med Educ, 2015. **49**(10): p. 983-92.
384. Kukielka, E., *How safety is compromised when hospital equipment is a poor fit for patients who are obese.* Patient Safety, 2020. **2**(1): p. 48-56.
385. *Nurses' Perceptions of Safety Concerns When Caring for Morbidly Obese Patients.* Bariatric Nursing and Surgical Patient Care, 2010. **5**(3): p. 243-247.
386. Hammond, K.L., *Practical issues in the surgical care of the obese patient.* Ochsner J, 2013. **13**(2): p. 224-7.
387. Puhl, R.M., T. Andreyeva, and K.D. Brownell, *Perceptions of weight discrimination: prevalence and comparison to race and gender discrimination in America.* International Journal of Obesity, 2008. **32**(6): p. 992-1000.
388. Puhl, R.M. and K.D. Brownell, *Confronting and coping with weight stigma: an investigation of overweight and obese adults.* Obesity (Silver Spring), 2006. **14**(10): p. 1802-15.
389. Puhl, R.M. and C.A. Heuer, *The Stigma of Obesity: A Review and Update.* Obesity, 2009. **17**(5): p. 941-964.
390. Tomiyama, A.J., et al., *How and why weight stigma drives the obesity 'epidemic' and harms health.* BMC Medicine, 2018. **16**(1): p. 123.
391. Al Zoubi, F., P.E. Beaulé, and P. Fallavollita, *Factors influencing delays and overtime during surgery: a descriptive analytics for high volume arthroplasty procedures.* Frontiers in Surgery, 2024. **10**.
392. Zheng, B., O.N. Panton, and T.A. Al-Tayeb, *Operative length independently affected by surgical team size: data from 2 Canadian hospitals.* Can J Surg, 2012. **55**(6): p. 371-6.
393. Carter, D., *The surgeon as a risk factor.* Bmj, 2003. **326**(7394): p. 832-3.

394. Kim, Y., et al., *Clinical impact of obesity on stability following revision total hip arthroplasty.* Clin Orthop Relat Res, 2006. **453**: p. 142-6.
395. Wagner, E.R., et al., *Effect of Body Mass Index on Complications and Reoperations After Total Hip Arthroplasty.* J Bone Joint Surg Am, 2016. **98**(3): p. 169-79.
396. Judge, A., et al., *Predictors of outcomes of total knee replacement surgery.* Rheumatology (Oxford), 2012. **51**(10): p. 1804-13.
397. Hawker, G., et al., *Health-related quality of life after knee replacement.* J Bone Joint Surg Am, 1998. **80**(2): p. 163-73.
398. Namba, R.S., et al., *Obesity and perioperative morbidity in total hip and total knee arthroplasty patients.* J Arthroplasty, 2005. **20**(7 Suppl 3): p. 46-50.
399. Martinez-Cano, J.P., et al., *Body mass index and knee arthroplasty.* J Clin Orthop Trauma, 2020. **11**(Suppl 5): p. S711-s716.
400. *BMI as A Risk Factor*. OrthoGuidelines; Available from: https://www.orthoguidelines.org/guideline-detail?id=1291.
401. *RISK FACTORS: BODY MASS INDEX (BMI)*. [cited 2024 Feb 13, 2024]; Available from: https://www.orthoguidelines.org/guideline-detail?id=1772&tab=all_guidelines.
402. Ogur, H.U., et al., *Does Body Mass Index Cause a Clinical Difference in Simultaneous Bilateral and Unilateral Knee Arthroplasty?* J Knee Surg, 2021. **34**(9): p. 1026-1032.

Appendix 1: Weight-based access to care barriers in orthopaedics

Abstract

Background - Many orthopedic surgeons choose not to perform joint arthroplasty on patients with a body mass index (BMI) of 35 or above, citing poorer outcomes and increased procedure risk. Identifying and addressing factors surgeons use to determine procedure BMI cutoffs are necessary to increase access to orthopaedic care for this growing patient population. This will help reduce healthcare disparities while also identifying clinical facilities, equipment, training, and procedures that require improvements to accommodate larger individuals.

Methods - Orthopaedic surgeons were surveyed to identify surgeon-specific BMI cutoffs for hip and knee arthroplasty. The survey was circulated within the California Orthopaedic Association (COA) report during March 2023. Questions aimed to identify BMI cutoffs and justifications such as infection risk, co-morbidities, inadequate equipment, and the American Academy of Orthopaedic Surgeons (AAOS) guidelines. Data on decision making about BMI cutoffs and exceptions were also collected.

Results - 75% of respondents use BMI cutoffs for hip and knee arthroplasty. 91% of respondents indicated they are either wholly or partially responsible for setting procedure BMI cutoffs. Mean hip and knee arthroplasty BMI cutoffs were 40.5 and 41, respectively. Four categories for BMI cutoff justifications were identified: 1) risk of complications; 2) surgery logistics; 3) concerns about facilities or resources; and 4) surgeon perception.

Conclusions – BMI-based justifications for denial of care define key addressable areas of improvement that can increase access to care for life-changing orthopaedic surgeries such as THA and TKA. Insight from the queried surgeons will help drive future research areas to address this need.

Key Words: BMI, arthroplasty, osteoarthritis, weight stigma

Introduction

The average weight of Americans has been increasing over the past several decades [347-350], and so is the demand for orthopaedic surgeries [351-353]. However, patients with larger body sizes may not have

the opportunity to pursue some elective orthopaedic procedures. Many orthopaedic surgeons have BMI limits, or cutoffs, for elective surgeries, citing poorer outcomes and increased procedure risk [354-357]. These risks can include increased infection rate, cardiac conditions, adverse reaction to anesthesia, and other life-threatening complications.

Total Hip Arthroplasty (THA) and Total Knee Arthroplasty (TKA) procedures are mainly conducted on patients with severe osteoarthritis (OA), many of whom have larger body sizes as high body mass has been identified as a risk factor for OA [358, 359]. Access to THA and TKA surgeries can be limited at the discretion of surgeons and medical facilities based on multiple risk factors. One of these risk factors is the Body Mass Index (BMI) of the patient. BMI was originally known as the Quetelet Index after the Belgian polymath who developed it in the 1830s to define the average man [360]. These statistics were based on Western European men of the time and did not consider other genders, ethnicities, or health factors [360, 361]. Ancel Keys [362, 363] rebranded the Quetelet Index to the Body Mass Index (BMI) in 1972 to support his nutritional assertions. It was later adopted by health insurance companies [364] and medical professionals as a quantitative metric to gauge the overall health of a patient [363, 364]. BMI is still being used today by many orthopaedic surgeons with the effect of restricting access to life-changing surgeries such as THA and TKA.

BMI cutoffs for THA and TKA are often as low as 30 or 35 [365]. Previous research and surveys have identified that risk of infections and complications are a major reason for these cutoffs[365], but do not go into specifics that can help drive research directions. The American Academy of Orthopaedic Surgeons (AAOS), the major professional organization for orthopedic surgeons in the US, recommends that THA and TKA surgeries should have a BMI cutoff of 40 [366]. The reason for differences between the AAOS guidelines and practicing California surgeon BMI cutoffs is unknown. To investigate the specifics of this discrepancy and the prevalence of BMI cutoffs in the state, we designed a survey for distribution to members of the California Orthopaedic Association (COA). The survey audience was orthopaedic surgeons

who regularly perform THA and/or TKAs. This study does not aim to identify if a patient should lose weight, but rather what barriers exist that prevent a patient at a higher weight in undergoing THA or TKA from a qualified orthopaedic surgeon. The questions were focused on identifying BMI cutoffs, pinpointing justifications for these cutoffs, and organizing these justifications into actionable categories to help reduce access to care disparities for individuals with a BMI over 35. With insight from these practicing orthopaedic surgeons, this study aimed to identify future areas of research that can increase access to care and clinical outcomes for millions. Specifically, we wanted to 1) discover the prevalence of BMI cutoffs; 2) identify BMI cutoff decision-making authorities; 3) identify currently used BMI Cutoffs, where applicable; and 4) document the BMI Cutoff Justifications used by California orthopaedic surgeons.

Materials and Methods

Survey Design and Distribution:

This survey was designed to identify key factors impacting access to hip and knee arthroplasty based on patient BMI in California. It was optimized to meet this goal with guidance from the UC Davis Health School of Medicine Office of Research Evaluation unit. The survey was pretested by an experienced orthopaedic surgeon (GCP) and questions were modified for clarity. The University of California, Davis Institutional Review Board determined this research was exempt from IRB approval as no personal identifying information or patient information was collected. The questions were distributed as a cross-sectional survey in Qualitrics (Qualtrics XM, Seattle, WA) within the California Orthopaedic Association (COA) report, the weekly COA newsletter, during March 2023. Members who had signed up to receive email alerts received this email. The report is also available online to the public on the COA Report website. It was designed as a preliminary study that would later be used to gauge nationwide BMI cutoff usage and justifications.

This survey consisted of 13 questions, the first of which collected data about the respondent's surgical practice. Subsequent questions were aimed at gauging the prevalence and degree of BMI cutoffs currently employed by Californian orthopaedic surgeons for THA and TKA. Years of practice, whether the surgeons use BMI cutoffs, and the respective BMI limits for surgeries were requested. To identify reasons surgeons used BMI cutoffs, the survey asked who is wholly or partially responsible for BMI decisions for both THA and TKA, as well as what factors or justifications were used to determine these limits. Multiple selections were allowed via a "select all that apply" instructions, and additional factors could be added through an "other: please specify" option. Justifications were categorized in the analysis as a framework for future investigation on this topic. All responses were required except for one which asked for any additional comments respondents would like to offer. Full survey questions are available in Appendix A.

Collected Responses: Out of 39 respondents, 33 completed the questionnaire (84.6% completion rate). This study was designed to assess California orthopaedic surgeons who perform THA/TKA. Therefore, this analysis includes data from 32 respondents who reported that they performed hip and/or knee arthroplasties. One respondent stated that they did not perform those surgeries, so their responses were not included in the analysis.

Data analysis: Data analysis was conducted on Microsoft Excel (Redmond, WA, USA) and Prism 10 (La Jolla, CA, USA).

Results

Prevalence of BMI Cutoffs:

Overall, 75% of respondents that perform THA and/or TKA self-reported using BMI cutoffs. Surgeons with more years of experience were less likely to use BMI cutoffs for these surgeries (Fig. 1). All respondents with 15 or fewer years of experience used BMI cutoffs for both THA and TKA. For surgeons with 16-20 years of experience, all used BMI cutoffs for THA, but only 75% used cutoffs for TKA. A majority of surgeons with over 20 years of experience used BMI cutoffs for both THA and TKA, but the prevalence of BMI cutoff use tended to decrease with more years of experience.

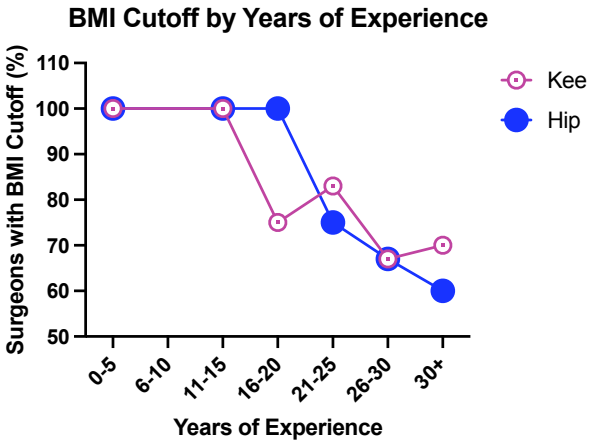

Figure 1. Percent of Californian orthopaedic surgeons with BMI cutoffs for knee and hip arthroplasties as a function of years of practice. (Abbreviations: BMI: Body Mass Index)

BMI Cutoff Decision Making:

Surgeons were asked, in general for both surgeries, about their BMI cutoff decision making. 91% of surgeons said they had partial or total decision-making power about whether to use a BMI cutoff for THA and TKA surgeries and what cutoff number to use (Fig. 2). 69% reported the cutoff was at their sole decision. Only 6% of respondents listed their department or another entity as the sole decision makers.

BMI Cutoffs Numbers:

Mean THA and TKA BMI cutoffs were 40.5 and 41, respectively (Fig. 3). Many surgeons used BMI cutoff numbers that were higher or lower than suggested by the AAOS.

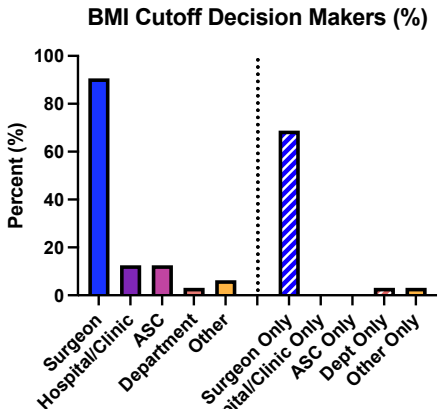

Figure 2. Who determines BMI cutoffs for hip and knee joint arthroplasties in California. (Abbreviations: BMI: Body Mass Index, ASC: Ambulatory surgery center)

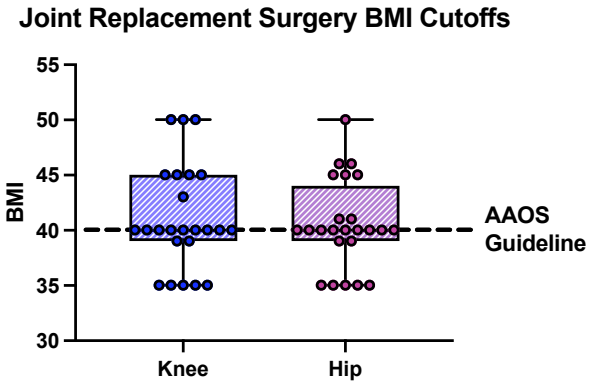

Figure 17.Self-reported BMI Cutoffs of Californian Orthopaedic Surgeons as they compare to the AAOS BMI guidelines. (Abbreviations: BMI: Body Mass Index, AAOS: American Academy of Orthopaedic Surgeons)

BMI Cutoff Justifications:

Surgeons were asked to identify justifications in their BMI cutoff decisions for both THA and TKA. The most common justifications identified by respondents were infection rate (75%) and difficulty of surgery (59%)

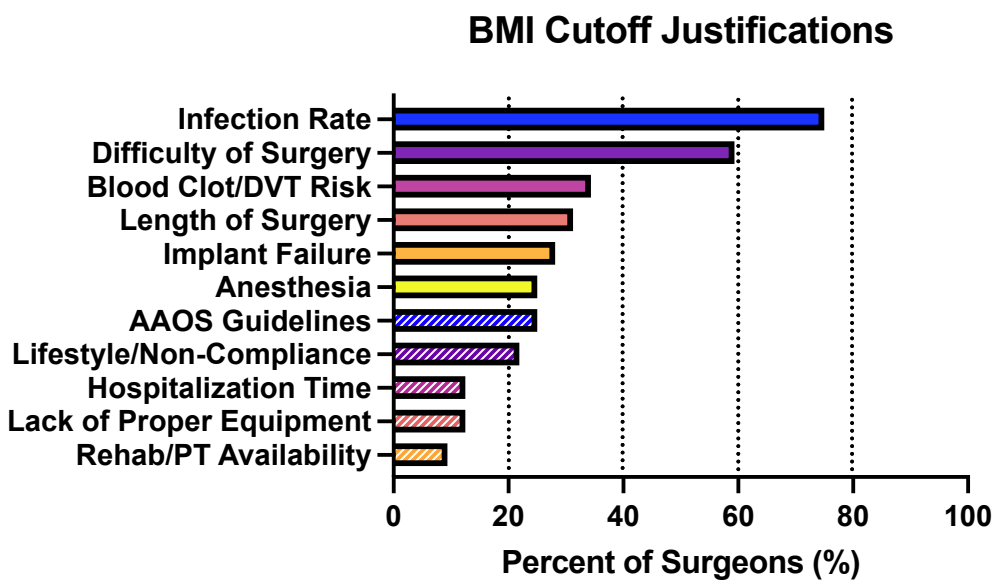

Figure 4. BMI Cutoff justifications for Californian orthopedic surgeons performing hip and knee arthroplasties. (Abbreviations: BMI: Body Mass Index, DVT: Deep vein thrombosis, AAOS: American Academy of Orthopaedic Surgeons)

(Fig. 4). Other justifications based on complications with surgery included blood clot/DVT risk (38%) and concerns about anesthesia (25%). Other concerns with performing the surgery included the increased length of surgery (30%). Justifications based on surgeon perception included the risk of implant failure (27%) and concerns about patient lifestyle or non-compliance (21%). Relatively few respondents were concerned about facilities or resources including hospitalization time (15%), lack of proper equipment (15%), and rehab/PT availability (9%). For further analysis, these justifications were categorized (Fig. 5). This included possible areas to be address by future research (Fig. 5A), issues that could be addressed with additional training (Fig. 5B), issues that could be addressed with updated facilities and resources (Fig. 5C), and issues that may be due to surgeon perception or bias (Fig. 5D).

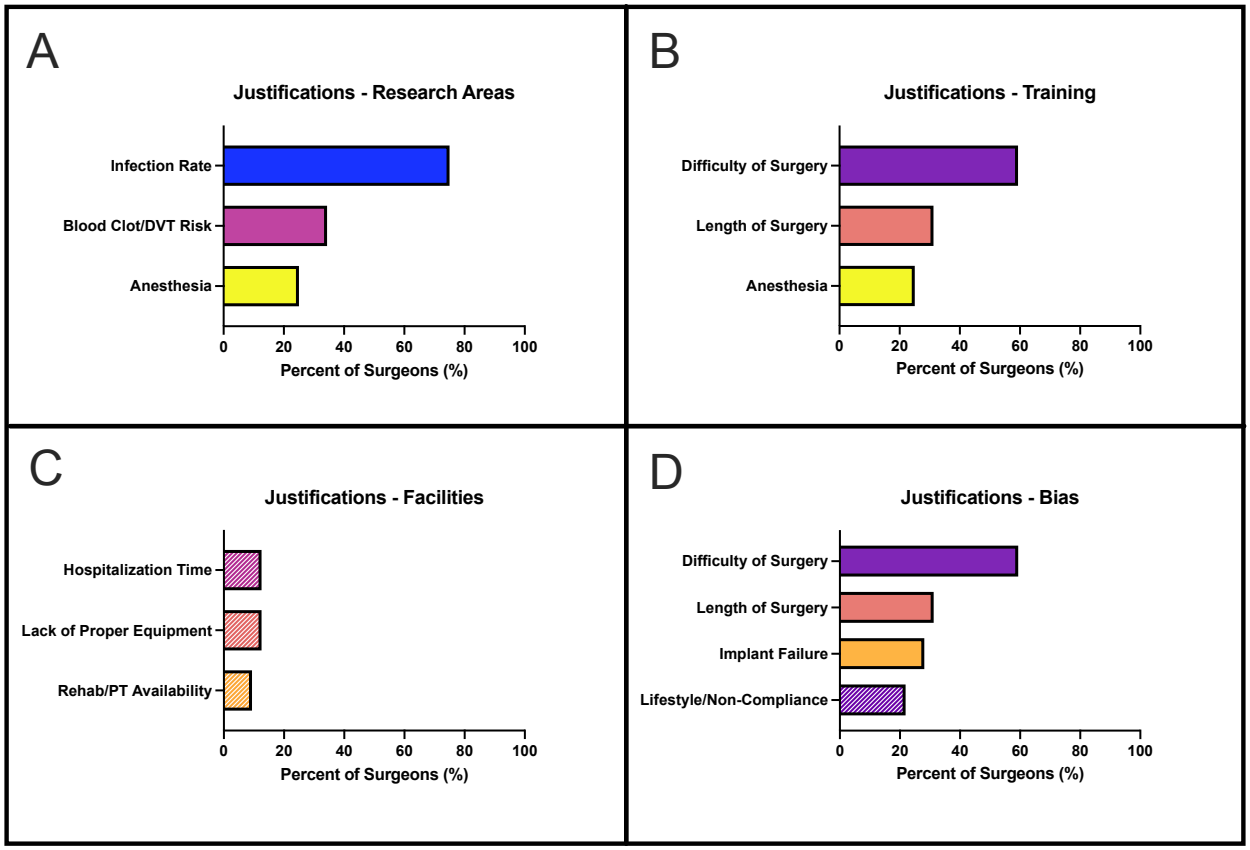

Figure 5. Categorized BMI Cutoff justifications for Californian orthopedic surgeons performing hip and knee arthroplasties. Four categories for BMI cutoff justifications were identified: A) increased risk of complications, B) logistics for performing surgeries, C) concerns about facilities or resources, and E) surgeon perception. (Abbreviations: BMI: Body Mass Index, DVT: Deep vein thrombosis, AAOS: American Academy of Orthopaedic Surgeons).

Discussion

In this study we surveyed California orthopaedic surgeons who regularly perform THA and/or TKA about BMI cutoffs for these procedures. This preliminary survey was only circulated among members of the California Orthopaedics Association so surgeons practicing THA and TKA in California that were not part of this organization may not be properly represented. Additionally, these responses may not represent the policies and decision making of surgeons outside of California. The survey received a small number of responses compared to the number of orthopaedic surgeons in California. However, the COA website lists 295 "total joint" surgeons in their member directory, leading us to believe our 32 responses is a large enough

proportion of relevant surgeons to glean important information regarding BMI cutoffs for these surgeries. Through their responses, we were able to assess the prevalence and specific cutoff numbers for these procedures. We also identified four categories for BMI cutoff justifications including 1) increased risk of complications, 2) logistics for performing surgeries, 3) concerns about facilities or resources, and 4) surgeon perception.

Our resulting average values (BMI cutoffs of 40.5 and 41 for THA and TKA, respectively) are in line with another survey distributed nationally to the American Association of Hip and Knee Surgeons Research Committee members, though the western/Pacific northwest portion of their respondents had a markedly lower BMI cutoff than present in our data [365]. The Western/Pacific northwestern portion makes up just 13% of their total study population, so their aggregated findings may not represent Californian surgeons.

Research Gaps

Justifications for denying a THA or TKA due to a high BMI pertaining to surgery-related complications represent areas for future research (Fig. 4B). Medical complications can arise during surgery, perioperatively, and post-operatively with varying levels of severity. Database studies frequently compare the rate of complications as a function of BMI category (underweight, normal weight, overweight, and the obesity classes). Complications that correlate with increased BMI can include cardio-respiratory issues, infection, and the need for revisions [367]. Surgery-related issues can lead to longer hospital stays and increased resource utilization and cost of care [368, 369], but not in all cases [369, 370]. Additionally, the literature currently has no consensus on the prevalence of these issues after THA and TKA in different BMI categories. Certain clotting conditions, such as pulmonary embolism, exhibit a higher likelihood in individuals with elevated BMI, whereas others, like deep vein thrombosis, remain unaffected by variations in patient weight [371]. Readmission and infections, including surgical site infections and perioperative joint infections, are one of the most identified risks of high BMI individuals [369, 372-375], though the correlation of BMI and infection risk is not clear for all surgeons or operations [376]. There is also no

consensus as to the impact of BMI on THA and TKA on overall functional outcomes [369, 377-379]. The pro-inflammatory state in an high BMI patient puts them at a higher risk of Perioperative cardiac and respiratory complications [380]. Due to the metabolic syndrome seen in bariatric patients, there is an increased risk of cardiac morbidity and mortality, in general, but this has not been defined in the joint arthroplasty population due to the extremely low mortality rates. Similarly, respiratory challenges in high BMI patients during and after surgery include hypoxia, need for higher positive end-expiratory pressure (PEEP), higher incidence of OSA (Obstructive Sleep Apnea) and higher risk of intensive care unit (ICU) admissions [381]. There is some evidence to suggest that operative times are also increased in patients with higher BMI [367, 382].

Orthopaedic research may be able to close several knowledge gaps that prevent safe surgeries on high BMI individuals including infection rate, blood clot/DVT risk, and adverse effects of anesthetics. Understanding the mechanisms that increase these issues in higher weight bodies, whether biological or procedure based, will help advance translational research that benefits patients of all sizes. As the average BMI of Americans increases, new research should be conducted to apply treatments of past studies to larger body sizes. Future medical studies and clinical trials should include a range of BMIs to reflect the impact of these treatments on a representative sample of patients that represent all patient populations.

Training

Perceived difficulty of surgery, increased length of surgery, and adverse effects of anesthetics on high BMI patients may be addressable by increased and specific training on caring for patients with larger body sizes (Fig. 4C) [380]. With practice, surgery difficulty and length can be reduced, and anesthesia application can be improved. Additionally, the negative correlation between years of experience and percentage of surgeons implementing BMI cutoffs for joint arthroplasty could represent a variety of training-related issues. These concerns could indicate that medical schools and residency programs are not adequately preparing trainees for operating on high BMI individuals, requiring years of post-graduation and post-residency experience to

adequately serve these patients. This is consistent with research about bias in medical schools and those training in healthcare fields [383]. Additionally, it is a possibility that the more experienced surgeons can handle the complexities of the surgery better than their younger counterparts or that they are just not aware of the AAOS guidelines (or chose to ignore them because of lived experience).

Facilities

Hospitalization time, lack of proper equipment, and rehabilitation/physical training availability were less influential on a surgeon's chosen BMI cutoff (Fig. 4D). However, these factors are still a systemic concern for hospitals around the US [384-386]. Developing a system to share equipment between orthopaedic surgery and bariatric surgery centers could help address any concerns related to access to appropriate facilities and equipment.

Surgeon Perception and Bias

In some cases, surgeons being unable or unwilling to operate on higher BMI individuals may be influenced by implicit or explicit anti-fat bias. Concerns about lifestyle and assumed non-compliance after surgery indicate an unspoken moral standard has been applied to high BMI patients. These prejudices heavily impact patient wellbeing beyond denial of care [387-390]. Patients that experience weight stigma have worse outcomes and morbidities compared to high BMI patients that have not experienced this stigma [390]. Increased body size may add difficulty or length to surgery, but these concerns would likely be mitigated with proper training and resources. Length of surgery as a justification to avoid high BMI joint arthroplasty patients may also reflect anti-fat bias. A metadata analysis of over 5 million patients found that mean surgery times were increased for high BMI patients by just 6 minutes for all surgeries (from 83 to 89 minutes) and 7 minutes for orthopaedic surgeries (from 76 to 83 minutes) [367]. THA and TKA surgeries carry a much shorter operation time than other elective orthopaedic procedures, and length of surgery can be impacted by many factors beyond weight, including inter-surgeon variability, available support staff, and even day of the week [391-393]. Inadequate training, education, and facilities, as well as provider bias,

all impact the ability of high BMI individuals to receive life-changing healthcare. This is a growing issue in many medical fields. As the population weight increases, so will the medical costs associated with delayed or avoided medical care. A scarcity of orthopaedic surgeons that are able and willing to perform surgeries on larger individuals will increase these issues unless policies and medical training are modified to be more accommodating of high BMI patients.

There is currently no consensus about the impact of BMI on implant failure based on implant survival and surgery outcomes [356, 377, 394-397]. Studies have found that there is no difference in knee prosthesis failures or outcomes regarding BMI or total body weight [356, 396, 397]. Others suggests that high BMI demonstrate increased infection rates in THA and TKA, and that reduced outcomes may be due to higher BMI at younger ages [398, 399]. Research has demonstrated increased dislocations of hip arthroplasty related to BMI [394, 395], but that mechanical failure and aseptic loosening were not correlated with BMI [395]. Several implant manufacturers include high BMI as a contradiction for the use of their products, though some researchers have shown that the forces on an implant reduce with height more so than weight, so BMI based cutoffs may be unjustified with respect to implant failure [377]. Despite these conflicting studies, the majority acknowledge that joint arthroplasty surgeries still provide a vast improvement to the quality of life of high BMI patients. THA and TKA surgeries carry extremely high success and satisfaction rates compared to other elective surgeries, so while many factors go into a surgeon's decision about whether to operate on a patient, concerns about implant failure should not be primary factor affecting this decision.

Professional Organization Guidelines

We found that less than 1 out of 4 Californian orthopaedic surgeons used the national AAOS guidelines as a key factor for their BMI cutoff selection. Current AAOS guidelines cite reduced clinical outcomes for individuals with high BMI based on “strong evidence.” However, a review of the few provided publications cited on the AAOS OrthoGuildelines website at the time of publication [400, 401] demonstrated conflicting evidence. BMI/Obesity received their highest risk factor recommendation of “Strong Recommendation”

for TKA based on the articles cited on these pages. However, several of these publications stated that outcomes are not correlated with BMI. [356, 396, 400-402]. For example, Judge et al determined that there were no reduced outcomes in higher BMI individuals, and that BMI should not be an access to care barrier given the benefits of TKA [396, 397]. The main risk factors listed for high BMI individuals were wound complications, such as surgical site infections, and reduced functional outcomes. However, outcomes such as Knee Society scored were still higher for high BMI patients post-TKA than their pre-clinical range and function scores [357], demonstrating that this surgery still provided an improvement in function for these individuals. The AAOS and similar professional organizations should revisit their BMI cutoff guidelines and justifications to better mirror current understandings in the field, such as those cited by this study, which Californian surgeons are currently using to inform their own BMI cutoffs.

Conclusions

Access to THA and TKA for high BMI individuals in California is mostly determined by the orthopaedic surgeon that would perform their surgery. These orthopaedic surgeons, as well as the medical facilities where they practice, have an opportunity to provide life-changing relief to osteoarthritis patients suffering from pain and mobility issues. Improvements in training, more accommodating facilities, updated institutional policies, bias training, and orthopaedic research aimed at addressing surgical complications in high BMI individuals may increase equitable access to healthcare to high BMI patients.

Appendix 2: Differentially expressed genes (tibia)

Ensembl ID	baseMean	log2FoldChange	lfcSE	stat	pvalue	padj	symbol
ENSMUSG00000059824	130.803727	-1.5224962	0.22245952	-6.8439246	7.71E-12	1.31E-07	Dbp
ENSMUSG00000008874	432.126679	-1.5315917	0.25949292	-5.9022486	3.59E-09	3.05E-05	Clec3a
ENSMUSG00000144056	723.622077	-1.3736004	0.27079555	-5.072463	3.93E-07	0.0022236	
ENSMUSG00000035258	291.324618	-0.6938897	0.13851094	-5.0096379	5.45E-07	0.00231586	Abi3bp
ENSMUSG00000038119	164.8287	-0.9911091	0.20189498	-4.9090328	9.15E-07	0.00310953	Cdon
ENSMUSG00000127251	5822.28349	1.16039474	0.23922136	4.85071538	1.23E-06	0.00348282	
ENSMUSG00000004105	305.95374	-0.7073859	0.14962685	-4.7276669	2.27E-06	0.00482249	Angptl2
ENSMUSG00000028957	247.904145	-0.7336977	0.15463779	-4.7446208	2.09E-06	0.00482249	Per3
ENSMUSG00000026574	84.6325984	-1.2358126	0.26724476	-4.6242723	3.76E-06	0.00660539	Dpt
ENSMUSG00000034463	635.262584	-0.5019602	0.108714	-4.6172547	3.89E-06	0.00660539	Scara3
ENSMUSG00000066687	80.1998874	1.34487995	0.30128684	4.46378584	8.05E-06	0.01243511	Zbtb16
ENSMUSG00000004709	120.151565	0.99859044	0.23229284	4.29884304	1.72E-05	0.02430443	Cd244a
ENSMUSG00000028780	56.2889923	-0.9846243	0.23474025	-4.194527	2.73E-05	0.034838	Sema3c
ENSMUSG00000037406	89.8072545	-1.2867991	0.30759294	-4.183448	2.87E-05	0.034838	Htra4
ENSMUSG00000040280	102.095053	-0.9162507	0.2243126	-4.0847046	4.41E-05	0.04997906	Ndufa4l2

Appendix 3: Differentially expressed genes (soleus)

	baseMean	log2FoldChange	lfcSE	stat	pvalue	padj	symbol
ENSMUSG00000066687	66.9582806	-1.6561282	0.26015398	6.36595362	1.94E-10	1.68E-06	Zbtb16
ENSMUSG00000033124	28.3977905	-1.4952745	0.26403183	5.66323571	1.49E-08	3.24E-05	Atg9a
ENSMUSG00000131965	21.4064155	-1.7147351	0.30281931	5.66256847	1.49E-08	3.24E-05	
ENSMUSG00000033624	18.3117907	-1.7393344	0.30191459	5.76101461	8.36E-09	3.24E-05	Pdpr
ENSMUSG00000141867	40.0555421	-1.3604412	0.24333238	5.59087604	2.26E-08	3.92E-05	
ENSMUSG00000131051	21.600001	-1.562156	0.29635188	5.2712877	1.35E-07	0.00016796	
ENSMUSG00000114382	126.706682	-1.4257837	0.27036593	5.27353312	1.34E-07	0.00016796	Gm4814
ENSMUSG00000022822	94.233606	0.83013043	0.15965122	-5.1996499	2.00E-07	0.00021661	Abcc5
ENSMUSG00000143965	22.820776	-1.6050406	0.31490096	5.09696931	3.45E-07	0.00033282	
ENSMUSG00000120539	22.2766691	-1.362763	0.27072108	5.03382677	4.81E-07	0.00041727	Gm56507
ENSMUSG00000026950	4921.46903	-0.6298586	0.12613326	4.99359668	5.93E-07	0.00042863	Neb
ENSMUSG00000137922	17.5829444	-1.904634	0.3805197	5.00534924	5.58E-07	0.00042863	
ENSMUSG00000109017	153.709618	-1.0622111	0.22207267	4.7831689	1.73E-06	0.00106971	Gm38979
ENSMUSG00000114968	22.1161428	-1.9514247	0.40695515	4.79518364	1.63E-06	0.00106971	A630019I02Rik
ENSMUSG00000087530	53.5958438	-1.5070964	0.31951187	4.71687137	2.39E-06	0.00138574	Gm15533
ENSMUSG00000138003	12.3383941	-1.6667797	0.35482539	4.69746469	2.63E-06	0.00142884	
ENSMUSG00000086741	108.532256	-0.9942374	0.2136618	4.65332301	3.27E-06	0.00157489	Gm15816
ENSMUSG00000069601	143.866752	-0.7486505	0.16066372	4.65973606	3.17E-06	0.00157489	Ank3
ENSMUSG00000110711	95.7656979	-1.4515919	0.3164542	4.58705212	4.50E-06	0.00195082	Gm45760
ENSMUSG00000087253	27.5927736	-1.8352837	0.39938032	4.59532841	4.32E-06	0.00195082	Gm12043
ENSMUSG00000142523	12.6437899	-1.8543854	0.41187057	4.50234993	6.72E-06	0.00277754	
ENSMUSG00000038034	99.8210316	-0.7891417	0.17571476	4.49103831	7.09E-06	0.00279609	Igsf8
ENSMUSG00000032393	99.141508	-0.7971579	0.17879163	4.45858612	8.25E-06	0.00302939	Dpp8
ENSMUSG00000112841	36.2768348	-1.8630679	0.41816786	4.45531099	8.38E-06	0.00302939	Gm48752
ENSMUSG00000056071	35.3938028	-5.3894066	1.21404319	4.43922143	9.03E-06	0.00313433	S100a9
ENSMUSG00000033400	314.362194	-1.205822	0.27240701	4.42654564	9.58E-06	0.00319635	Agl
ENSMUSG00000040118	276.773235	-0.5713993	0.13086748	4.36624324	1.26E-05	0.00396808	Cacna2d1
ENSMUSG00000030753	179.613648	-0.723951	0.16648842	4.34835647	1.37E-05	0.00396808	Thap12
ENSMUSG00000061983	349.792599	0.58389512	0.13409313	-4.3543998	1.33E-05	0.00396808	Rps12
ENSMUSG00000073375	75.4863103	-1.0084682	0.23175084	4.35151918	1.35E-05	0.00396808	Lrrc30
ENSMUSG00000051391	285.342729	-0.5765755	0.1335686	4.31669947	1.58E-05	0.00429555	Ywhag
ENSMUSG00000022139	253.694966	-0.8096339	0.18750309	4.31797612	1.57E-05	0.00429555	Mbnl2
ENSMUSG00002076463	21.9433113	-1.18772	0.27603177	4.30283794	1.69E-05	0.00443482	Gm55944
ENSMUSG00000025006	70.1393175	-1.1456037	0.2676879	4.27962469	1.87E-05	0.00477878	Sorbs1
ENSMUSG00000026123	61.9506637	-0.7943376	0.18635052	4.2625991	2.02E-05	0.00490024	Plekhb2
ENSMUSG00000120290	14.0814816	-1.4598168	0.34257705	4.26128018	2.03E-05	0.00490024	Gm56959

ENSMUSG00000131897	33.0803131	-1.0387093	0.24469295	4.24494975	2.19E-05	0.0049605	
ENSMUSG00000055053	235.712545	-0.710484	0.16711477	4.25147329	2.12E-05	0.0049605	Nfic
ENSMUSG00000009073	80.8100961	-0.6596732	0.15556064	4.24061783	2.23E-05	0.0049605	Nf2
ENSMUSG00000020634	44.3616878	-1.1308123	0.26706343	4.23424612	2.29E-05	0.00497566	Ubxn2a
ENSMUSG00000032484	27.6372515	-6.6896852	1.60266157	4.17410973	2.99E-05	0.00633257	Ngp
ENSMUSG00000033863	143.08753	-0.9213789	0.22238662	4.14314025	3.43E-05	0.00707922	Klf9
ENSMUSG00000026883	85.6549363	-0.7885814	0.19115773	4.12529202	3.70E-05	0.00747332	Dab2ip
ENSMUSG00000031543	289.152853	-0.8165419	0.19833206	4.11704422	3.84E-05	0.00756971	Ank1
ENSMUSG00000025326	80.6091901	-0.5818145	0.1419832	4.09777006	4.17E-05	0.00804542	Ube3a
ENSMUSG00000129224	12.7429544	-1.3799741	0.33839605	4.07798516	4.54E-05	0.00857102	
ENSMUSG00000093674	330.777086	0.51662618	0.12810689	-4.0327742	5.51E-05	0.00996679	Rpl41
ENSMUSG00000036450	129.311899	-0.7886387	0.19553975	4.03313748	5.50E-05	0.00996679	Hif1an
ENSMUSG00000028766	12.465005	-1.3909365	0.34736841	4.00421122	6.22E-05	0.0110214	Alpl
ENSMUSG00000067279	243.723512	-1.2983739	0.32488213	3.99644588	6.43E-05	0.01116129	Ppp1r3c
ENSMUSG00000047419	1478.54308	-0.9653547	0.24234351	3.98341455	6.79E-05	0.01156045	Cmya5
ENSMUSG00000131335	14.2683369	-1.4673797	0.3698882	3.96708986	7.28E-05	0.01214318	
ENSMUSG00000020671	243.98499	-0.7564574	0.19180829	3.94381999	8.02E-05	0.01313212	Rab10
ENSMUSG00000020821	587.13151	-0.7634295	0.19426842	3.92976635	8.50E-05	0.01366596	Kif1c
ENSMUSG00000027288	841.157718	-0.7453266	0.19232421	3.87536529	0.00010646	0.01517756	Zfp106
ENSMUSG00000038375	351.528723	-0.7783521	0.200871	3.87488543	0.00010667	0.01517756	Trp53inp2
ENSMUSG00000037111	132.145228	-0.8239279	0.2114937	3.895756	9.79E-05	0.01517756	Setd7
ENSMUSG00000144165	27.1921147	-1.0599335	0.27337234	3.87725233	0.00010564	0.01517756	
ENSMUSG00000040550	53.7967749	-0.7156491	0.18429016	3.88327356	0.00010306	0.01517756	Otud6b
ENSMUSG00000039952	175.641905	-0.8629373	0.22232769	3.88137565	0.00010387	0.01517756	Dag1
ENSMUSG00000042524	107.018098	-0.6547064	0.16833821	3.88923211	0.00010056	0.01517756	Sun2
ENSMUSG00000130634	14.0776455	-1.321154	0.34218935	3.86088579	0.00011298	0.01581492	
ENSMUSG00000121052	139.469893	-1.0663515	0.27688561	3.85123483	0.00011752	0.01619029	Gm56551
ENSMUSG00000034055	326.990252	-1.3062172	0.33960478	3.84628632	0.00011992	0.0162625	Phka1
ENSMUSG00000120274	43.1260795	-1.237213	0.3222967	3.83873916	0.00012367	0.01651249	Gm56882
ENSMUSG00000090990	179.545301	-1.6012743	0.41841611	3.82699	0.00012972	0.01705815	Gm17197
ENSMUSG00000000131	138.487541	0.85798926	0.22464641	-3.8192877	0.00013384	0.01707308	Xpo6
ENSMUSG00000051236	87.9006887	-0.5607078	0.14708016	3.81225988	0.0001377	0.01707308	Msrb3
ENSMUSG00000139856	17.6280905	-1.4341432	0.37526324	3.82169925	0.00013254	0.01707308	
ENSMUSG00000031010	36.1279726	-0.8558406	0.22429849	3.81563261	0.00013583	0.01707308	Usp9x
ENSMUSG00000044461	37.1141315	-0.9909682	0.26048109	3.80437681	0.00014216	0.01737776	Shisa2
ENSMUSG00000009112	66.1690817	-0.665101	0.17504536	3.79959207	0.00014493	0.01747064	Bcl2l13
ENSMUSG00000020067	447.636843	-0.6604317	0.17461387	3.78224107	0.00015542	0.01798552	Mypn
ENSMUSG00000120133	90.7748026	-1.004554	0.26517888	3.78821277	0.00015173	0.01798552	Gm56945
ENSMUSG00000048546	79.2292114	-0.8911449	0.23554171	3.78338447	0.00015471	0.01798552	Tob2

ENSMUSG00000045983	477.521134	-0.5333902	0.1418748	3.75958382	0.0001702	0.01943596	Eif4g1
ENSMUSG00000021096	138.000263	-0.489614	0.13047996	3.75240722	0.00017514	0.01974131	Ppm1a
ENSMUSG00000026229	103.605864	-1.0022662	0.26940864	3.7202452	0.00019903	0.02214585	Psmd1
ENSMUSG00000032050	162.619092	-0.4396871	0.11855034	3.70886443	0.00020819	0.02287201	Rdx
ENSMUSG00000123692	15.4417824	-2.2521	0.61036383	3.68976645	0.00022446	0.02435042	
ENSMUSG00000143258	330.222249	-1.6417867	0.44533753	3.68661205	0.00022726	0.02435042	
ENSMUSG00000086297	14.0355711	-1.4159879	0.38517737	3.67619696	0.00023674	0.02505657	Gm15632
ENSMUSG00000052337	208.118852	-0.5477798	0.14944939	3.66531954	0.00024703	0.02552349	Immt
ENSMUSG00000021061	239.787525	-0.9260816	0.25262512	3.66583329	0.00024653	0.02552349	Sptb
ENSMUSG00000037573	205.572246	-0.7430021	0.20360681	3.64920047	0.00026306	0.02654742	Tob1
ENSMUSG00000024163	62.5272646	0.61005161	0.16708774	-3.6510854	0.00026113	0.02654742	Mapk8ip3
ENSMUSG00000056054	28.8226381	-4.5615873	1.25159438	3.64462114	0.00026779	0.02671396	S100a8
ENSMUSG00000038170	2371.47994	-0.6806122	0.18793651	3.62150066	0.0002929	0.02883094	Pde4dip
ENSMUSG00000021495	53.6942793	0.73311522	0.20256943	-3.6190812	0.00029565	0.02883094	Fam193b
ENSMUSG00000026822	21.9216741	-3.7023768	1.02405292	3.61541548	0.00029987	0.02891711	Lcn2
ENSMUSG00000022265	165.407057	-0.5991612	0.16658478	3.59673404	0.00032224	0.03054856	Ank
ENSMUSG00000038084	74.3336538	-0.6057859	0.16848653	3.59545598	0.00032382	0.03054856	Opa1
ENSMUSG00000038615	795.945115	-0.6307775	0.17567847	3.59052249	0.00033002	0.03079792	Nfe2l1
ENSMUSG00000034472	14.0021782	-3.4493283	0.96158843	3.58711498	0.00033436	0.0308711	Rasd2
ENSMUSG00000027651	47.5397955	-0.6466983	0.18070138	3.57882335	0.00034514	0.03151617	Rprd1b
ENSMUSG00000037622	106.04727	-0.7113582	0.19891376	3.5762142	0.00034861	0.03151617	Wdtc1
ENSMUSG00000092596	14.1465424	-1.2359863	0.34633991	3.56870889	0.00035874	0.03177088	Gm20490
ENSMUSG00000138621	14.8188268	-1.1243458	0.31501539	3.56917745	0.0003581	0.03177088	
ENSMUSG00000008226	38.4185325	-0.853887	0.24007311	3.556779	0.00037543	0.03182313	Scrn3
ENSMUSG00000051747	9359.88362	-0.5774108	0.1621687	3.56055628	0.00037007	0.03182313	Ttn
ENSMUSG00000068823	712.84525	-0.6511395	0.18328146	3.55267526	0.00038133	0.03182313	Csde1
ENSMUSG00000038708	436.635723	-0.6818572	0.19155424	3.55960377	0.00037141	0.03182313	Golga4
ENSMUSG00000020169	12.3433664	-1.254861	0.35211188	3.5638132	0.00036551	0.03182313	Best3
ENSMUSG00000041329	88.5004442	-1.9220966	0.5407347	3.55460197	0.00037855	0.03182313	Atp1b2
ENSMUSG00000030554	414.643958	-0.8201133	0.23120534	3.54712102	0.00038947	0.03200834	Synm
ENSMUSG00000013076	677.076759	-0.7805252	0.22021329	3.54440567	0.0003935	0.03200834	Amotl1
ENSMUSG00000025161	47.0383711	-2.059686	0.58123176	3.54365697	0.00039462	0.03200834	Slc16a3
ENSMUSG00000073702	260.383491	0.4238872	0.12018193	-3.5270461	0.00042022	0.03302715	Rpl31
ENSMUSG00000106375	71.7202272	-2.0592899	0.58395927	3.5264272	0.00042121	0.03302715	Gm43361
ENSMUSG00000035284	17.2458633	-0.9220151	0.26180737	3.52173102	0.00042874	0.03302715	Vps13c
ENSMUSG00000086918	46.839937	-0.7013625	0.19917789	3.52128694	0.00042946	0.03302715	4930429F24Rik
ENSMUSG00000057181	27.7673104	-0.8570395	0.24286788	3.52883003	0.0004174	0.03302715	5730455P16Rik
ENSMUSG00000097413	52.923861	-0.8881793	0.25225591	3.52094531	0.00043001	0.03302715	A830052D11Rik
ENSMUSG00000042686	209.790492	-0.8195174	0.23348241	3.50997505	0.00044815	0.03310073	Jph1

ENSMUSG00000051000	28.8331143	-0.9728809	0.27691601	3.51327083	0.00044263	0.03310073	Fhip1a
ENSMUSG00000015714	69.2927165	0.60942729	0.17349359	-3.5126791	0.00044361	0.03310073	Cers2
ENSMUSG00000130125	28.2850665	-1.5377388	0.43824507	3.50885589	0.00045004	0.03310073	
ENSMUSG00000004798	79.0612699	-0.5712165	0.16237313	3.51792541	0.00043493	0.03310073	Ulk2
ENSMUSG00000126148	40.717275	-0.8138454	0.23213729	3.50587961	0.0004551	0.03319178	
ENSMUSG00000120060	149.496838	0.57240118	0.16349826	-3.5009618	0.00046358	0.03352858	Gm56964
ENSMUSG00000041695	46.6902176	-0.8657802	0.24822498	3.48788493	0.00048686	0.03463473	Kcnj2
ENSMUSG00000022371	14.1972082	2.16302115	0.61991529	-3.4892205	0.00048443	0.03463473	Col14a1
ENSMUSG00000021390	50.6638703	1.59939669	0.45979466	-3.4785021	0.00050422	0.03557858	Ogn
ENSMUSG00000026827	60.3028654	-1.8197546	0.52585812	3.46054298	0.00053909	0.0374299	Gpd2
ENSMUSG00000125611	81.7725315	-0.9472726	0.27357944	3.46251396	0.00053515	0.0374299	
ENSMUSG00000021557	44.8447305	-0.5930385	0.17147937	3.45836647	0.00054346	0.03743415	Agtpbp1
ENSMUSG00000002222	141.57191	-0.4910627	0.14228907	3.45116229	0.00055818	0.03755368	Rmnd5a
ENSMUSG00000030730	17020.1396	-1.1766713	0.34053761	3.45533435	0.00054961	0.03755368	Atp2a1
ENSMUSG00000141911	24.9045773	-1.0040126	0.2907855	3.45276028	0.00055488	0.03755368	
ENSMUSG00000022508	76.7363129	-0.9262923	0.26883934	3.44552358	0.00056995	0.03805102	Bcl6
ENSMUSG00000050708	185.073634	0.53978386	0.15710532	-3.4358088	0.00059079	0.0391192	Ftl1
ENSMUSG00000032418	135.293786	-0.669794	0.19505358	3.43389767	0.00059497	0.0391192	Me1
ENSMUSG00000014956	422.63516	-0.4195499	0.12245107	3.42626528	0.00061194	0.03993269	Ppp1cb
ENSMUSG00000018800	33.4418612	-0.693827	0.20266897	3.42344943	0.00061832	0.0400476	Abca5
ENSMUSG00000043923	40.7203083	0.72820279	0.21286932	-3.4208912	0.00062416	0.04012675	Cenatac
ENSMUSG00000028518	102.949188	-1.0051565	0.29406339	3.41816264	0.00063045	0.04023318	Prkaa2
ENSMUSG00000025404	125.549296	-0.5098851	0.14936445	3.41369799	0.00064088	0.04059971	R3hdm2
ENSMUSG00000024286	91.2438602	-0.4701499	0.13801545	3.40650191	0.00065801	0.04138316	Ccny
ENSMUSG00000056602	87.5181018	-0.5885044	0.17308926	3.40000521	0.00067385	0.04207415	Fry
ENSMUSG00000041028	490.342455	-0.5287912	0.15582359	3.3935245	0.00068999	0.04247132	Ghitm
ENSMUSG00000024588	112.173215	-0.6794651	0.20019364	3.39403942	0.0006887	0.04247132	Fech
ENSMUSG00000028278	126.243816	-0.7933319	0.235283	3.37181983	0.00074673	0.0456401	Rragd
ENSMUSG00000079278	30.907969	-1.982712	0.58905096	3.3659431	0.00076282	0.04627236	Tmem233
ENSMUSG00000021451	35.2670494	-1.2821928	0.3811319	3.36417066	0.00076774	0.04627236	Sema4d
ENSMUSG00000026457	251.378735	-0.5970324	0.17774351	3.35895489	0.00078238	0.04682939	Adipor1
ENSMUSG00000058975	52.9469104	-1.0680818	0.31837463	3.35479574	0.00079424	0.04721353	Kcnc1
ENSMUSG00000030089	28.2131427	-1.429391	0.42672919	3.34964423	0.00080915	0.04764291	Slc41a3
ENSMUSG00000079641	128.153185	0.41742933	0.12466077	-3.3485221	0.00081244	0.04764291	Rpl39